U.S. DEPARTMENT OF COMMERCE
National Technical Information Service
PB-284 099

Study of the Subarctic Heat Island at Fairbanks, Alaska

Alaska Univ, College Geophysical Inst

Prepared for

Environmental Sciences Research Lab, Research Triangle Park, N C

Jun 78

United States
Environmental Protection
Agency

Environmental Sciences Research
Laboratory
Research Triangle Park NC 27711

EPA-600/4-78-027
June 1978

Research and Development

PB 284 099

EPA

Study of the Subarctic Heat Island at Fairbanks, Alaska

REPRODUCED BY
NATIONAL TECHNICAL
INFORMATION SERVICE
U. S. DEPARTMENT OF COMMERCE
SPRINGFIELD, VA. 22161

RESEARCH REPORTING SERIES

Research reports of the Office of Research and Development, U.S. Environmental Protection Agency, have been grouped into nine series. These nine broad categories were established to facilitate further development and application of environmental technology. Elimination of traditional grouping was consciously planned to foster technology transfer and a maximum interface in related fields. The nine series are:

1. Environmental Health Effects Research
2. Environmental Protection Technology
3. Ecological Research
4. Environmental Monitoring
5. Socioeconomic Environmental Studies
6. Scientific and Technical Assessment Reports (STAR)
7. Interagency Energy-Environment Research and Development
8. "Special" Reports
9. Miscellaneous Reports

This report has been assigned to the ENVIRONMENTAL MONITORING series. This series describes research conducted to develop new or improved methods and instrumentation for the identification and quantification of environmental pollutants at the lowest conceivably significant concentrations. It also includes studies to determine the ambient concentrations of pollutants in the environment and/or the variance of pollutants as a function of time or meteorological factors.

This document is available to the public through the National Technical Information Service, Springfield, Virginia 22161.

TECHNICAL REPORT DATA
(Please read Instructions on the reverse before completing)

1. REPORT NO. EPA-600/4-78-027	2.	3. RECIPIENT'S ACCESSION NO. PB284099
4. TITLE AND SUBTITLE STUDY OF THE SUBARCTIC HEAT ISLAND AT FAIRBANKS, ALASKA		5. REPORT DATE June 1978 6. PERFORMING ORGANIZATION CODE
7. AUTHOR(S) S. A. Bowling C. S. Benson		8. PERFORMING ORGANIZATION REPORT NO.
9. PERFORMING ORGANIZATION NAME AND ADDRESS Geophysical Institute Fairbanks, AK 99701		10. PROGRAM ELEMENT NO. 1AA603 AE-29 (FY-78) 11. XXXXXXXX/GRANT NO. 802999
12. SPONSORING AGENCY NAME AND ADDRESS Environmental Sciences Research Laboratory - RTP, NC Office of Research and Development U.S. Environmental Protection Agency Research Triangle Park, North Carolina 27711		13. TYPE OF REPORT AND PERIOD COVERED Final 8/74-4/78 14. SPONSORING AGENCY CODE EPA/600/09
15. SUPPLEMENTARY NOTES		

16. ABSTRACT

The heat island associated with the City of Fairbanks, Alaska was studied as a means of isolating the effects of self-heating modified radiative transfer from other causes of heat islands. Minimal winter insolation virtually eliminated the effects of variable albedo and the daily temperature cycle; snow cover and dormant vegetation made differences in evapotranspiration unimportant, and very low wind speeds minimized the effect of surface roughness. The observed steady-state heat island under clear skies and low wind speeds was around 10°C, with transient values reaching 14°C. This high value is probably due to the extremely steep ground inversions known to exist in Fairbanks, as the heat island intensity correlated well with the strength of the inversion between 2 and 60 meters elevation. The depth of the mixing layer was less than 90 meters, but the temperature structure at higher levels was disturbed, apparently by coherent lifting of the stable air. The wind field was extremely complex in both time and space, with strong vertical shears, horizontal eddies with scales superimposed on gravity drainage. Speeds were generally too low for accurate measurements. A self-heating term of 10KW person^{-1} in winter and 5KW person^{-1} in summer was derived from the fuel inventory carried out as part of the project. The winter value, applied in a simple model of a heat island over a conducting and radiating city, gave realistic heat island values with wind speeds under 1 m sec^{-1}.

17. KEY WORDS AND DOCUMENT ANALYSIS

a. DESCRIPTORS	b. IDENTIFIERS/OPEN ENDED TERMS	c. COSATI Field/Group
* Meteorology Heating * Insolation Temperature inversions Wind (meteorology)	Heat island effect Fairbanks, AL	04B 13A 04A

18. DISTRIBUTION STATEMENT RELEASE TO PUBLIC	19. SECURITY CLASS *(This Report)* UNCLASSIFIED	21. NO. OF PAGES 168
	20. SECURITY CLASS *(This page)* UNCLASSIFIED	22. PRICE A08 / MF A01

EPA Form 2220-1 (9-73)

EPA-600/4-78-027
June 1978

STUDY OF THE SUBARCTIC HEAT ISLAND AT FAIRBANKS, ALASKA

by

S. A. Bowling and C. S. Benson
Geophysical Institute
Fairbanks, Alaska 99701

Grant No. 80299

Project Officer

George C. Holzworth
Meteorology and Assessment Division
Environmental Sciences Research Laboratory
Research Triangle Park, North Carolina 27711

ENVIRONMENTAL SCIENCES RESEARCH LABORATORY
OFFICE OF RESEARCH AND DEVELOPMENT
UNITED STATES ENVIRONMENTAL PROTECTION AGENCY
RESEARCH TRIANGLE PARK, NORTH CAROLINA 27711

DISCLAIMER

This report has been reviewed by the Office of Research and Monitoring, U. S. Environmental Protection Agency, and approved for publication. Approval does not signify that the contents necessarily reflect the views and policies of the U. S. Environmental Protection Agency, nor does mention of trade names or commercial products constitute endorsement or recommendation for use.

ABSTRACT

The heat island associated with the city of Fairbanks, Alaska was studied as a means of isolating the effects of self-heating and modified radiative transfer from other causes of heat islands. Minimal winter insolation virtually eliminated the effects of variable albedo and the daily temperature cycle; snow cover and dormant vegetation made differences in evapotranspiration unimportant, and very low wind speeds minimized the effect of surface roughness.

The observed steady-state heat island under clear skies and low wind speeds was around 10°C, with transient values reaching 14°C. This high value is probably due to the extremely steep ground inversions known to exist in Fairbanks, as the heat island intensity correlated well with the strength of the inversion between 2 and 60 meters elevation. The depth of the mixing layer was less than 90 meters, but the temperature structure at higher levels was disturbed, apparently by coherent lifting of the stable air. The mean surface wind field was extremely complex in both time and space, with strong vertical shears, horizontal eddies with scales from a few hundred meters to several kilometers, and seiche oscillations at several scales superimposed on gravity drainage. Speeds were generally too low for accurate measurement.

A self-heating term of 10KW person^{-1} in winter and 5KW person^{-1} in summer was derived from the fuel inventory carried out as part of the project. The winter value, applied in a simple model of a heat island over a conducting and radiating city, gave realistic heat island values with wind speeds under 1 m sec^{-1}.

CONTENTS

Abstract iii
Figures v
Tables xvi
Acknowledgement xviii
1. Introduction 1
2. Conclusions 4
3. Recommendations 6
4. Background Information 8
The geographic setting 8
Historical data 11
5. The Surface Temperature Field 17
Measurements 17
Results 35
6. The Three-Dimensional Heat Island 61
Measurements 61
Results 63
7. The Wind Field 72
Measurements 72
Results 75
8. Fairbanks Energy-Use Inventory 85
Electricity 85
Coal 85
Gasoline 89
Fuel oil 94
Total energy 100
Breakdown of energy use 101
Production of unavoidable combustion products 108
9. Theory 110
Introduction 110
The effect of the form of the temperature profile 119
Conductive/convective and radiative energy losses 131
References 147

Preceding page blank

FIGURES

Number Page

1 Fairbanks and surroundings as seen by LANDSAT. The outlined area is that shown in Figure 2. North is at the top. 9

2 Map of the Fairbanks area, showing thermograph sites and traverse routes. Routes most often used were University Avenue, Airport Road, Cushman Street and College Road. Letter codes are as follows: Thermographs: AL Alaskaland, CF Creamer's Field, CL City Parking lot, FS Fire Station, FW Farm Woods, LF Lower Farm, PR Peger Road, SR Sears Roebuck Co, UF Upper Farm (=University Exp. Station climatological station). Creamer's Field and Peger Road had wind data available during part of the second year. Other data: WS NOAA Weather Service, A site of acoustic sounder/boundary layer profiles study, B Borough-operated wind sensor, N anemometer at North Slope Batteries. Thermograph sites CL and SR were "downtown", FS and AL were suburban, and the remaining sites were rural. Shading indicates elevation, with unshaded areas 130 to 152m MSL, lightly shaded areas 152 to 305m MSL and heavily shaded areas above 305m. North is at the top of the figure. 10

3 Fairbanks heat island, 13 December 1964 (Traverse V). Contours labeled in °C. 12

4 Differences in monthly mean temperatures for November, downtown Fairbanks minus the Experimental Farm. All years but 1933 had downtown thermometers at 3m height; 1933 was 20m temperatures. Negative temperature differences in most years are due to intense inversions (Experimental Farm was 18m higher than downtown) 16

FIGURES

Number Page

5 Summary of weather and data collection activity, Nov. 1974 through April 1975. From top to bottom: Double line graph gives daily maximum and minimum temperatures. Dots in line with TR show traverse times; x's in line with FL indicate aircraft observations. Under wind, W's indicate multiple-observer wind observations; single lines indicate one wind recorder in operation, double lines indicate two or more recording anemometer records available. Sky conditions: filled curve gives sky coverage by cloud in tenths; open curve gives sky obscuration by ice fog. Horizontal lines: periods of thermograph records; code letters are the same as in Figure 2.. 18

6 Same as 5 but for May, 1975 through October, 1975. 19

7 Same as 5 but for November, 1975 through May, 1976.. 20

8 Locations of thermistor sensors on traverse vehicle. (a) side view; (b) front view; (c) detail of thermistor shield (used for late-spring and summer daytime runs.) 24

9 Vertical view of downtown Fairbanks, showing the heat island core area (white arrow) and the thermograph site CL, 21 April 1975 . . . 27

10 Thermograph site CL, looking south-southeast, in late April, 1976.. 28

11 Vertical view of Creamer's Field, College Road at lower edge, showing thermograph site CF, 21 April 1975. 29

12 Thermograph site CF, looking NNE, April, 1975 30

FIGURES

Number		Page
13	Vertical view of Peger Road area, 21 April 1975, Tanana River at lower part of photo. Peger Road thermograph locations marked by PR	31
14	Original site PR looking west from access road, summer 1975.	32
15	Both PR sites, photo taken in April 1976 from the same location as was Figure 14. The tallest spruces at the left mark the old site; the thermograph shelter is at the new site.	33
16	Both PR sites, looking SE, anemometer at the new site in the foreground.	33
17	Thermograph temperatures, night of March 3-4, 1975 (23). Stations keyed to Figure 2. Note that station UF is about 12 m higher than the other stations.	34
18	Temperature contours at 2m elevation for a typical heavy ice-fog situation, 1300-1400 January 3, 1975 (8). Contours labeled in °C. .	36
19	Aerial view of Fairbanks during traverse 8, 3 January 1975.	37
20	Temperature contours at 2m elevation for Traverse 13, 1600-1900 January 10, 1975. Moderate ice-fog.	38
21	Temperature contours at 2m elevation for Traverse 29, 2000-2200 December 1, 1975. Moderate ice-fog.	39
22	Comparison of low-level sounding data for times near Traverses 8, (1/3/75), 11 (1/7/75), 13 (1/10/75), all based on rawinsonde data, and traverse 29 (12/1/75), based on helicopter data. Traverse 11 had the weakest nighttime heat island in the study..	40

FIGURES

Number Page

23 Temperature contours at 2m elevation for Traverse 24, 2320 13-0120 14 March, 1975. Clear skies. 42

24 Temperature contours at 2m elevation for Traverse 38, 2100-2230 February 26, 1976. Clear skies. Measured wind directions shown by heavy arrows; wind directions inferred from plume drift shown by light solid arrows (ground level) or light dashed arrows (high stack plumes). 43

25 Temperature contours at 2m elevation for Traverse 17, 1430-1600 January 25, 1975. Overcast skies. Arrows show approximate mean wind directions over the half hour period 1440-1510. 44

26 Thermal infrared imagery of the Alaskaland (AL) area, 0500 March 4, 1975. The general gradient of density from light at the bottom to dark at the top is an artifact of processing and should be ignored. (Photo courtesy of U. S. Army 172nd MID(AS) and Cold Regions Research and Engineering Laboratory). 49

27 Thermal infrared image of part of downtown Fairbanks, about 5 a.m. on a clear March morning. Note the importance of the river as a heat source, especially downstream of the Municipal Utilities System power plant near the center of the picture. The general gradient of density from light at the bottom to dark at the top is an artifact of processing and should be ignored. (Photo courtesy of U.S. Army 172nd MID(AS) and Cold Regions Research and Engineering Laboratory). 49

28 An example of daily temperature variations in town (solid line, thermograph CL) and at Creamer's Field (dashed line) very early in the snowmelt season. Skies were clear throughout.. 51

FIGURES

Number		Page
29	Comparison of daily minimum temperatures at four locations in March. Heavy solid line is site CL (downtown), light solid line is the official weather service temperature recorded at the airport (WS), dashed line is Creamer's Field (CF) and dotted line is Peger Road (PR), both outlying stations. Squares show sky conditions, with open squares for clear skies, black squares for complete overcast and intermediate shading for intermediate conditions. Slant of shading indicates increasing (up to right) decreasing (down to right) or constant (crossed lines) cloudiness.	52
30	Oblique aerial photograph of Fairbanks, Alaska, looking north, taken during the snowmelt season, April 21, 1975. Note the lack of snow on roads and in the city core area just south of the wider bridge (Cushman Street). For comparison with Figure 2, the broad E-W highway near the bottom of the figure is Airport Road and the road bordering the snow-covered field at top is College Road. The Creamer's Field thermograph is at the end of the side road north near the west edge of the subdivision roads south of College Road.. .	54
31	An example of daily temperature variations in town (solid line) and at Creamer's Field (dashed line) quite late in the snowmelt season. The curve at the bottom of the figure gives cloud cover in tenths.	55
32	Temperatures and cloud cover during a relatively clear period in early July, 1975. Stations are the same as Figure 29.	56
33	Thermal infrared imagery of the Fairbanks area in summer. Site CF is at the top edge. This scene was dated to approximately summer 1970 largely on the state of completion of the intersection of Airport Road and Cushman streets, near the lower edge.	57

FIGURES

Number Page

34 Vertical profiles of temperature, acoustic sounder backscatter and wind velocity in a relatively undisturbed area (From Holmgren et. al., 1975). 63

35 Comparison of heat island intensity and approximate 60 m inversion strength (Geophysical Institute temperature minus the same background temperature used in computing the heat island intensity). . . 65

36 Plot of crossover height against inversion strength based on empirical relationship between heat island intensity and 60m inverson and assumed constant background lapse rate. Assymptotic approach tc Z = 45m for strong inversions is physically unrealistic and indicates probable non-constant background lapse rates for these conditions. 67

37 Limiting values for city lapse rate. Heavy dots are measured temperatures; light line is the adiabatic lapse rate over the city; dashed line is the background temperature profile assuming a constant lapse rate to 60m; dash-dot line is a more realistic background temperature profile. Cross shows calculated crosssover height, circled cross, a more realistic value. The true city temperature profile must lie within the triangle formed by the heavy solid lines. 68

38 Thermistor traces across town during Traverse 23 at an elevation of 90m. Left side - North to South and return along Cushman Street; right side - East to west along the line of Airport Road.. 69

39 North-South temperature cross section of the air over Fairbanks, based on data obtained midnight to 0100 March 14, 1975 (Traverse 24).. 70

FIGURES

Number Page

40 Photo of the Fairbanks area, looking east, taken 3 January 1975 with a temperature of -42.5° measured at the city core. East, west, and north winds may be observed to affect plumes emitted at different levels. 74

41 Comparison of winds at three sites through the course of a day. . . . 76

42 Suites of wind directions for various simple wind fields for comparison with Figure 41. Wind measuring sites coded same as Figure 41. 76

43 Wind vectors for 2 two-minute measuring periods during Traverse 20 (0900-1000 8 February 1975). The lengths of solid arrows indicate measured wind speeds; dashed arrows indicate that only wind direction was available. Filled arrowheads-0925; open arrowheads 1000. 77

44 Low-level wind roses at sites in the Fairbanks area for 4 periods of light ice fog in 1969-1970.. 78

45 Surface flow pattern for ice fog deduced from the data in Figure 44. 82

46 Cumulative commerical electricity production as a function of time in and for the Fairbanks area. Note that the top line is the sum of all commercial generation in the area.. 87

47 Cumulative coal consumption by power plants in the Fairbanks area in thousands of tons. 88

48 Gasoline consumption in the Fairbanks area. Heavy line - adjusted tax data; light line - Alaska Railroad imports. 92

FIGURES

Number Page

49 Gasoline imported to Fairbanks and Fort Wainwight prior to 1965 (not cumulative). 93

50 Cumulative fuel oil use in the Fairbanks area. 100

51 Fuel oil imported to the Fairbanks area prior to 1965 (not cumulative).. 101

52 Total cumulative energy use in the Fairbanks area broken down by fuel type and compared with monthly mean temperatures. 105

53 Surface and fog-top energy balances for (a) clear background area; (b) clear city; (c) foggy city. 114

54 Cross section through a hypothetical city, wind from left to right in all cases. Panel a: assumed heat input, h, and heat transferred to the air, q. Panel b: Values of ΔT_{eq} and observed ΔT for the given values of h and q. Panel C: Height of mixed layer, Z, and development of inversion downwind of maximum heat island under clear conditions. Panel d: Height of mixed layer, Z, and cooling downwind of maximum heat island under foggy conditions. . . .117

55 City vs. background soundings for clear and city-fog cases. Both city soundings have had the same net heat addition, q, which is in each case proportional to the shaded area between the unmodified and modified soundings. The fog case has some negative area (horizontally shaded) due to cooling from the fog top, which is balanced by an increase in the positive area, the increase being shown by the fine vertical lines.
$\Delta\theta_C = \Delta T_C$ = Heat Island intensity for the clear case
$\Delta\theta_F = \Delta T_F$ = Heat Island intensity for the foggy case.. 119

FIGURES

Number | Page

56 Development of mixing layer as background air moves into the city. y' is the particular value of y selected for the right hand panel. Left panel - background sounding. Center panel - cross section showing increase of Z (for non-uniform q) as air moves into city. Right panel - sounding at y = y' within the city. Shaded area = ${}^{Z}_{0}(\theta(z) - \theta(z))dz$ is equal to Q(y). 120

57 Potential temperature profiles for which calculations were made of mixing height and heat island intensity. Light lines - lapse rates with the 100 meter potential temperature difference equal to 15.22°C. Plain line - linear case; line with crosses - logarithmic case; dashed line - stepped case; dotted line - capping inversion case. Heavy lines - linear and logarithmic profiles for 100 meter potential temperature differences of 4.6°C (3.6°C/100 m inversion). 128

58 Mixing height, Z, as a function of accumulated bottom heating, Q(y), in °K m. Line types as in Figure 57. Short double lines indicate the 100 m level. 129

59 Heat island intensity, $\Delta\theta$, as a function of Q(y). Line types as in Figure 57. Short double lines indicate where the heat island extends above 100 m. 130

60 Development of city fog sounding. 139

61 Dependence of city center heat island intensity on population. Heavy lines include the effect of thermal radiative loss, light lines give heat island intensity neglecting radiative effects. 144

62 Dependence of city center heat island intensity on energy release per person (solid lines) and potential lapse rate (dashed lines). Light and heavy lines as in Figure 61. 144

FIGURES

Number

Page

63 Dependence of city center heat island intensity on wind speed (solid lines) and area per person (dashed lines). Light and heavy lines as in Figure 61. 145

TABLES

Number Page

1 Monthly mean differences in winter daily minimum temperatures between Experimental Farm and Weeks Field Stations before and after Experimental Farm move. 14

2 Comparison of the Fairbanks winter heat island in 1929-42 with that in 1974-76. 15

3 Summary of Traverse Data. 21

4 Day length and maximum solar elevation at Fairbanks as a function of time of year. 46

5 Thermal properties of various substrates found in the Fairbanks area. 48

6 Approximate height of Fairbanks heat island as a function of inversion strength. 66

7 Electricity imported to Fairbanks. 86

8 Fairbanks area coal usage by year. 90

9 Monthly power plant coal use breakdown in 10^3 tons - 1974 and 1975. . 91

10 Total coal use in the Fairbanks area. 92

11 Fairbanks area gasoline consumption. 95

12 Ratio of taxed yearly sales of diesel oil to those of gasoline for the IV Judicial District. 96

TABLES

Number Page

13 Fairbanks area fuel oil consumption. 98

14 Total energy use in the Fairbanks area. 102

15 Average power consumption per person (including waste heat) in the Fairbanks area for 3 winter and 2 summer months. 106

16 Breakdown by point of release of energy used in the Fairbanks area. .107

17 Production rates of H_2O and CO_2 by fuel types. 108

18 H_2O and CO_2 generated by fossil fuel combustion in the Fairbanks area in 1975. 109

19 Symbols used. 121

20 Temperatures from two helicopter traverses. 130

21 K/J as a function of AB/J 133

22 Typical values of A and B 134

23 Predicted heat islands. 137

24 Maximum ratios of foggy/clear values of mixing depth ($\sqrt{J/K}$) and ΔT (m). 140

25 Combination of ϕ, G, and K observed for urban areas 143

26 Variation of ΔT with population, area per person, energy release per person, lapse rate and wind speed 146

ACKNOWLEDGMENTS

Section 8 of this report is based on data provided by a number of organizations and businesses. These included:

- Alaska Dept. of Revenue
- Alaska Railroad
- Federal Energy Administration
- Fort Wainwright Power Plants (U.S. Army)
- Golden Valley Electrical Assn.
- Municipal Utilities System
- Univ. of Alaska Heating Plant
- Alyeska Pipeline Company
- Fairbanks Fuel Supply
- Johnny's Express
- Kobuk Oil Company
- Northern Heating Oil
- Peters Express
- Petroleum Sales Limited
- Shell Heating Oil
- Sourdough Heating Inc.

We would like to thank all of the above, and to express our special gratitude to the power and heating plants, which provided pre-1967 data, and to the managers of Sourdough Heating and Fairbanks Fuel Supply, who supplied the long-term monthly data which allowed us to extend the data from other oil suppliers backward in time.

SECTION 1

INTRODUCTION

"Urban heat island" is a term used to indicate the effect of a city on the temperature measured within that city. Its existence has been noticed since 1833, and various detailed studies have been made over most of the last 50 years (Duckworth and Sandberg, 1954). Ideally, the magnitude of the heat island is the difference between the temperature measured within a city and the temperature which would be measured at the same point if the city were not present. In practice, the temperature difference between the city and its surroundings is used. Heat islands may be positive or negative, although the negative type is rarely considered.

The most obvious effect of a heat island is, of course, the direct effect on temperature. Hot summer nights are even hotter in large cities. But probably the most compelling immediate reason for studying the urban heat island is the interaction between the heat island and air pollution. Pollutant concentrations are critically dependent on local air motion and temperature structure. In order to develop realistic models for pollutant dispersal, the heat island structure and its dependence on conditions that may change with time must be considered.

A heat island is produced by a combination of many factors, which often oppose each other (Myrup, 1969). The major factors leading to an increase in city temperature are: (1) the heat exhausted to the atmosphere from energy sources within the city (anthropogenic heat or self-heating), which might be considered analogous to thermal pollution of surface waters, (2) a decrease in the area of transpiring plants within the city, (3) The high heat capacity and conductivity of building materials and the generally increased roughness of cities over their surroundings tend to decrease the amplitude of the daily temperature wave (Nappo, 1972). (This will tend to increase further the night-time temperature, but decrease the temperature at midday.) (4) The radiative effects of dirty city air also have an influence on the city air temperature (Atwater, 1971), and if the city albedo differs from that of its surroundings, this will also have an effect.

A high-latitude city, such as Fairbanks, Alaska, provides separation of these causative factors, especially in winter. Once the winter snow cover is established (usually sometime in October) differences in evaporation become unimportant. Even where snow is removed from the main roads enough of a veneer of ice remains that saturation of air in contact with the surface is assured. During December and the first half of January the sun is above the horizon for less than five hours a day, with a maximum elevation above the horizon of only about three and a half degrees. (The minimum values are 3 1/2 hours daylight with noon-time solar angle of 1.5°.) With so little incoming solar energy and the presence of a high-albedo snow surface to reflect most of this slight amount back to space, it is not surprising that the "normal" daily rise in temperature cannot be detected without statistical techniques. This in turn means that the difference in heat capacity and conductivity between the city and the surrounding contryside affects the heat island intensity only during changes from one type of weather to another. The very low wind speeds typical of Fairbanks in winter also minimize the effect of differing roughness in and out of the city. On the other hand, Fairbanks is subject to high concentrations of several pollutants, with one component of the air pollution -- ice fog -- having particulary marked effects on radiative transfer. In addition, the per capita energy consumption in winter is comparable to that of the heavily urbanized strip along the east coast of the U. S. Thus the Fairbanks heat island in winter is dependent primarily on anthropogenic heating, with ice fog being present at some times.

As the seasons progress, other factors begin to influence the Fairbanks heat island. By February, a normal daily temperature cycle is present but melting is still generally absent. Substrate properties become important, but evapotranspiration can still be neglected. The latent heat of melting snow - a factor not normally considered in heat island studies - becomes important in April. By mid-May to June vegetation is in full and extremely rapid growth under uninterrupted daylight and approximately twenty hours a day of possible sunlight. At the same time, the anthropogenic heating has decreased to about half of its winter value. Thus in summer, conditions are similar to those normally encountered in temperate latitudes.

The following report details an observational and theoretical study of the Fairbanks heat island. This information should prove useful in evaluating the relative importance of the causative factors in other areas as well.

SECTION 2

CONCLUSIONS

Our investigations have demonstrated that the Fairbanks area, with an estimated population of 65,000, frequently has a winter heat island intensity of 10°C, and intensities of up to 14°C have been observed. Thus self-heating with some disturbance by buildings of thermal infrared transfer is adequate to produce a substantial heat island. The magnitude of the night-time heat island is only slightly less in the summer months. The daytime heat island disappears from March to September except for a short period in late spring when snowmelt is complete in the city but not in the surrounding area. The effect of ice fog is to decrease the heat island intensity. This effect is probably due to the fact that ice fog affects the background areas as well as the city.

The Fairbanks heat island appears to extend to roughly 60m above the city. Temperatures at 90m are warmer than those at street level under clear and slightly foggy conditions, but greater mixing depths may exist in dense fog. The heat island intensity correlates well with the intensity of the inversion in the lowest 60m of the atmosphere.

The wind field was found to be extremely complex, with 180° shears being common over distances of 200m in the horizontal and 25 m in the vertical. Fluctuations with time are also substantial. It was not possible to determine unequivocally the effect of the heat island on the wind field.

Fairbanks is hardly an industrialized area, but the fuel use inventory gave per capita winter energy consumptions of the order of 10 KW /person. This is comparable to Los Angeles or the east coast urbanized strip from Boston to Washington, D. C. (SMIC, 1971). Summer energy use is about 5 KW/person.

A simple theoretical analysis, including both radiative and convective losses from the surface, gives fairly good agreement with the observed winter heat island, but only if regional wind speeds are kept well below 1 m/sec. This figure is compatible with our observations of the wind field.

In summary, our investigations have demonstrated that a strong heat island can exist even when the only contributing factors are self heating and some disturbance of radiative transfer due to the presence of sizeable buildings. The heat island thus produced is not, however, strong enough to break the Fairbanks inversion even up to 100 m, at least under clear-night conditions.

SECTION 3

RECOMMENDATIONS

Although the horizontal distribution of temperature around and in Fairbanks and its variation with season and time of day are now reasonably well understood, some questions remain unanswered. These problems concern the wind field and the detailed vertical temperature structure within the downtown area, both of which are of major inportance for any continued air pollution studies in the Fairbanks area. The vertical temperature structure outside the city has been examined in detail in the past (Holmgren et al, 1975).

As pointed out in Section 7, the wind field is now known to be extremely complex, and a complete formulation based on any number of point measurements at any one time would be of questionable utility even if it could be achieved. On the other hand, the construction of a refinery at North Pole (about 20 km ESE of Fairbanks) and the proposed further industrialization of that area have made an understanding of the wind fields actually involved in pollutant transport of immediate practical importance. We strongly recommend that tracer studies be carried out in the area. If the emissions from the North Pole refinery prove to have a sufficiently unique trace element "fingerprint", they may themselves act as an automatically released tracer. Their usefulness should be confirmed by an inert tracer such as SF_6 or a Freon not normally used in the area, which could also be used to check flow from possible source areas other than North Pole. The manager of the North Pole refinery has indicated a willingness to cooperate in such studies. As an adjunct to such a study, the time-lapse photography of vapor plumes carried out experimentally during the heat island project and more intensively during the 1976-1977 winter should be continued and expanded.

Another portion of the study which was not as complete as we would have liked was the vertical temperature profile within the city. It appears likely from the helicopter measurements that the vertical temperature structure within the city, studied in detail, might show horizontal variability approaching that of the wind field. (In fact the vertical structure must be tied to the convergence of the wind field by simple conservation of mass). Pilot ballons and a thermistor are not adequate (see Section 6). Radio-controlled model airplanes, also considered, will not operate reliably at temperatures below -20°C. Probably the best way of studying the 2-100 m region would be something like the Institute's boundary layer profiling (BLP) system (part or all of which was unfortunately in Antarctica during our study) but mounted in a trailer or truck. This system consists of an instrument package lifted to as much as 500 m by a 3.2 m^3 aerodynamic balloon, with temperature, pressure, and wind speed telemetered back to the ground. It has previously been used in a stationary mode in the flat, undeveloped area between Fairbanks and the University of Alaska. Some results from the system are cited in Section 6. We would recommend the use of such a system in conjunction with mobile measurements of air chemistry currently in the planning stage.

SECTION 4

BACKGROUND INFORMATION

THE GEOGRAPHIC SETTING

Fairbanks is located on the floodplain of the Chena River near its confluence with the Tanana River. South of the town site, very gently sloping outwash plains extend roughly 100 km from the Tanana River to the Alaska Range. From southwest through northwest to northeast of Fairbanks proper, residential areas extend up into the Tanana-Yukon uplands. East and southeast of town the uplands are farther away (30 to 50 km), but even at this distance the influence of the hills on the wind field cannot be neglected under strong inversions. Figure 1 shows the topography of the area as seen from space, while the smaller scale topography and the locations of thermograph sites and roads used for traverses are shown in Figure 2.

Because of the intense winter ground inversions, (Benson, 1970), topography has an overwhelming influence on both the wind and the temperature fields in the area, as will be discussed in Sections 6 and 7. In considering background temperature sites comparable to the downtown area (which is right on the river bank) any area which is in the hills may be eliminated at once. Luckily the break in slope between the flood plain (locally referred to as "the flats") and the hills is usually abrupt. Even within the flats, however, filled-in sloughs and similar very slight depressions may be considerably colder than nearby areas which are not obviously higher. The infrared images reproduced in Section 5 make this quite evident.

In considering how the site on which Fairbanks is built would fit into the natural temperature field if the city were not there, two types of information were considered. The first was the distribution of water depths

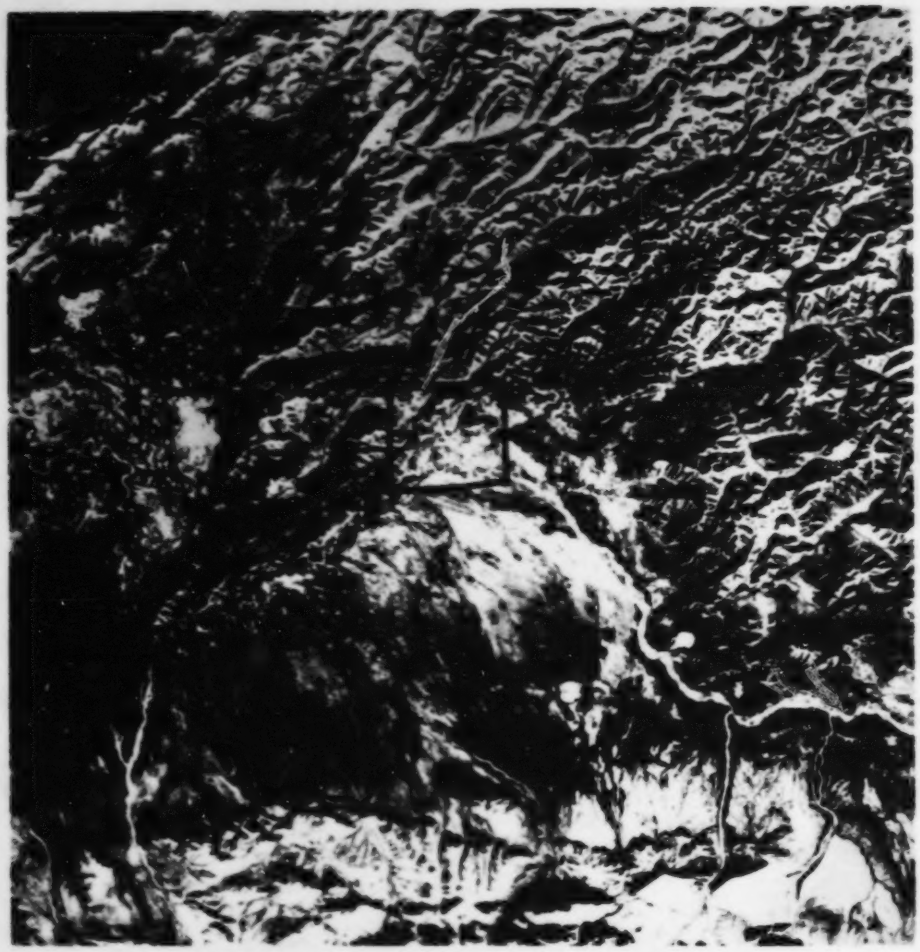

Figure 1. Fairbanks and surroundings as seen by LANDSAT. The outlined area is that shown in Figure 2. North is at the top.

during the Fairbanks Flood of August 1967 (Childers and Meckel, 1967). Virtually everything within the city limits of Fairbanks and a large area outside the city were under 2 to 5 feet of water. Of the background thermograph sites selected, Creamers Field was under approximately 2 feet of water, Peger Road under 3 feet, and Lower Farm was out of the flooded area. The heat island core at Second Avenue and Cushman Street was under 2.7 feet of water. Thus to the extent that water flows in the same way as cold air, the background sites should have temperatures similar to or higher than that of the heat island core. (It is probably worth noting that the Airport, where weather records are now taken, was an island above the flood waters.)

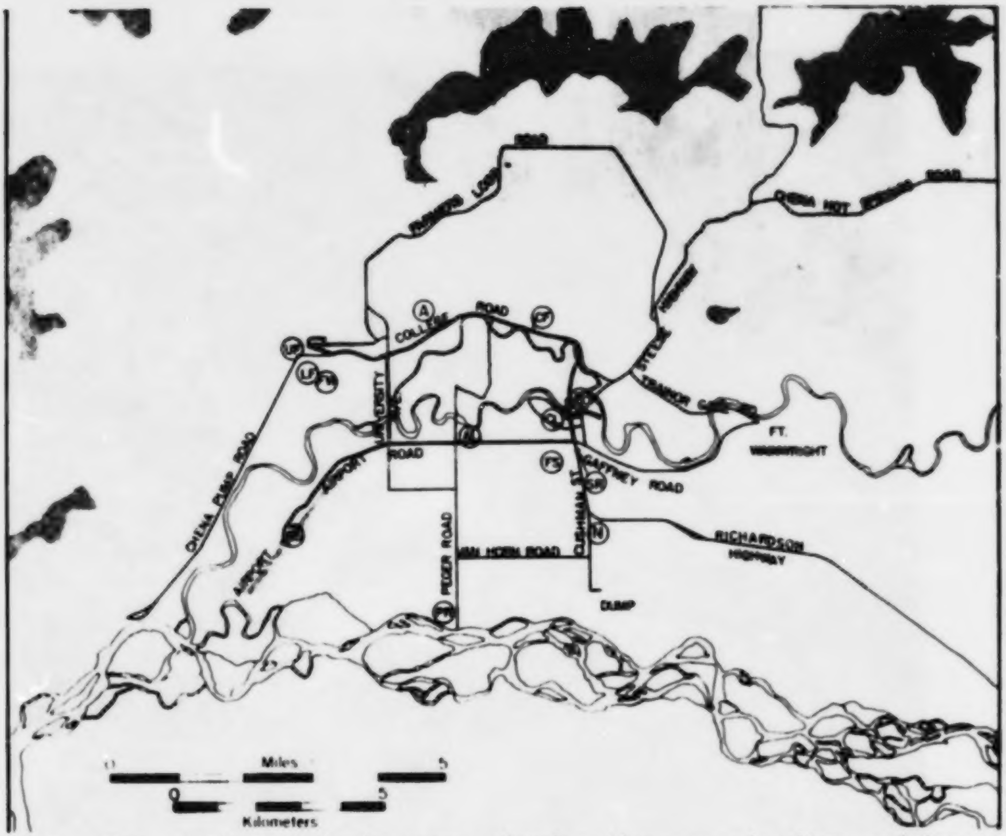
FARMERS LOOP ROAD
CHENA HOT SPRINGS ROAD
STEESE HIGHWAY
COLLEGE ROAD
UNIVERSITY AVE
TRAINOR GATE ROAD
FT. WAINWRIGHT
AIRPORT ROAD
GAFFNEY ROAD
CHENA PUMP ROAD
PEGER ROAD
VAN HORN ROAD
CUSHMAN ST
RICHARDSON HIGHWAY
DUMP
A
UF
LF
FW
CF
CL
SR
FS
AL
WS
B
N
PR
Miles
0
5
0
5
Kilometers

Figure 2. Map of the Fairbanks area, showing thermograph sites and traverse routes. Routes most often used were University Avenue, Airport Road, Cushman Street and College Road. Letter codes are as follows: Thermographs: AL Alaskaland, CF Creamer's Field, CL City Parking lot, FS Fire Station, FW Farm Woods, LF Lower Farm, PR Peger Road, SR Sears Roebuck Co, UF Upper Farm (=University Exp. Station climatological station). Creamer's Field and Peger Road had wind data available during part of the second year. Other data: WS NOAA Weather Service, A site of acoustic sounder/boundary layer profiler study, B Borough-operated wind sensor, N anemometer at North Slope Batteries. Thermograph sites CL and SR were "downtown", FS and AL were suburban, and the remaining sites were rural. Shading indicates elevation, with unshaded areas 130 to 152m MSL, lightly shaded areas 152 to 305m MSL and heavily shaded areas above 305m. North is at the top of the figure.

In addition, the lowest temperature ever recorded by the weather service in the Fairbanks area, -66°F (-54.4°C) on January 14, 1934, was recorded at Second and Cushman--the heart of the present day heat island. As discussed in the next subsection, this temperature was itself probably influenced by the

Fairbanks heat island. A quick check of other interior Alaska stations in operation since 1934 indicated that the 1934 cold spell, although certainly severe, has been equalled or exceeded since--but not in Fairbanks, where the weather station has been moved to other sites. We concluded that the natural background temperature at Second and Cushman was probably comparable to those observed at our colder background sites.

The final choice of Creamers Field rather than Peger Road as the primary background site was based on winds. Although the wind field in the Fairbanks basin is extremely complex, topography and strong radiative cooling do drive a very slow downslope motion (north to south) at low levels. Seiche oscillations, the influence of the regional wind field, Coriolis effects on the downslope winds, and local eddies and waves would exist even in the absence of the city (see Section 7), but only the gravity drainage (modified by Coriolis effects) produces a consistent direction of transport. As a consequence, Creamers Field, which is north of town, is usually sampling the clean air coming into the town while Peger Road air has often been through Fairbanks. The distribution of ice fog, which under light to moderate fog conditions was normally absent at Creamers' Field and present at Peger Road, confirms this. (Creamer's Field is actually closer to heavy traffic.) Under heavy fog conditions Creamer's Field is often fogged in also, and in fact the apparent weakening of the heat island under these conditions (see Section 5) may be because we have been unable to locate an accessible background site in the flats upwind of and uninfluenced by the City of Fairbanks.

HISTORICAL DATA

Most heat island studies are confined to data collected after the study is started. In Fairbanks, data from two earlier periods are also available. Benson (1970) made several temperature traverses under ice fog and partially overcast conditions during the course of his ice fog investigations in the early 1960's. (See Roman-numbered traverses in Table 3, Section 4.) In addition, some evidence for heat island intensity is available from the 1930's.

Benson's traverses generally showed temperatures similar to those observed during our ice fog measurements in 1974-1976, except that the secondary maximum temperature at Cushman and Airport Road was not so pronounced during the earlier study. Figure 3 is a plot of one of these early traverses, which may be compared with plots at similar temperatures (Figures 18, 20, 21, 23, and 24) in Section 5. His traverses at higher temperatures showed generally weak heat islands.

The data for the 1930's comes from the fact that Fairbanks has had both a Weather Bureau Station and a climatological station at the University Experimental Farm since the summer of 1929. Although both stations have been moved, there is enough common data that we can compensate for the experimental

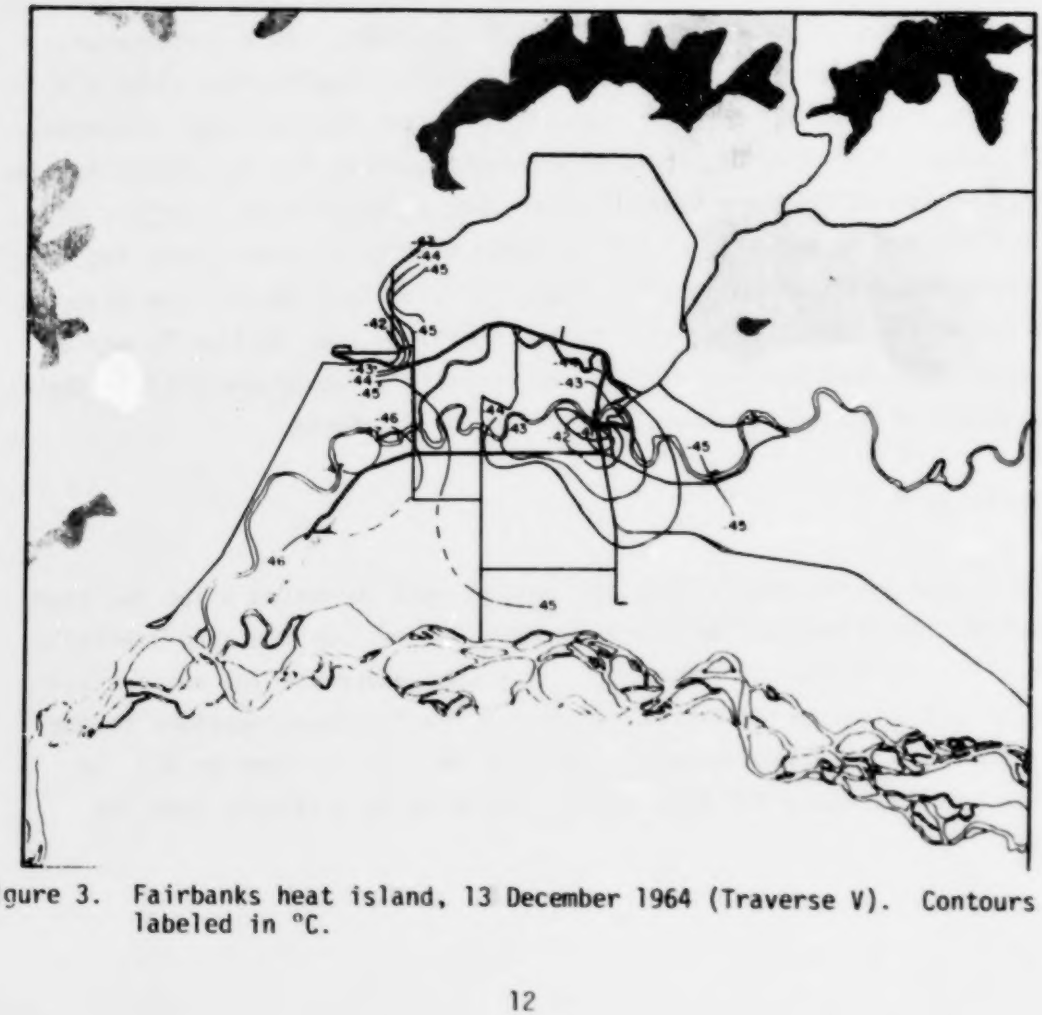

Figure 3. Fairbanks heat island, 13 December 1964 (Traverse V). Contours labeled in °C.

farm move in the late 1940's. It is then possible to compare the temperature differences between the two stations in the 1930's (when the Weather Bureau was located in the heart of downtown Fairbanks, within a block of the present heat island maximum at Second and Cushman) with those available for the period when thermograph records were available from downtown during 1974-76.

Compensation for the change in Experimental Farm location is based on the period from 1943 to 1951 when the Fairbanks station was located at Weeks Field (north of Airport Road and west of Cushman Street; see Figure 2). Prior to 1943 the Fairbanks station was at Ladd Air Force Base (now Ft. Wainwright) or downtown; since 1951 it has been at the present International Airport. The Climatological Record for Alaska shows that the University Experiment Station changed from 500' (152 m) to 475' (145 m) msl elevation in the summer of 1947. Internal evidence in the temperature records suggests that the actual movement of the station may have taken place in the summer of 1946, so the 1946-47 winter was excluded from the analysis. Both the old and the new station locations are on an exposed south slope, the new location being the one marked UF in Figure 2. (By comparison, the City of Fairbanks is at 440' [134 m]). In order to avoid insolation effects, only December and January monthly means of daily minima were used. Temperature differences between the two stations for the three years before the move and the four years after are given in Table 1. If the Weeks Field location remained unchanged, comparison of means for the two periods gives a 2.5°C temperature change due to the move of the Experimental Farm. If the apparent trends within the two short periods are real and due to an increased effect of the Fairbanks heat island on the Weeks Field location, the change could be as little as 1.5°C or even 1°C. We have used the 2.5°C correction in Table 2, recognizing that the corrected values could be as much as 1.5°C too high. The Experimental Farm location itself has been changed by paving the road 100 m to the south and by addition of a small modular building south of the measurement area. Possible effects of these changes have been neglected.

As the Experimental Farm site is definitely higher and warmer than the flat area around Fairbanks, a final correction was made by using the available data from Creamer's Field for the 1974-76 December and January minimum temperatures. The resulting mean heat island intensities (with the 1° correction for the location of the downtown thermograph) are given in Table 2 for the

Table 1. MONTHLY MEAN DIFFERENCES IN WINTER DAILY MINIMUM TEMPERATURES BETWEEN EXPERIMENTAL FARM AND WEEKS FIELD STATIONS BEFORE AND AFTER EXPERIMENTAL FARM STATION MOVE. POSITIVE VALUES INDICATE THAT THE EXPERIMENTAL FARM WAS WARMER THAN WEEKS FIELD.

500' location		475' location	
Dec 43	3.9	Dec 47	0.7
Jan 44	3.3	Jan 48	1.9
Dec 44	2.4	Dec 48	0.3
Jan 45	3.7	Jan 49	0.7
Dec 45	3.0	Dec 49	0.1
Jan 46	2.1	Jan 50	-0.3
Dec mean	3.1	Dec 50	0
Jan mean	3.0	Jan 51	-0.2
Dec-Jan means	3.1	Dec mean	0.3
		Jan mean	0.5
Change: ∿2.5°C		Dec-Jan means	0.4

recent data. The difference between the temperatures from the Experimental Farm and those from Creamer's Field ranged from 2 to 4.5°C, averaging 3.3°C. In order to estimate the heat islands of earlier years, 3.3°C was added to the site-corrected figures for 1929-42. The results are shown in Table 2. Census populations were 2100 for 1930 and 3450 for 1940, as compared with 18,400 for 1970; so the change from the thirties to the mid-seventies is in fact very nearly proportional to the change in the fourth root of population (see Section 9).

One other point of interest may be gleaned from the records of the 1930's. In 1933, when the Weather Service moved from First and Cushman to Second and Cushman, the thermometer, previously maintained at a height of 3 m, was installed at a height of 20 m from July through November. By late November, it had become obvious that the change in height was affecting recorded temperatures and the thermometer was moved back to a 3 m height. Figure 4 shows the

TABLE 2. COMPARISON OF THE FAIRBANKS WINTER HEAT ISLAND IN 1929-1942 WITH THAT IN 1974-1976. ALL FIGURES ARE DIFFERENCES (IN °C) BETWEEN MONTHLY MEANS OF DAILY MINIMUM TEMPERATURES, CITY MINUS EXPERIMENTAL FARM. 1929-1933 CITY TEMPERATURES FROM FIRST AND CUSHMAN, 1933-42 FROM SECOND AND CUSHMAN. 1974-1976 FROM BARNETTE (TWO BLOCKS WEST OF CUSHMAN) BETWEEN THIRD AND FOURTH. SECOND AND CUSHMAN IS CURRENTLY THE PRIMARY MAXIMUM OF THE HEAT ISLAND, WITH THE BARNETTE STREET LOCATION BEING 2°C COLDER DURING STRONG HEAT ISLAND CONDITIONS AND AN ESTIMATED 1°C COLDER ON A MONTHLY MEAN BASIS. STATION LOCATION CORRECTIONS ARE +2.5°C PRIOR TO 1947 (CORRECTION FOR EXPERIMENTAL FARM SITE CHANGE) AND + 1° IN 1974 IN 1974-1976 (CORRECTION FOR THERMOGRAPH SITE LOCATION RELATIVE TO SECOND AND CUSHMAN).

Year	Raw Differences	Corrected for Site Changes	Corrected for Background Temperatures
December			
1929-30	-1.9	0.6	3.9
1930-31	-2.1	0.4	3.7
1931-32	-1.4	1.1	4.4
1932-33	-2.5	0	3.3
1933-34	-0.8	1.7	5.0
1934-35	-2.5	0	3.3
1935-36	-0.8	1.7	5.0
1936-37	-0.9	1.6	4.9
1937-38	-2.2	0.3	3.6
1938-39	-0.8	1.7	5.0
1939-40	0.9	3.4	6.7
1940-41	0.9	3.4	6.7
1941-42	-2.6	-0.1	3.2
Mean		1.2	4.5
1974-75	2.8	3.8	8.2*
1975-76	2.6	3.6	5.9*
Mean		3.7	7.0
January			
1929-30	-3.6	-1.1	2.2
1930-31	-2.7	-0.2	3.1
1931-32	-2.3	0.2	3.5
1932-33	-2.3	0.2	3.5
1933-34	-1.3	1.2	4.5
1934-35	-7.9	-5.4	-2.1
1935-36	-3.2	-0.7	2.6
1936-37	0.7	3.2	6.5
1937-38	-2.1	0.4	3.7
1938-39	-0.9	1.6	4.9
1939-40	-1.5	1.0	4.3
1940-41	-0.3	2.2	5.5
1941-42	-3.1	-0.6	2.7
Mean		0.2	3.5
1974-75	1.0	2.0	6.6*
1975-76	2.7	3.7	5.6*
Mean		2.8	6.1

* Measured values (downtown-Creamer's Field thermograph, +1° correction for downtown thermograph site). These are the values used to estimate the 3.3°C correction (2° to 4.5°) to the earlier data.

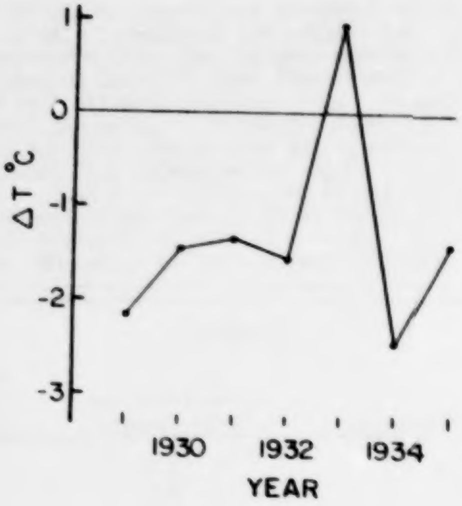

Figure 4. Differences in monthly mean temperatures for November, downtown Fairbanks minus the Experimental Farm. All years but 1933 had downtown thermometers at 3 m height; 1933 was 20 m temperatures.

November monthly temperature differences between the city site and the Experimental Farm, from which it appears that the 3 m to 20 m inversion in the City in 1933 may have averaged around 2°C, for a near-ground inversion strength of around 12°C/100 m. (The warmer temperatures at the Experimental Farm are an elevation effect due to the background inversion.) This is in sharp contrast with present day conditions because inversions are now rare in the lowest 20 m in the city. City lapse rates are probably normal to around 50 m and the city mixing depth is almost certainly more than 20 m. (Present-day lapse rates are discussed in detail in Section 6).

SECTION 5

THE SURFACE TEMPERATURE FIELD

MEASUREMENTS

Information on the distribution of near-surface temperatures in the Fairbanks area was obtained from automobile traverses, from a variable number of thermograph stations, and from regular NOAA weather service observations at Fairbanks International Airport (WS in Figure 2). Time distribution of traverses and thermograph data is shown, together with data on temperature and sky cover, in Figures 5 through 7. In addition, qualitative data on actual surface temperatures are available from two sets of aerial thermal infrared imagery.

Traverses

Table 3 summarizes the results of the 43 surface traverses carried out in the course of the project. The traverse vehicle had a mast mounted on the right front bumper and extending 2m above the ground (see Figure 8). All traverses except 18 were carried out with a YSI thermistor probe, mounted at 2 m on the mast. The 2 m temperature was normally observed on a YSI telethermometer and recorded manually together with location, time, sky conditions, wind directions as indicated by vapor plumes, and any other pertinent data. Attempts were made to record temperature with a battery-operated millivolt recorder, but the combined problems of calibration, vibration, and of keeping a record of location on the moving strip chart made the manual method easier and more accurate. Temperatures were normally read to .1°C from a scale with 1°C divisions; reading accuracy varied from about ±.2°C on smooth pavement to +.5°C or more on very rough roads.

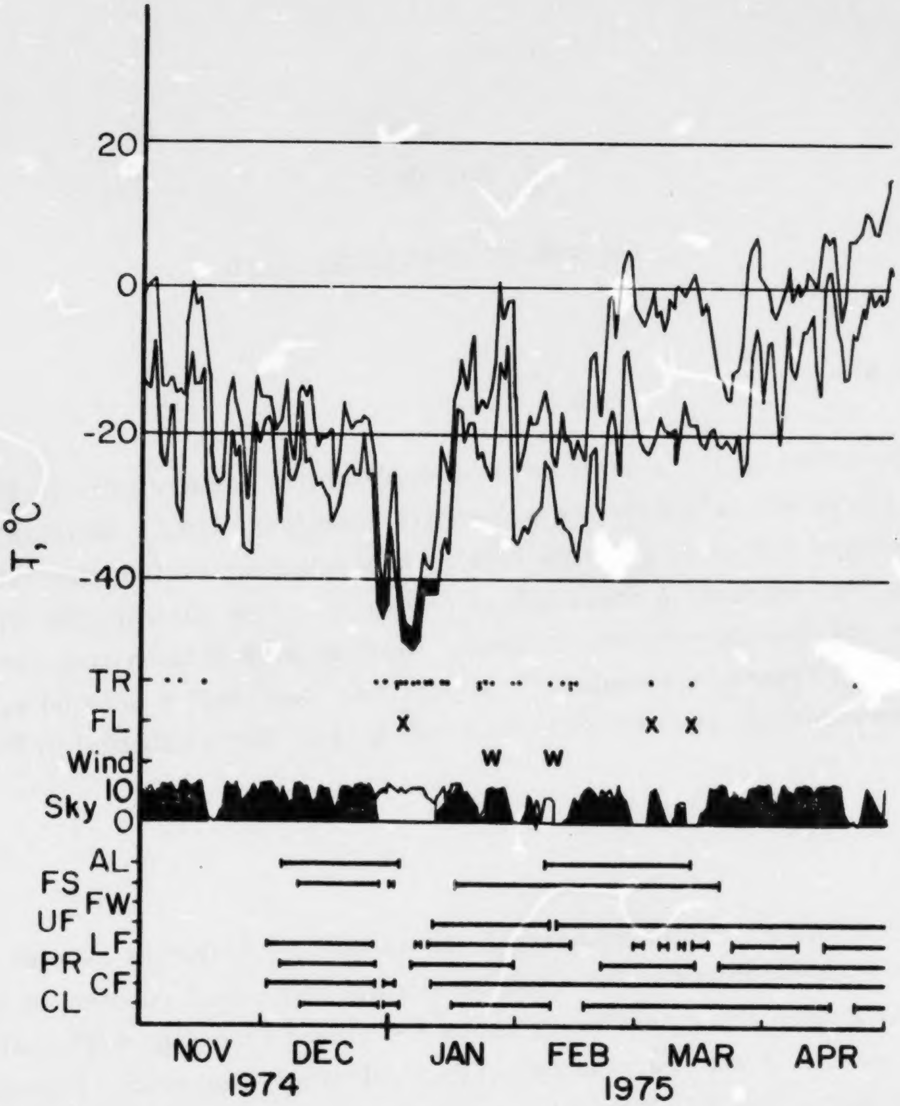

Figure 5. Summary of weather and data collection activity, Nov. 1974 through April 1975. From top to bottom: Double line graph gives daily maximum and minimum temperatures. Dots in line with TR show traverse times; x's in line with FL indicate aircraft observations. Under wind, W's indicate multiple-observer wind observations; single lines indicate one wind recorder in operation, double lines indicate two or more recording anemometer records available. Sky conditions: filled curve gives sky coverage by cloud in tenths; open curve gives sky obscuration by ice fog. Horizontal lines: periods of thermograph records; code letters are the same as in Figure 2.

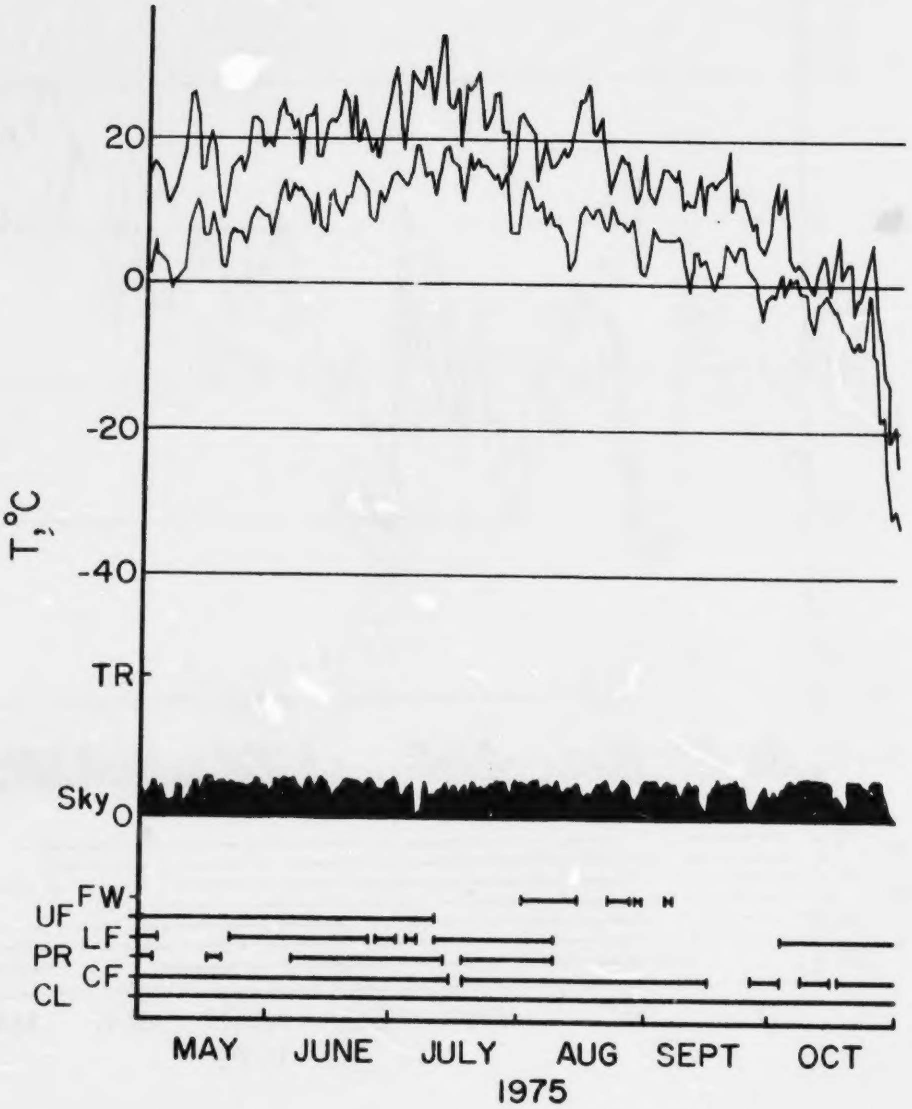

Figure 6. Same as 5 but for May, 1975 through October, 1975.

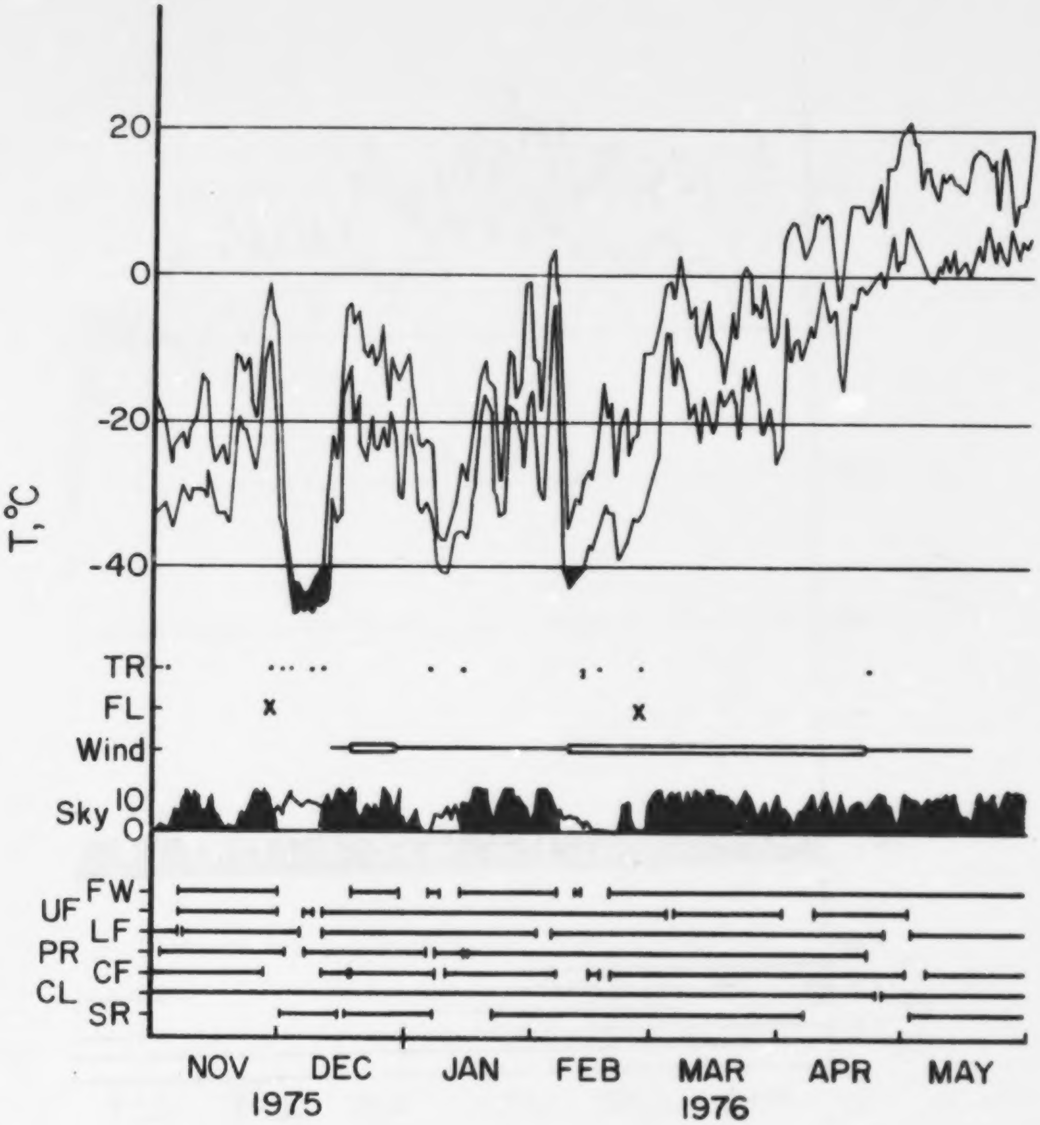

Figure 7. Same as 5 but for November, 1975 through May, 1976.

TABLE 3. SUMMARY OF TRAVERSE DATA. ALL TEMPERATURES IN C; WIND (AT THE AIRPORT) IN, KNOTS AIRPORT SKY COVER IN TENTHS CLOUD. "MEAN BACKGROUND" IS THE AVERAGE OF THE COLDEST TEMPERATURES ENCOUNTERED ON EACH OF SEVERAL ROADS. "TEMPERATURE TREND" IS THE TEMPERATURE CHANGE OBSERVED AT THE AIRPORT DURING THE TRAVERSE. TRAVERSES MARKED "INVERSION" HAD THERMISTORS MOUNTED AT .5 m AS WELL AS 2 m.

Traverse	Date	AST time	Temp. Trend	Wind	Sky	Lowest	Mean Background	City Core	ΔT Max.	ΔT Mean	Other Observation
I	12/7/63	23-01	+1.5	NE 2-C	5/10 Ci	-23.0	-21	-19.0	4	2	
II	1/4/64	15-16	+ .5	C	10/10	-16.0	-15	-12	4	3	
III	1/6/64	20-21^{30}	-1	C	3/10	-31.4	-31	-27.5	3.9	3.5	
IV	12/9/64	21-23	0	C	IF	-23	-23	-19	4	4	
V	12/13/64	14^{30}-18^{30}	0	C	IF	-47.6	-46	-38.2	9.4	7.8	
VI	12/14/64	13-15^{30}	+1	C	IF	-44.3	-43	-38.2	6.1	4.8	
VII	12/8/66	12-14	0	C	IF	-45	-42.5	-37.5	7.5	5.0	
VIII	1/5/73	22-24	-1	NW 3	IF	-46.5	-45	-40	6.5	5	
IX	1/25/73	9^{30}-11^{30}	0	C	IF	-43.5	-40	-38.	7	5.5	
X	2/1/73	11-13	+4	NE C-5	3/10 Ci	-33	-31	-26.	7	5	
1	11/7/74	21-22	0	SW 3	8/10	-16.9	-16	-14	2.9	2	
2	11/10/74	17-21	+5	N 4	10/10	-23.0	-23	-21	2	2	
3	11/16/74	21-22	0	ENE7-C	0/10	-28.0	-27.5	-21	7	6.5	
4	12/28/74	14-16	±1	C	IF	-45	-44	-37	8	7	
5	12/30/74	12-16	±1	WSW 3-6	7/10+IF	-38.6	-37	-34	4.6	3	
6	1/2/75	16-17	0	C	IF	-46	-46	-40*	6	6	
7	1/2/75	20-22	-1	NNE 3	IF	-47	-47	-41	6	6	

(Continued)

TABLE 3. Continued

Traverse	Date	AST time	Temp. Trend	Wind	Sky	Lowest	Mean Background	City Core	ΔT Max.	ΔT Mean	Other Observation
†8	1/3/75	13-14	-1	C	IF	-49	-48	-42.5	6.5	5.5	light airplane
9	1/4/75	15-19	0	C	IF	-49.8	-48.5	-41.5	8.3	7	
10	1/6/75	11-15	±1.5	C	extreme IF	-49.5	-49	-45.8	3.7	3.2	
11	1/7/75	13-15	0	C	IF	-42	-42	-40.5	1.5	1.5	
12*	1/9/75	11-12	0	C	IF	Lapse rate equipment test					2 m inversion
†13	1/10/75	16-19	-1	NE 3	IF	-44.5	-43	-34.8	9.7	8.2	inversion
14	1/13/75	15-16	-1	N 4	10/10	-28.5	-28.2	-25	3.5	3.2	
15	1/14/75	11-13	+1	N 7	4/10	-44	-40	-31.5	12.5	8.5	inversion
16A	1/22/75	13-15	+1	N, C-3	5/10 Ci	-20	-19.5	-12	8	7.5	inversion
16B	1/22/75	16^{30}-17^{30}	-.5	SW 3	2/10 Ci	-24	-22.5	-13.8	10.2	8.7	inversion
16C	1/23/75	8^{20}-9^{20}	0	C	2/10 Ci	-28	-27	-18	10.0	9.0	inversion
†17	1/25/75	14^{30}-16	1.5	C	10/10 Ac	-16.2	-16.1	-12.6	3.5	3.4	2 cars + wind observ.
18*	1/30/75	14-15	0	C→N5	0/10	-27	-26.5	-21	6.0	5.5	1 m temperature
19	1/31/75	15^{30}-16^{30}	-1.5	N 3	0/10	-30	-30	-24	6.0	6.0	inversion
20	2/8/75	9^{25}-11	±1	WSW 5	variable	-28.3	-26	-23.3	5.0	2.7	inversion, IR, winds
21	2/11/75	14-15	-1.5	NNE 4	0/10	-29	-27	-22.5	6.5	4.5	shielding test-no dif.
22A	2/13/75	14-15	-1	ENE 8	0/10	-28	-27	-22.9	5.1	4.1	shielding test-no dif.
22B	2/13/75	18-19	-1	SE4→NE8	0/10	-42	-38	-28	14	10	inversion, IR
22C	2/14/75	6^{30}-7^{30}	+.5	N 8	Patches IF	-42.8	-40	-32.5	10.3	7.5	inversion, IR
†23	3/3/75 3/4/75	23^{30}-01^{15}	±1		0/10	-24	-20	-13.8	10.2	6.2	helicopter

(Continued)

TABLE 3. Continued

Traverse	Date	AST time	Temp. Trend	Wind	Sky	Lowest	Mean Background	City Core	ΔT Max.	ΔT Mean	Other Observation
ˆ24	3/13/75 3/14/75	23^{20}-01^{20}	-1		0/10	-20	-18	-9	11	9	helicopter
25	4/22/75	3-4	-.5		0/10	-14	-12	-6.0	8	6	shielded
26	10/29/75	14^{30}-15^{30}	-1.5	S 3	0/10	23	23	-19.5	3.5	3.5	
27	10/29/75	19^{30}-20^{30}	±.5	E 4	0/10	-32	-30	-22	10	8	inversion
28	11/3/75	12-13	±1.5	N C-3	2/10+IF	-28	-27.5	-24	4	3.5	
ˆ29	12/1/75	20-22	0	NE4→NW6	IF	-40	39	-33.8	6.2	5.2	helicopter(inst.cond).
30	12/3/75	14-16	-.5	C→NW3	IF	-44	-43.5	-38.3	5.7	5.2	inversion
31	12/8/75	11-12	±1	N 3-C	heavy IF	-46	-46	-44	2	2	
32	12/11/75	14-15^{30}	0	C-NE 3	patchy IF	-46	-37 to -46	-35	11	?	during citywide power failure
33	1/6/76	19-20	0	W-SC	0/10	-35	-26E, -35W	-23	12?	?	
34	1/14/76	11-12	±1.5	C	0/10	-35	-33	-26.5	8.5	6.5	
35	2/12/76	9-10	±1.5	C	IF	-40.7	-39	-33.1	7.6	5.9	
36	2/12/76	pm	±1.5	C	0/10	-30	-29	-26	4	3	
37	2/17/76	22-23	± .5	C-N3	0/10	-32.8	-31	-26.2	6.6	4.8	
ˆ38	2/26/76	21-22^{30}	-5.5*	N6	0/10	-31	-30	-18.5	12.5	11.5	helicopter & tethered balloon
39	4/22/76	21-22^{30}	-2		2/10	- .5	+ 1	+ 5.1	5.6	4.1	shielded

*Not standard equipment

ˆPlot reproduced in this report

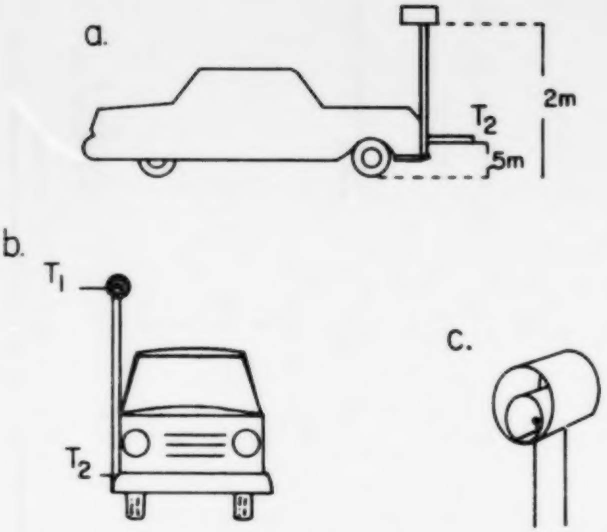

Figure 8. Locations of thermistor sensors on traverse vehicle. (a) side view; (b) front view; (c) detail of thermistor sheild (used for late spring and summer daytime runs.)

With the exception of daylight runs more than two months from the winter solstice, the thermistor was shielded only on an experimental basis. Shielded and unshielded thermistors operated side by side on a sunny February day indicated no difference in equilibrium temperature while the vehicle was moving, but a decided slowing of response in the shielded thermistor after stops. As only temperatures obtained while the traverse vehicle was in motion were being recorded, the shielding was considered a disadvantage.

Ground inversion strength was recorded by adding a second thermistor of the same type .5 m above the ground and approximately 30 to 40 cm in front of the mast (Figure 8). Traverses with this two-thermistor arrangement are marked "inversion" in Table 3. During the initial test run, 12, the second sensor was mounted on the bumper, but with this arrangement the engine and/or headlights of the traverse vehicle appeared to be heating the lower sensor. Inversion strength was recorded on a strip chart as the difference in voltage output from the two telethermometers. As the calibration of this arrangement was dependent on the temperature, an approximate calibration technique was used. Periodically during a run the observer would note the temperature difference between the two telethermometer dials and mark this on the strip chart. Location was also marked frequently. As the electronics were temperature sensitive, calibration also involved repeated re-zeroing of the telethermometers and (usually simultaneously) checking the zero on the portable recorder. The thermistor sensors were occasionally run side by side to confirm that they were in agreement with each other.

The noise level in these near-ground inversion strength records was quite high due to the fact that mechanical vibration of the glavanometer needles in the telethermometers added a spurious electrical signal to the recorder input -- and mechanical vibration on some of the roads used for traverses was considerable. Consequently, the .5 m to 2 m temperature difference normally had to be of the order of .5°C (a lapse rate or inversion of 33 times the adiabatic lapse rate) in order to be detected. Temperature differences considerably in excess of this amount were in fact detected frequently, as will be discussed below.

Attempts were made to observe the incoming infrared flux, using a pyrgeometer mounted on the roof of the traverse vehicle. Although the records obtained appeared to be of good quality, especially in comparison with those from the thermistors, attempts to relate them to physical reality suggested that the instrument was unreliable under conditions of rapid temperature change. Tests on a building roof confirmed that the pyrgeometer was in fact highly sensitive to heating of the (supposedly) infrared-transparent dome. As our primary interest was in comparing the incoming radiation at ground level in the warm, foggy city with that in the cold outlying areas, the pyrgeometer data were unsuitable. However the pyrgeometer demonstrated a significant increase in incoming radiation whenever the traverse vehicle passed under a visible stack plume from a power plant.

Traverses were heavily used in the winter months, when the diurnal temperature variation was small and the temperature curve was quite flat over at least part of the day. During the summer months the diurnal temperature cycle was far stronger, and periods of near-equilibrium temperature did not occur. No effort was made to run traverses under these conditions, as the differences in cooling and heating rates between city and background would have made interpretation of the results extremely difficult.

Thermographs

A thermograph network was maintained throughout the project, although the number of active instruments varied considerably. Each thermograph used was calibrated at least twice against the thermistor used for the traverses at 5°C to 10°C intervals from 0° C down to -45°C with the aid of a low-temperature freezer chest. (In most cases the full calibration was not possible, as the thermograph clocks and/or inking systems quit between -35°C and -40°C). At temperatures above 0°C, calibration was normally carried out in the open, with the thermistor as near as possible to the thermograph sensor element. Allowance was made for the poor ventilation of the thermistor sensor, and in any case the intercomparison among thermographs should not be affected by this. Those thermographs which required range changes between summer and winter were calibrated before and after each change.

Thermograph sites are shown by the circled pairs of letters on Figure 2 and the period of operation at each site is summarized in Figures 5-7. Gaps in the records are due to: (1) non-operation or illegible records at temperatures below -30°C; (2) inability to reach some sites under some weather conditions; (3) removal of thermographs for calibration and servicing; (4) thermographs being required for other projects; (5) one or more thermographs simply not working; (6) vandalism or wind damage to the shelters and (7) at Peger Road, interference from a sewer construction project. Whenever possible, we attempted to maintain records from City Lot (CL), Creamers Field (CF) and Peger Road (PR), in that order of priority, at the expense of the other stations if necessary.

Thermograph CL--

The maximum city temperature observed on traverses was generally located at 2nd Avenue and Cushman Street (Fig. 9). Thermograph site CL (City Lot) was located approximately 200 m south and the same distance west of this maximum, at the west end of a parking lot. Figure 10 shows the site as it appeared in spring 1976. Several traverses included a loop through this parking lot, after which the temperature recorded from the car was compared with that of the thermograph. At this location, thermograph and traverse temperatures were generally equal and, under strong heat island conditions, about 2°C lower than the temperature at 2nd and Cushman.

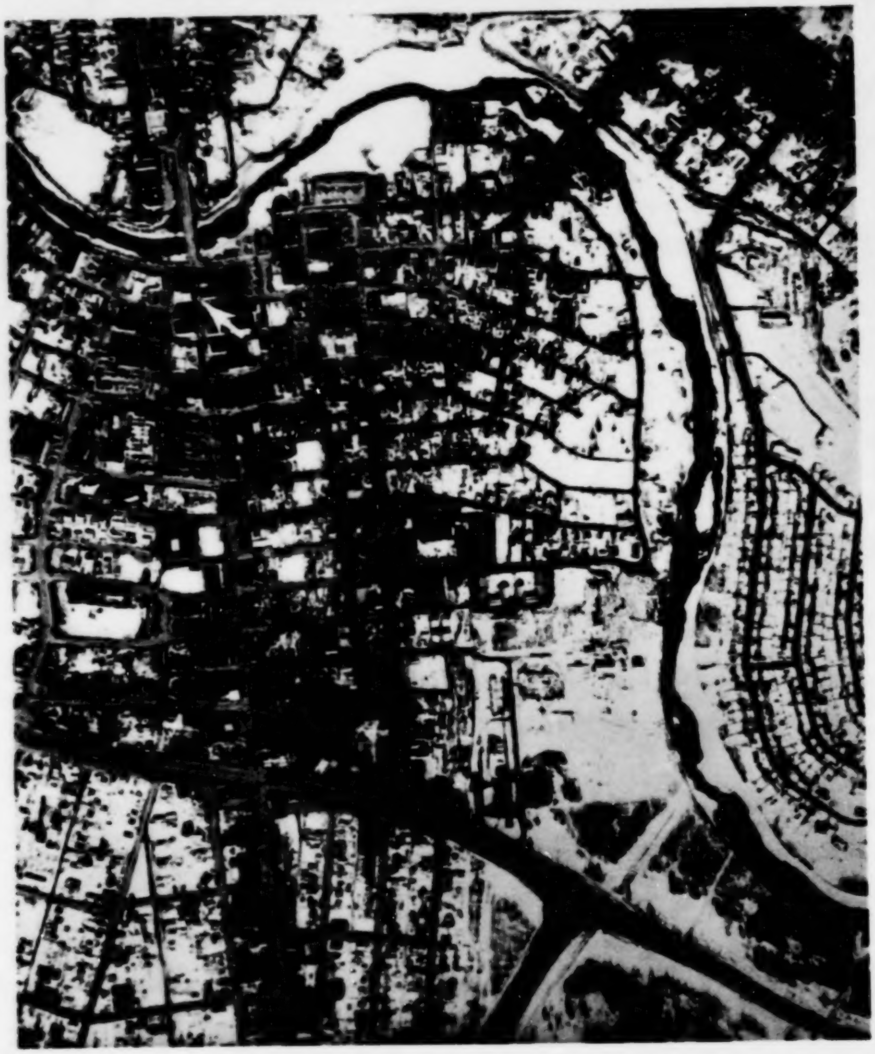

Figure 9. Vertical view of downtown Fairbanks, showing the heat island area (white arrow) and the thermograph site CL.

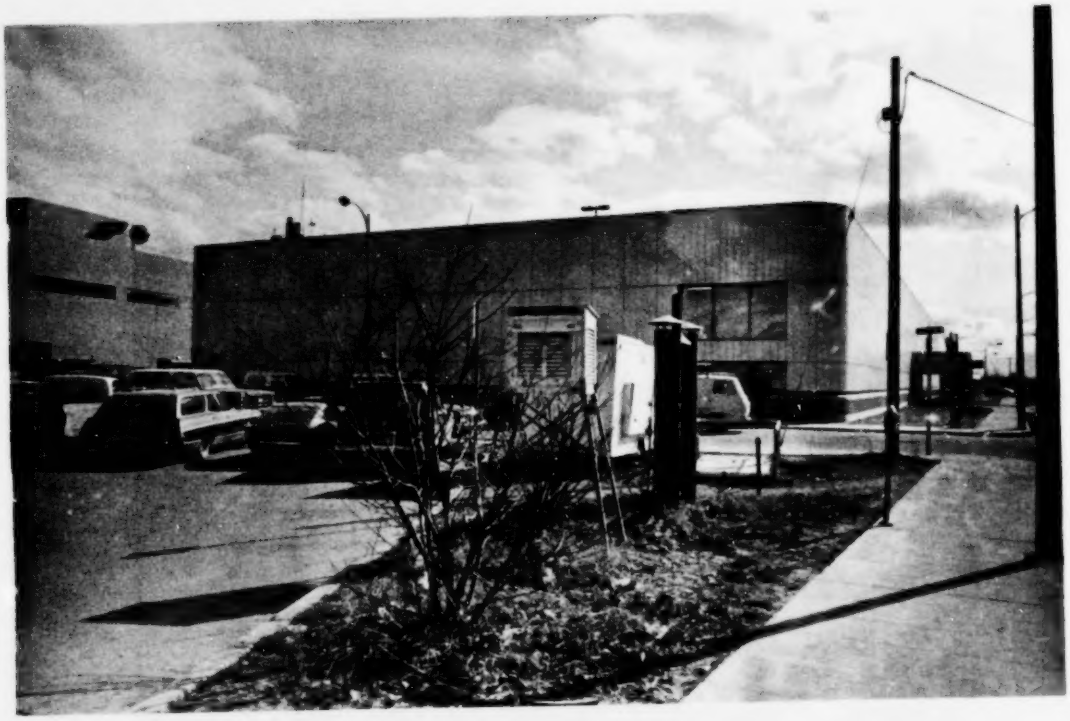

Figure 10. Thermograph site CL, looking south-southeast, in late April 1975.

temperatures were generally equal and, under strong heat island conditions, about 2°C lower than the temperature at 2nd and Cushman.

Thermograph CF--

Site CF (Creamers Field) was located at the site of a former dairy farm. Much of the area is now a wildlife refuge, primarily for northward-migrating waterfowl. Figure 11 shows the site as seen from the air; the peculiar grid pattern southeast of the thermograph site represents a snow clearance effort for the benefit of the wild geese which normally come through in late April. (This photo, along with Figures 9 and 13, was taken near noon on April 21, 1975). As can be seen from Figure 12, the area is quite flat, but not actually swampy except during breakup season; it is regularly sown to grain crops. This thermograph site and the road leading to it provided about half of the minimum temperatures in Table 3. As discussed in Section 4, this site was the closest we could come to a good background site "upwind" of town.

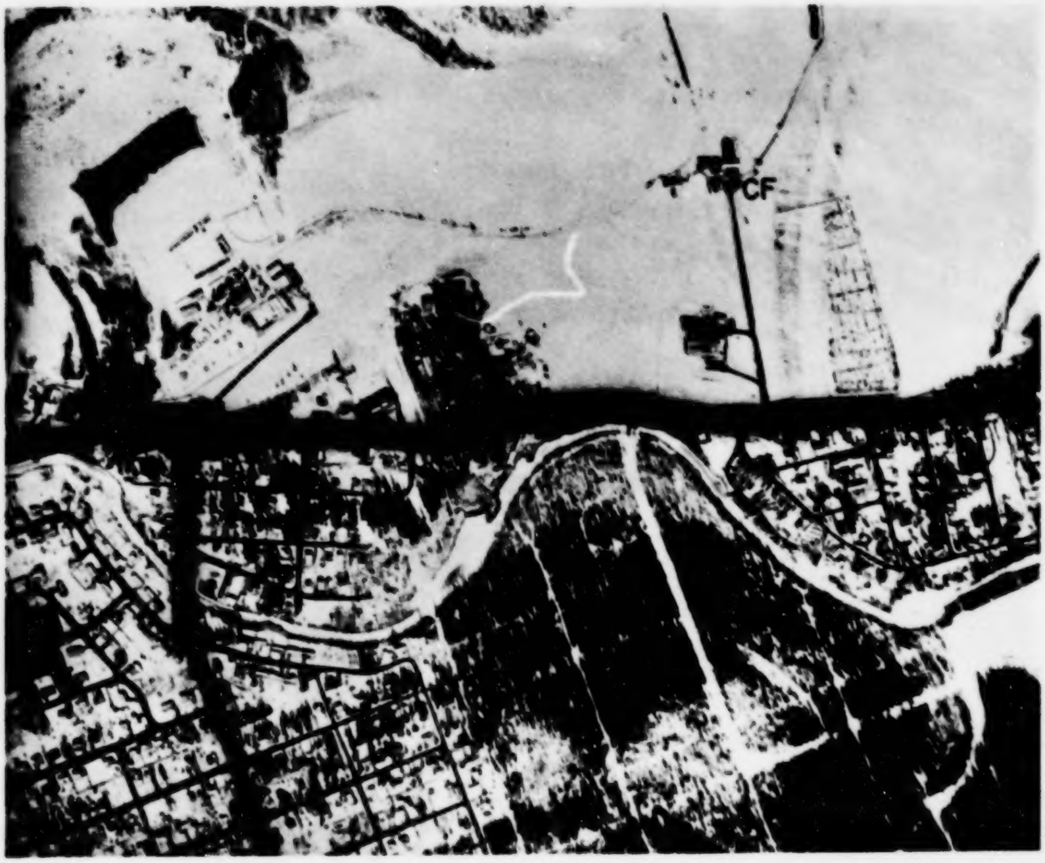

Figure 11. Vertical view of Creamer's Field, College Road at lower edge, showing thermograph site CF, 21 April 1975.

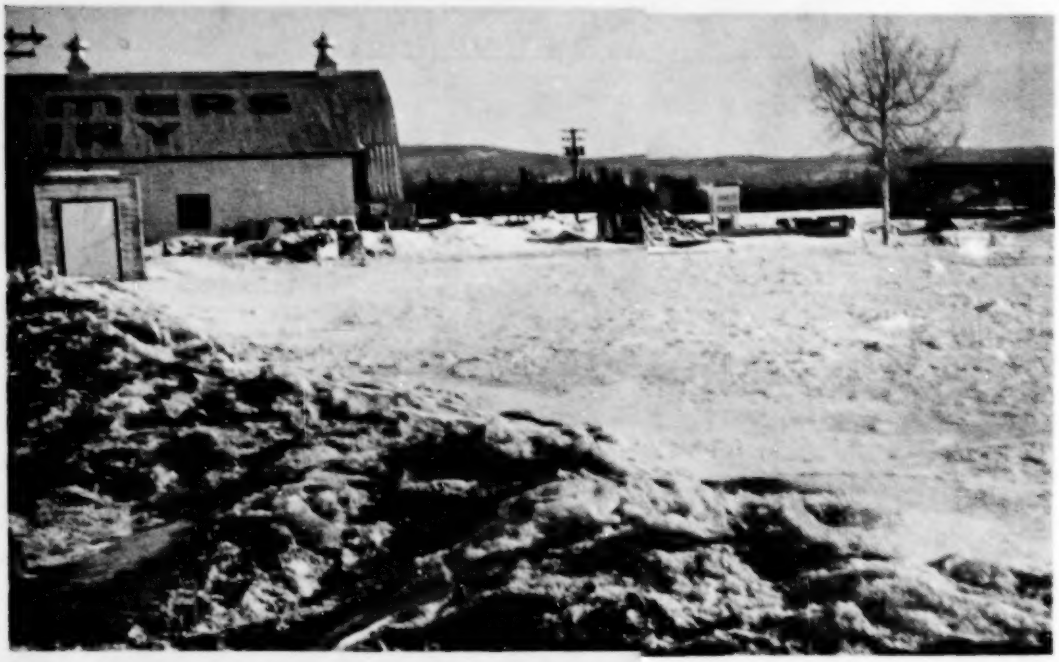

Figure 12. Thermograph site CF, looking NNE, April, 1975.

Thermograph PR--

Site PR (Peger Road) was initially located in natural muskeg vegetation near the north bank of the Tanana River (Figure 13). It was subject both to air drift from Fairbanks (as evidenced by ice fog) and to considerable site disruption. The shelter was initially installed in November, 1974. When the snow melted in April, it became apparent that a low area between the shelter and the road was actually a stagnant slough of the Tanana River. The area which appears grassy in Figure 14 was knee-deep or more in water through most of May and June. At roughly 10:00 p.m. on May 20th, an unknown person put a bullet through the thermograph drum, apparently while using the shelter (which had about 25 bullet holes in it) for target practice. The thermograph was replaced and serviced through July with the aid of hip boots, but of course the second calibration on the damaged instrument was lost. In August, excavation began for the new Fairbanks sewer outfall, and a water-filled ditch between the road and the shelter made access impossible until the pipe was installed and the ditch backfilled. We wanted a wind station in the area, so since the vegetation around the original site was thoroughly disrupted anyway, the site was moved about 100 m north to a flat area where both winds and temperature could be measured. Figure 15, taken from almost the same point as Figure 14, shows the new site as well as the two tall spruces (on the left) which had marked the original site. Site installation was further delayed by a bulldozer knocking down the anemometer support post (which was supposedly well out of the construction area). The thermograph was finally installed in early November, and wind records were started in December. The station was removed because of rising water in late April. Figure 16 was taken while the station was being dismantled.

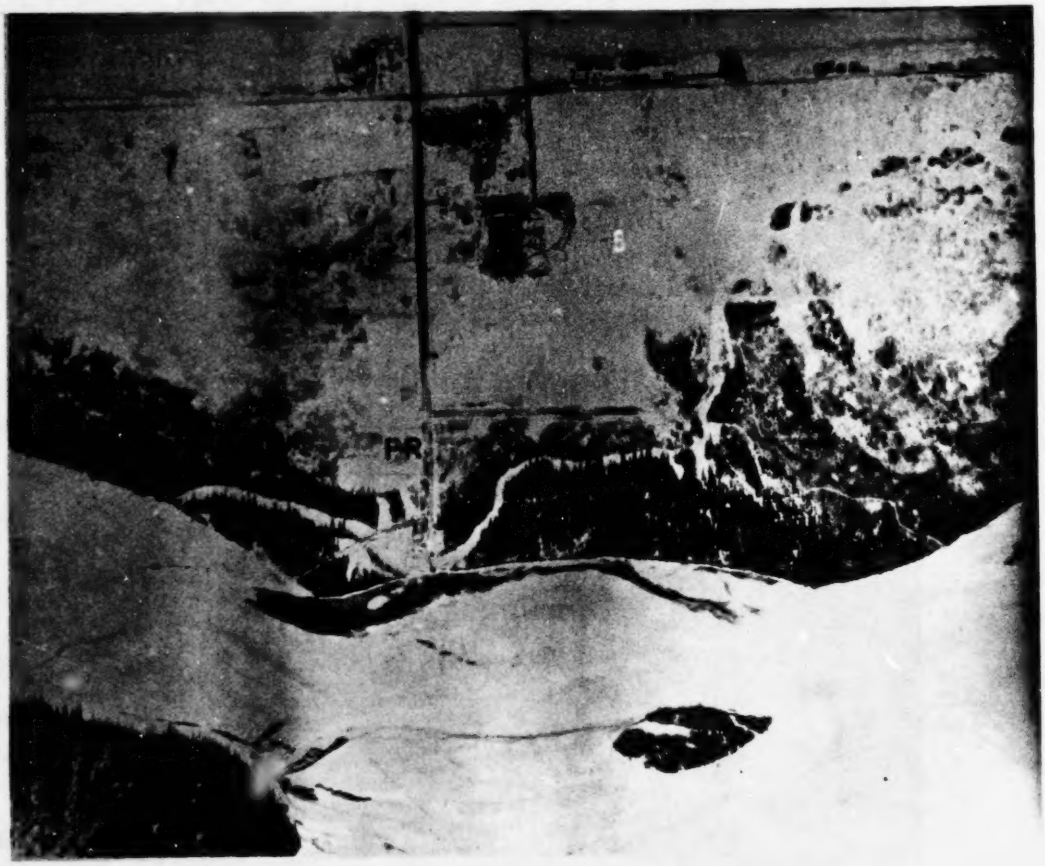

Figure 13. Vertical view of Peger Road area, 21 April 1975, Tanana River at lower part of photo. Peger Road thermograph locations marked by PR

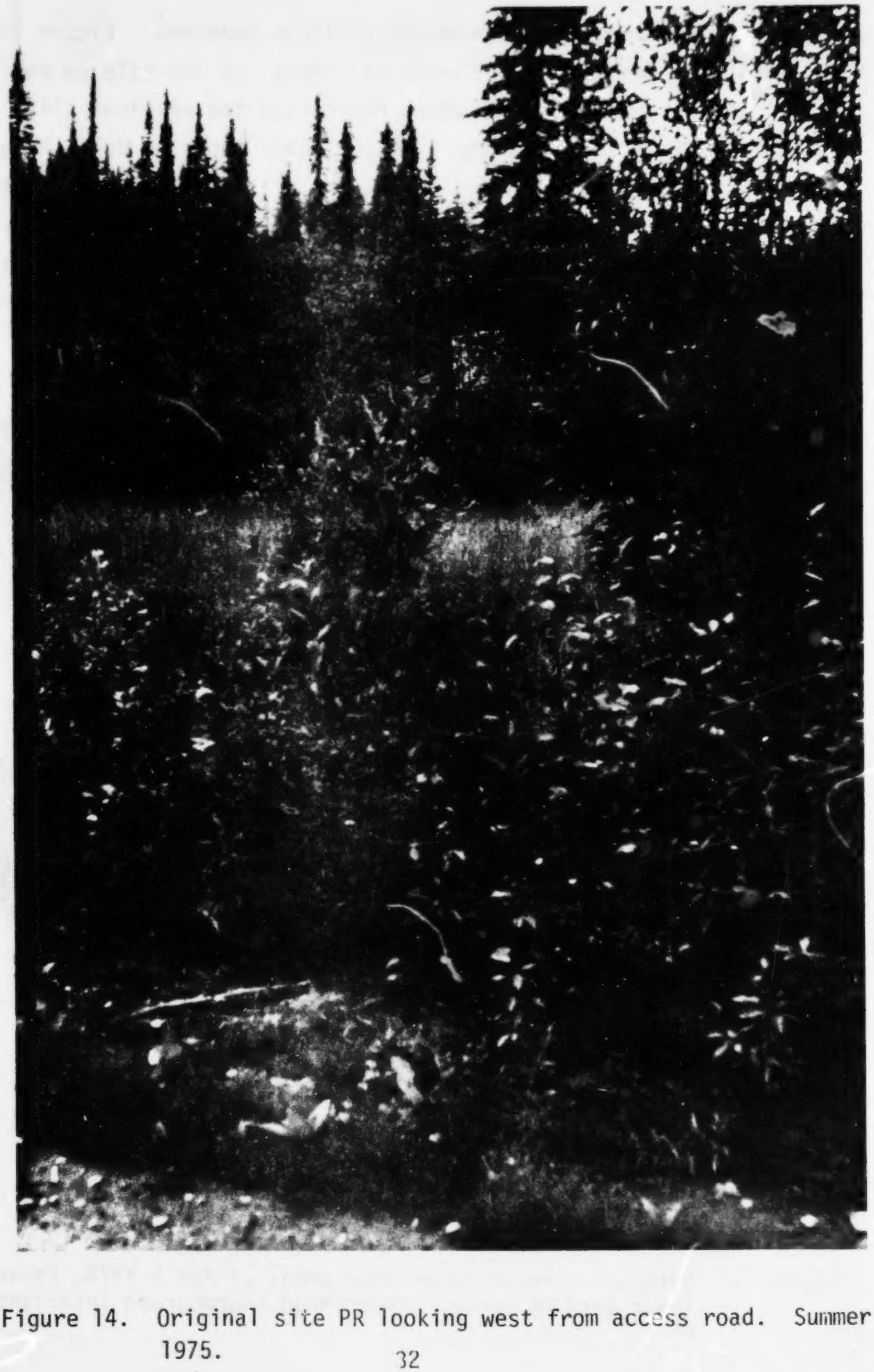

Figure 14. Original site PR looking west from access road. Summer 1975.

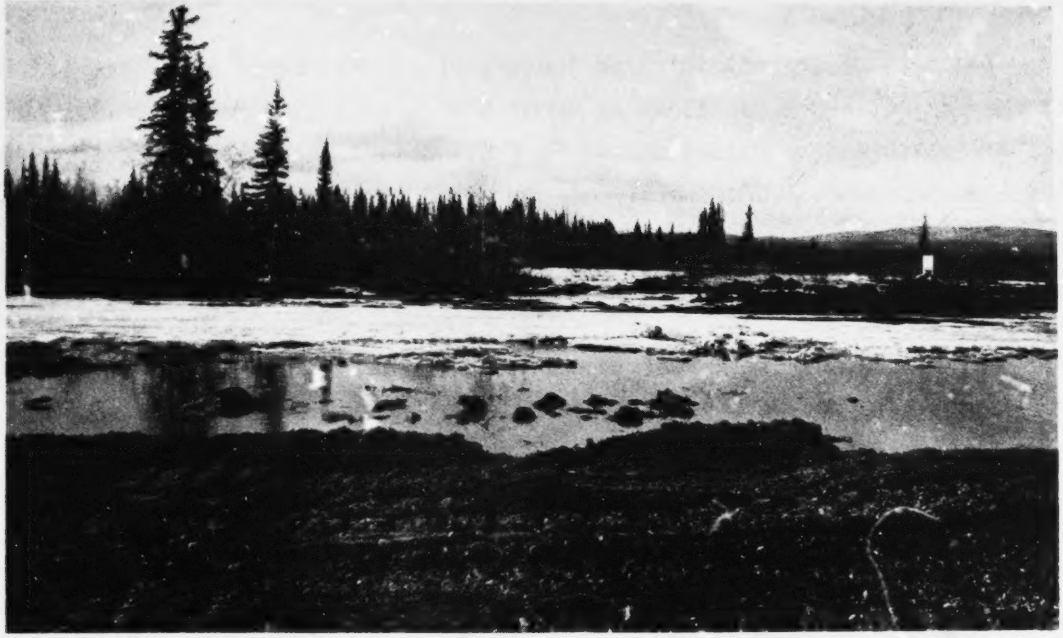

Figure 15. (Above) Both PR sites, photo taken April 1976 from the same location as was Figure 14. The tallest spruces at the left mark the old site; the thermograph shelter is at the new site.

Figure 16. (Below) Both PR sites, looking SE, anemometer at the new site in the foreground.

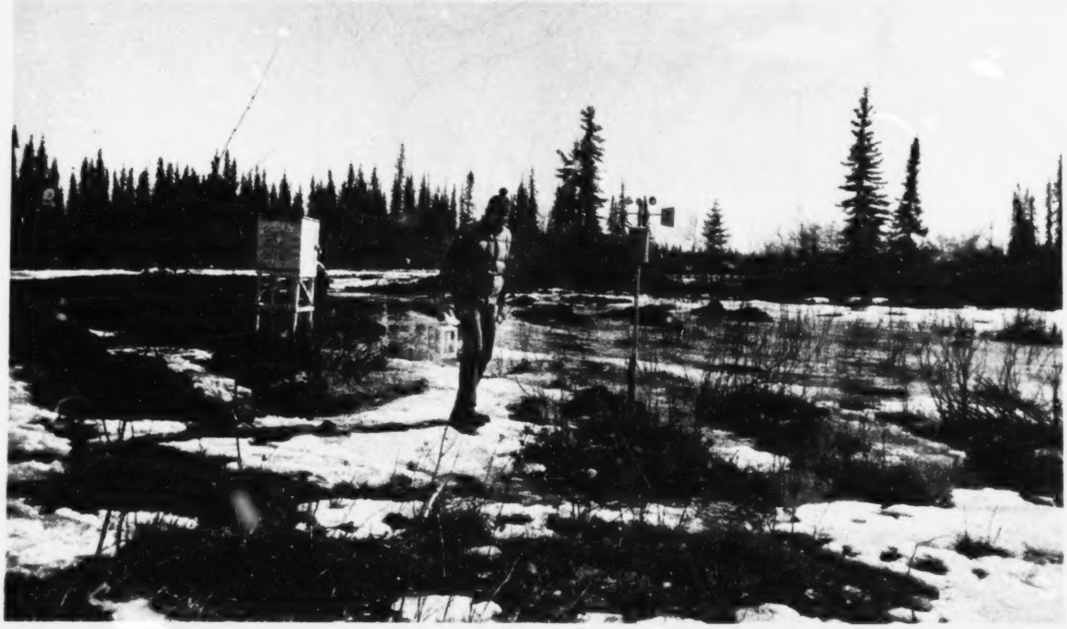

Thermal Infrared Imagery

Two sets of thermal infrared imagery of the Fairbanks area were available to the project. One was flown at about 5 am Alaska time March 4, 1975 by the 172nd MID(AS) operating out of Fort Wainwright, Alaska. Temperatures at 2 m elevation were approximately -14 to -24°C. Surface and helicopter measurements had been carried out between 23:30 and 01:30 the same night. Figure 17 shows the temperatures recorded by the thermograph network that night.

The second set of thermal imagery was flown sometime between July, 1969 and June, 1971, but we have not been able to trace the exact date or the organization responsible. On internal evidence it was flown in summer, probably at night in summer 1970.

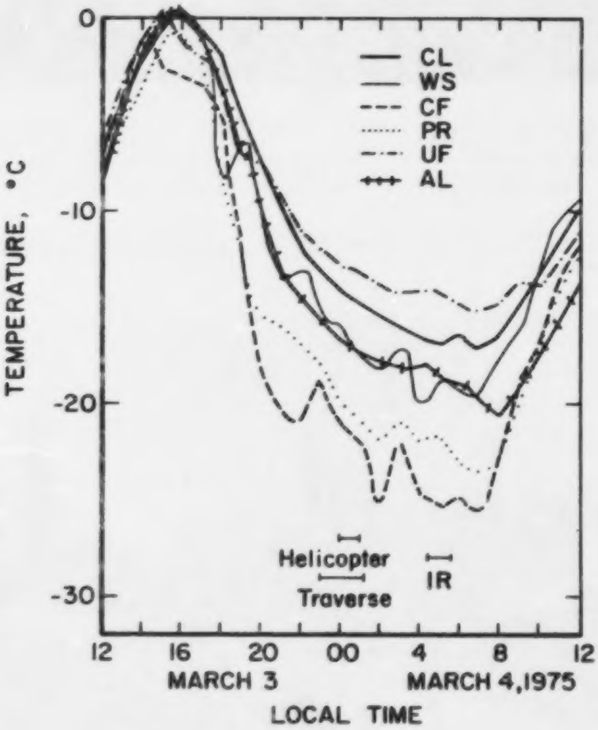

Figure 17. Thermograph temperatures, night of March 3-4, 1975 (23). Stations keyed to Figure 2.

The thermal infrared images provide excellent qualitative information on surface temperature variations, and thus on important heat sources for conductive/convective heating of the air. They do not normally provide information on heating of the air due to direct admixture with the ambient air of hot gases escaping from heated buildings or produced by combustion processes.

RESULTS

The simplest heat island to explain from a theoretical point of view was that observed under near steady-state conditions in mid winter. This type of heat island will be described first, followed by a discussion of how the heat island intensity changes with season and time of day. Finally the pattern of near-ground inversion strength will be considered.

The Winter-Night Heat Island

The winter heat island is of considerable interest both theoretically and because of practical observational aspects. The heat island at this time of year is due primarily to direct anthropogenic heating and effects of air pollution, with possible secondary effects from surface modification (packing and removal of snow). The diurnal thermal cycle is negligible from late November to the end of January and the nighttime temperature shows a distinct plateau (a period of several hours of fairly steady temperatures) from October through March. From a practical point of view, this allowed traverses to be carried out and interpreted without a great deal of correction for cooling or heating during the traverse. Also the plateau in temperature suggests a steady state thermal regime, and thus a steady state heat island.

Most of the traverse data listed in Table 3 were obtained under these plateau temperature conditions, the exceptions being 16A, 17, 19, 22A, 25, 26, 28, 35, 36, 38, and 39. Four of the winter cases, plus two in which some adjustment of temperature was necessary, are described below. These six cases were selected on the basis of completeness of coverage (four were run simultaneously with aerial observations, one had the best ground inversion data in ice fog, and one had simultaneous wind measurements) and variability in the degree of ice fog and cloud coverage.

Heavy Ice Fog; Traverse 8--

Figure 18 shows the pattern of temperatures around Fairbanks from 1300-1400 January 3, 1975. Ice fog was intense, with airport visibilities 1/4 mile during the traverse and dropping to 1/8 mile later in the day; horizontal visibility downtown was considerably less. Figure 19 gives a good impression of the density of the ice fog, which looked even thicker from the ground. The contrast between only slightly impeded vertical visibility and very poor slant or horizontal visibility is typical of ice fog.

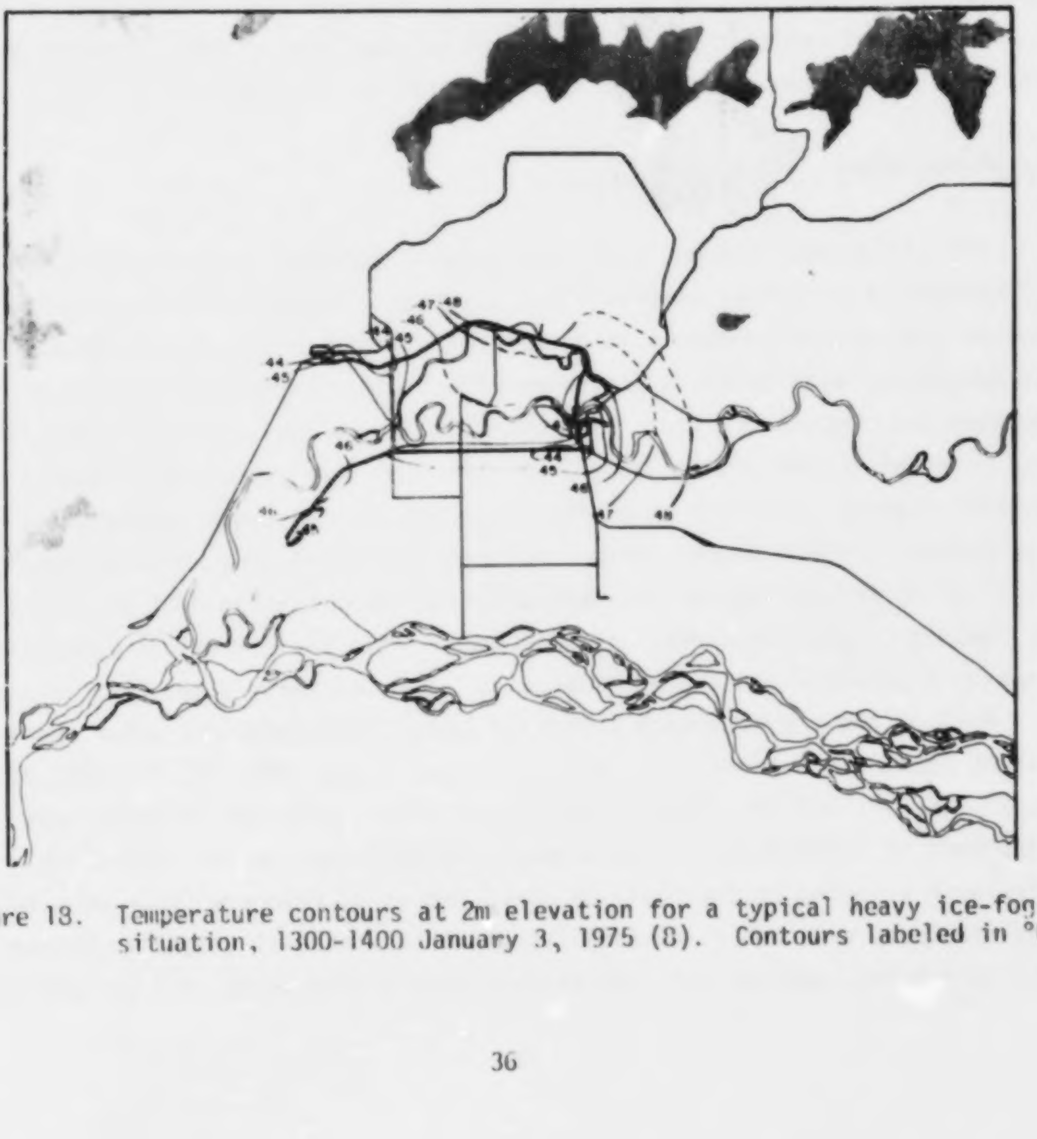

Figure 18. Temperature contours at 2m elevation for a typical heavy ice-fog situation, 1300-1400 January 3, 1975 (8). Contours labeled in °C.

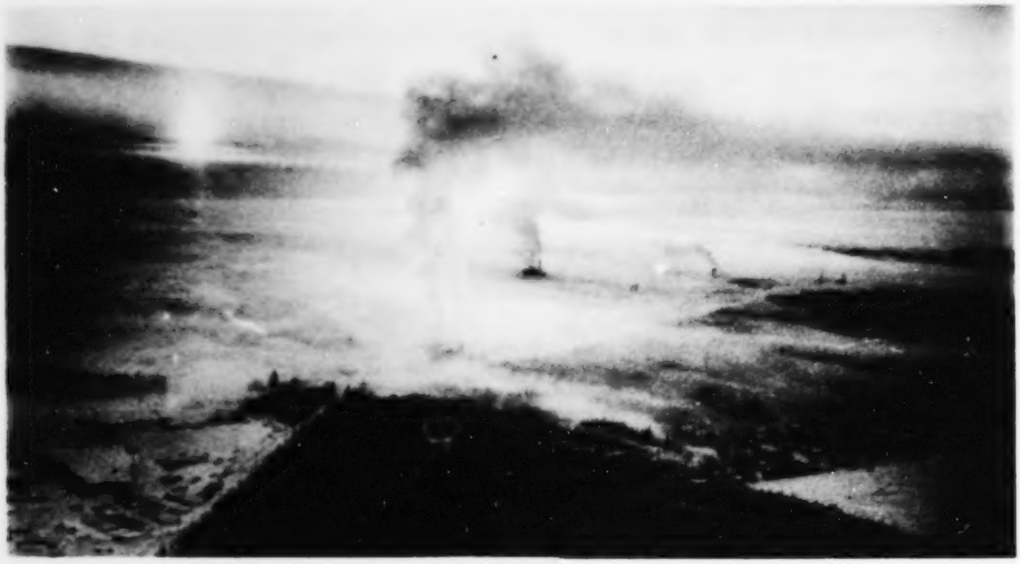

Figure 19. Aerial view of Fairbanks during traverse 8, 3 January 1975.

A light airplane with thermistor was flown during this traverse from an airstrip outside of the foggy area; the temperature measurements aloft are discussed in Section 6. Measurements are predominantly from above 200 m, as horizontal visibility at 200 m was too low for safe flying. Figures 19 and 40 were taken from this plane.

The temperature pattern is fairly typical of those observed with heavy ice fog. Thermal gradients were relatively weak except at the Chena River bridge north of town and along the hill slope by the University, and even in these two places they were weak compared with the clear-sky traverses, 24 and 38. The heat island intensity was about 5.5°C. Most likely this smoothing of horizontal temperature gradients is due to the reduction of vertical temperature gradients, as the "background" areas were generally fogged in during severe ice fog (see Section 9). If the temperature along the slope in front of the Geophysical Institute at a height of 60 m above the flats is taken to be an approximation of the 60 m free-air temperature, and Figure 35 (Section 6) is used as a guide to the relationship between heat island intensity and inversion strength, the ice-fog heat islands are within the expected range except for traverses 4, 6 and 7, in which the city heat islands are larger than would be predicted.

Even though the fog is not optically thick to a vertical beam, calculations using observed crystal size distributions and densities show that radiative transfer in the thermal infrared is probably sufficient to destabilize dense fogs, or even moderately dense fogs when anthropogenic heating is considered (Bowling, 1970). Weakened or missing inversions in the first 100 m of the atmosphere are not always visible on standard Weather Service Rawinsonde records, but occasional cases of normal lapse rates within layers of dense ice fog have been observed for over 20 years (Robinson and Bell, 1956).

Moderate Ice Fog; Traverses 13 and 29--

According to NOAA Weather Service observations, visibility at the airport was about 1 mile during traverse 29 (which was run simultaneously with a helicopter flight,) and 1/2 to 1/4 mile during traverse 13. Isotherms at 2 m elevation are shown in Figures 20 and 21. Horizontal temperature

Figure 20. Temperature contours at 2m elevation for Traverse 13, 1600-1900 January 10, 1975. Moderate ice-fog.

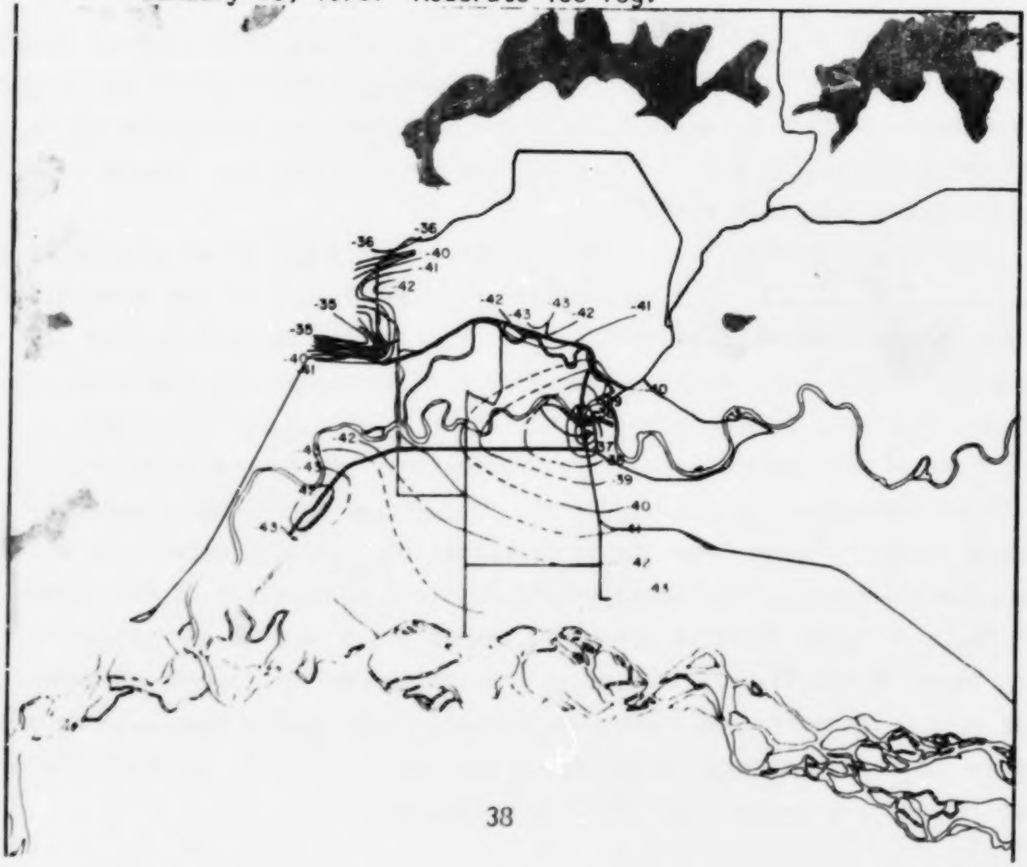

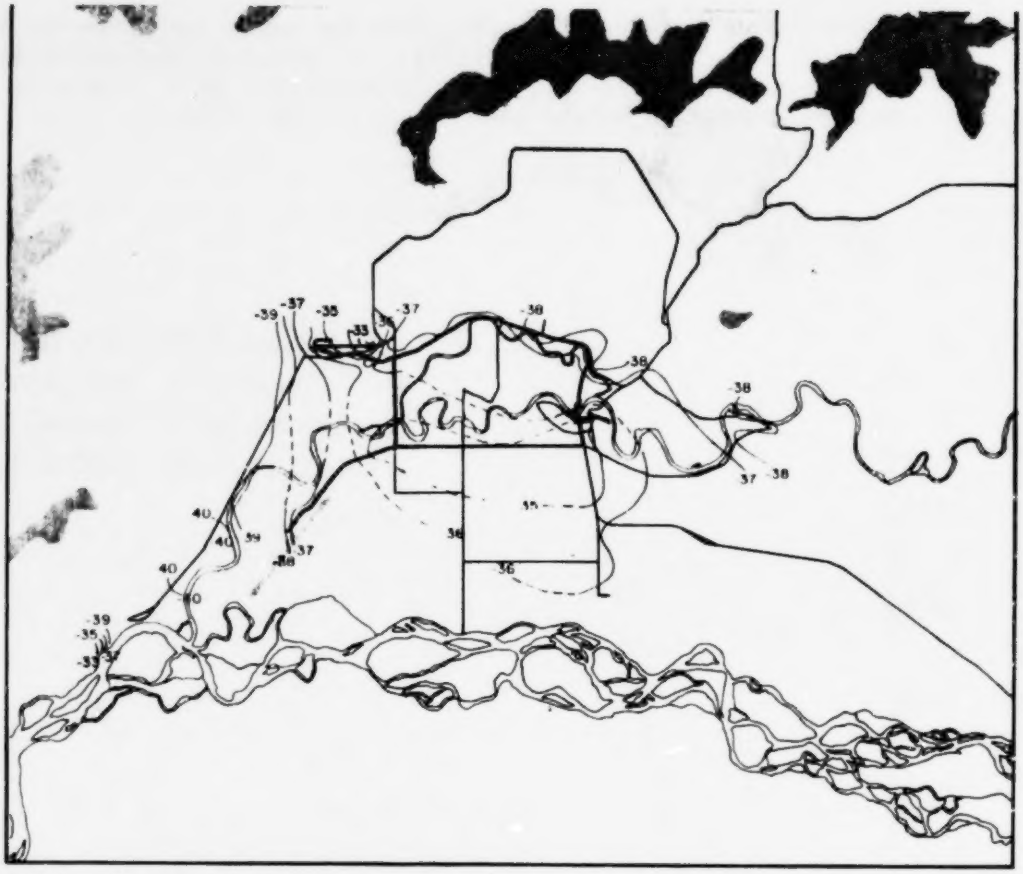

Figure 21. Temperature contours at 2m elevation for Traverse 29, 2000-2200 December 1, 1975. Moderate ice-fog.

gradients were strongest in traverse 13, and those in traverses 8 and 29 were rather similar in appearance. The shape of the heat island was similar in all three cases - a sharp maximum near Second Avenue and Cushman Street with a strong gradient just to the north at the Chena River and a more diffuse maximum to the south along Cushman Street and west along Airport Road.

Although the heat island intensity does not correlate well with ice fog density in these three cases, it does correlate well with inversion strength, as can be seen from Figure 22. The reason for the discrepancy between inversion strength and ice fog density may be found in the way an ice fog episode develops (Bowling et al., 1968). During the early stages (January 2 and 3, 1975 in this case) cold air advection aloft and radiative cooling

Figure 22. Comparison of low-level sounding data for times near Traverse 8, (1/3/76), 11 (1/7/75), 13 (1/10/75), all based on rawinsonde data, and traverse 29 (12/1/75), based on helicopter data. Traverse 11 had the weakest nighttime heat island in the study.

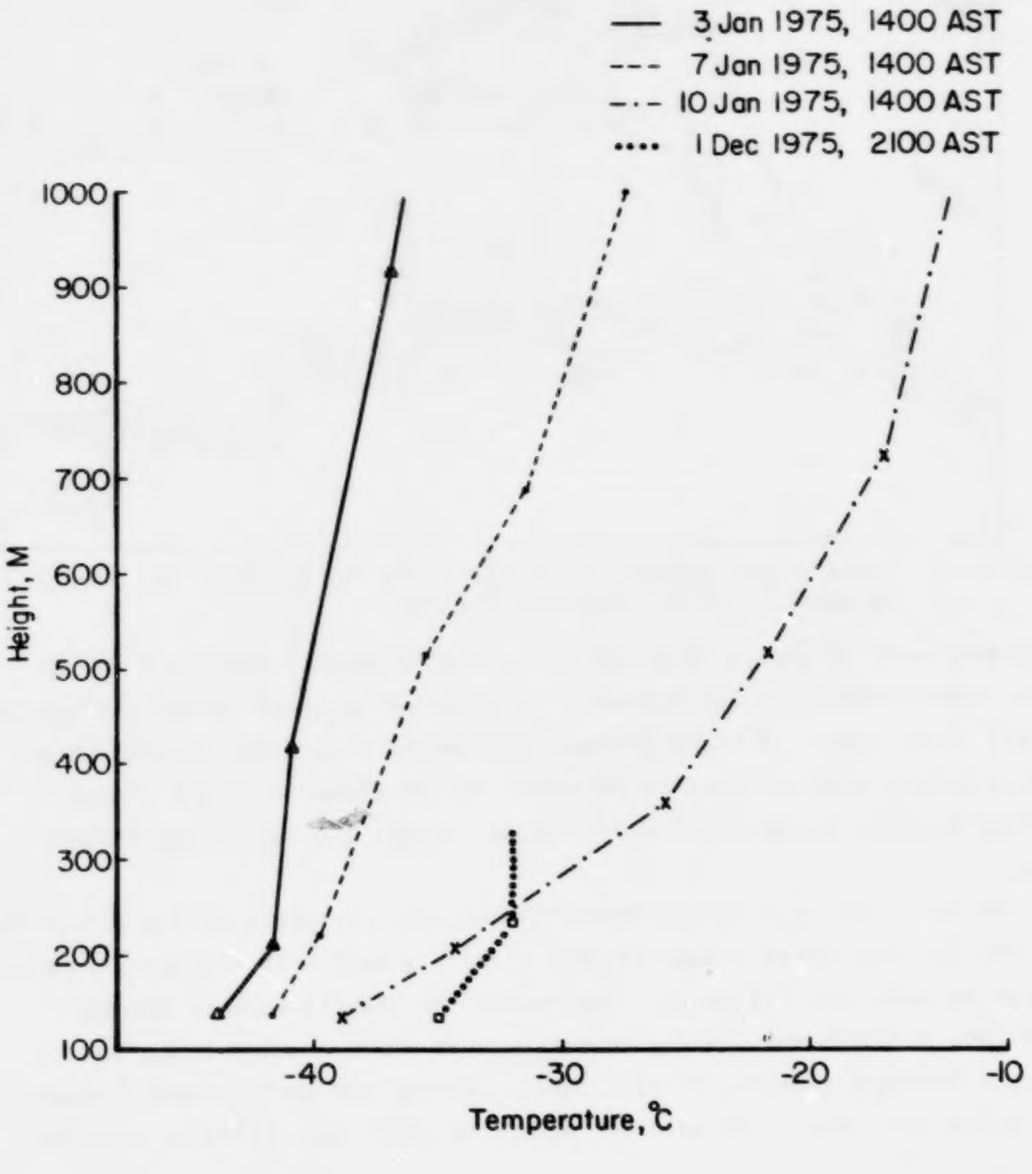

from the ground act together to lower the temperature of the entire air column. Warm air advection then takes over aloft but if sufficient ice fog is present to affect radiative cooling from the ground, the ground inversion may remain constant or weaken even while the overall inversion in the first kilometer strengthens. Three days of ground temperature below -45°C allowed buildup of enough ice fog to produce this situation by January 7. Near the end of an ice fog episode, warm air advection aloft strengthens markedly and extends to lower levels, resulting in the strength of the ground inversion being increased by heating from above. As this heating also erodes away the top of the ice fog, radiative cooling from the ground can also strengthen at this time -- thus the steeper inversion and stronger heat island while the ground level fog remains quite dense near the end of an ice fog episode.

Clear Skies; Traverses 24 and 38--

Winter and early spring nights (and December and early January days) with clear skies had the most intense temperature contrasts observed. Figures 23 and 24 show the results of two winter-night traverses. One feature of the clear-sky heat island which is immediately obvious in Figure 23 is the extreme variability of background temperature. Some features, such as the low temperatures and occasional sharp thermal gradients along College Road (northwest of the city core), are fairly consistant among traverses and probably reflect the gravity-driven micro and/or mesoscale circulation patterns of the area (see Section 7). The higher temperatures southeast and south of the city in Figure 23, however, are examples of "random" warm spots which occasionally appear in clear-sky night-time traverses. It should be noted that these warm spots represent a weakening but not any actual breaking of the thermal inversion - temperatures measured 100 m above the surface with a helicopter during the time covered in Figure 23 ranged from -3°C north of town to -5°C over the Tanana River (see Figure 39). The warm spots may be due to partial vertical mixing by local winds or to a combination of anthropogenic sources and local winds. Wind data were not available.

Returning to the more persistent features, essentially all the clear-sky nighttime traverses had primary temperature maxima at Second Avenue and Cushman Street and in front of the airport terminal building, with the

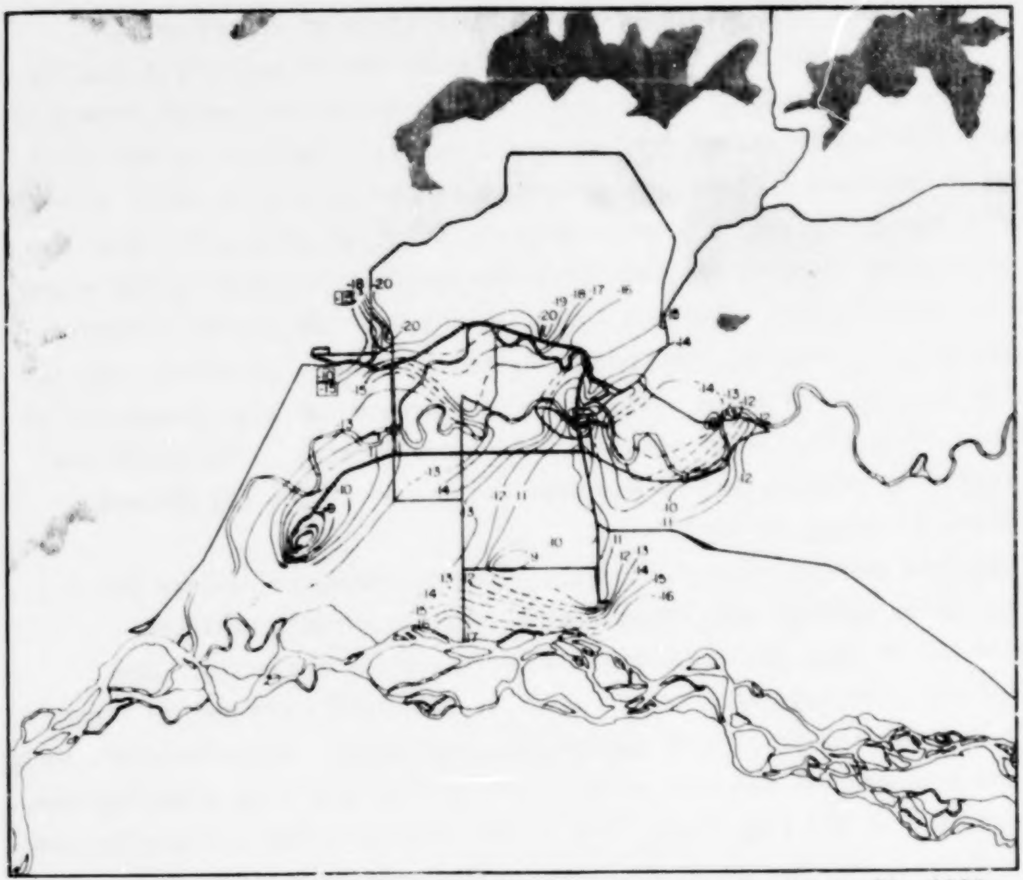

Figure 23. Temperature contours at 2m elevation for Traverse 24, 2320 13-0120 14 March, 1975. Clear skies.

downtown area generally showing a secondary maximum about a kilometer farther south, at the intersection of Cushman Street and Airport Road. (The warm area at the University, WNW of town, is due to the University being on a hill.) The lowest temperatures were normally found in isolated patches along College Road, often bounded by very sharp thermal gradients. These cold areas were interpreted as tongues of cold air flowing across College Road from the Creamer's Field area. Those traverses which extended west-southwest of the University (e.g., 38) frequently encountered an equally cold or even colder area, suggesting that these very low temperatures may have been realistic background temperatures. Temperatures south of town were generally lower than those in town, but not as low as those to the north. Figure 24, which shows the available wind directions as well as the

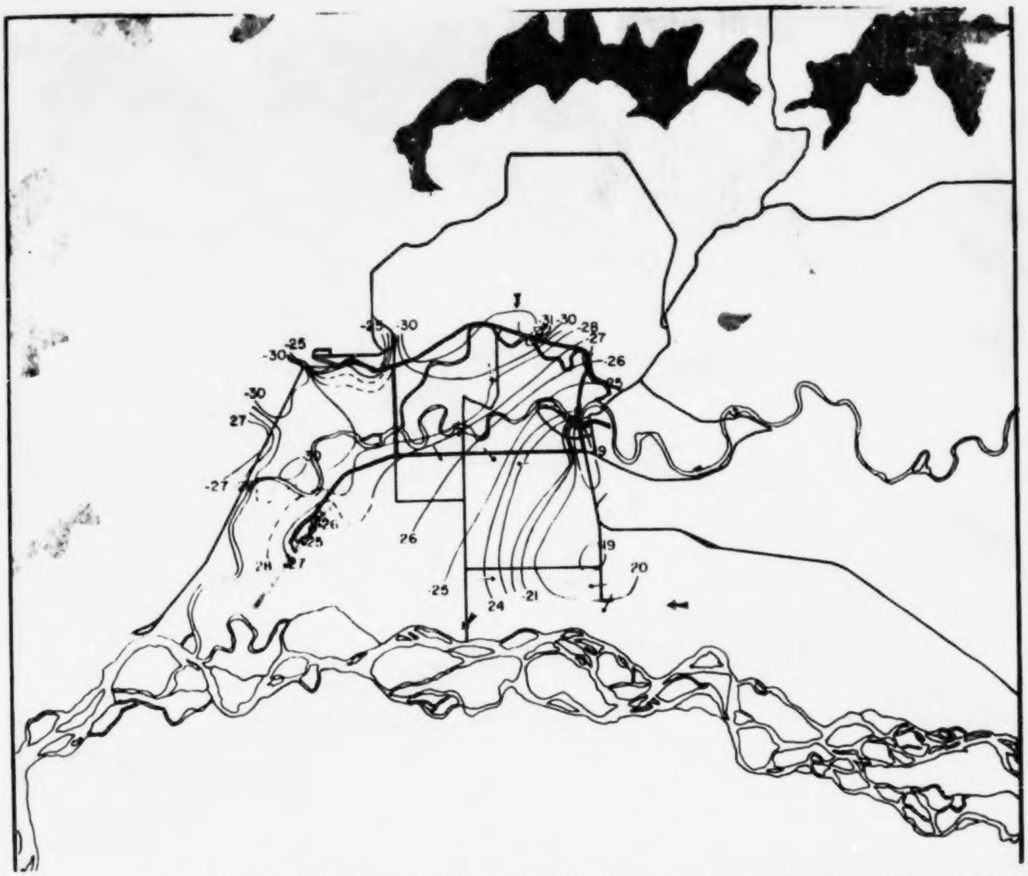

Figure 24. Temperature contours at 2m elevation for Traverse 38, 2100-2230 February 26, 1976. Clear skies. Measured wind directions shown by heavy arrows; wind directions inferred from plume drift shown by light solid arrows (ground level) or light dashed arrows (high stack plumes).

temperature field, suggests that the difference could be due to the fact that air encountered south of town had mostly been heated as it moved through the built-up area and was cooling again.

Cloud Cover; Traverse 17--

During the five traverses described so far, skies as seen from hills in the area were clear. Traverse 17, however, was carried out under a complete overcast, with ceiling at about 12,000 feet (3500 m). Figure 25 shows the resulting temperatures and general wind directions. The 60 m inversion as measured between the Geophysical Institute and the coldest background station was only 3°C, and the heat island was correspondingly weak. Even

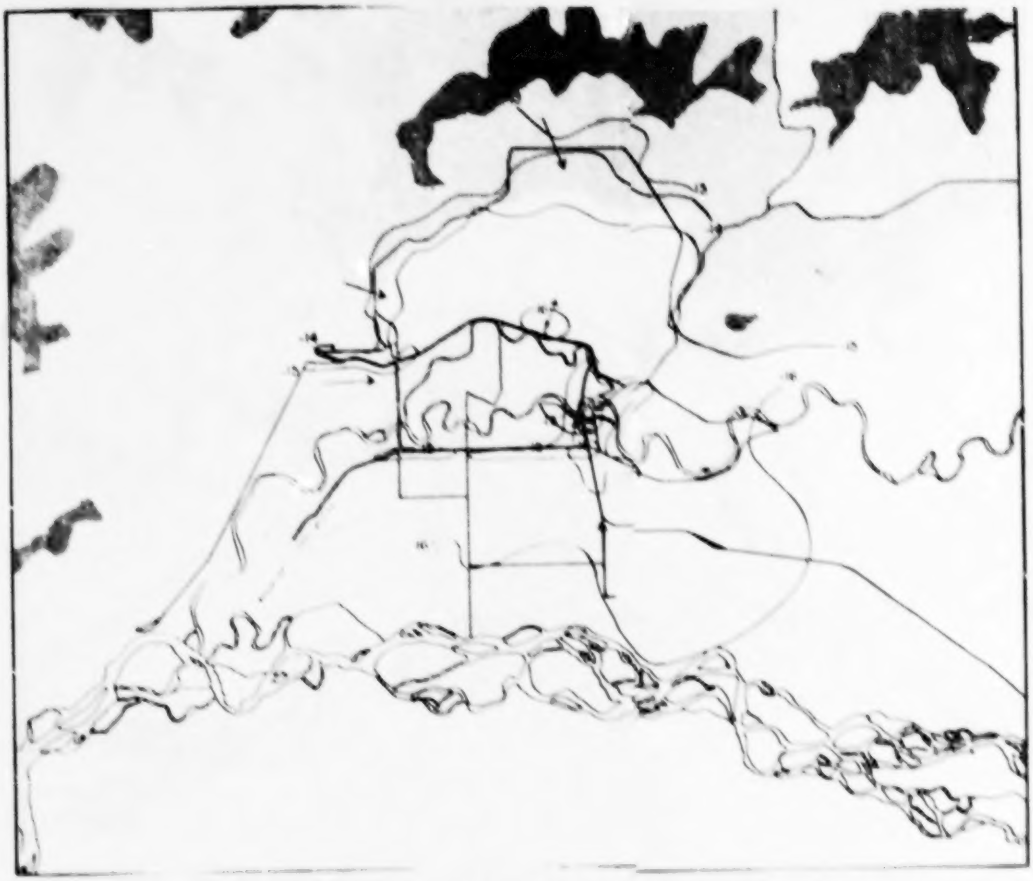

Figure 25. Temperature contours at 2m elevation for Traverse 17, 1430-1600 January 25, 1975. Overcast skies. Arrows show approximate mean wind directions over the half hour period 1440-1510.

the gradient at the Chena river crossing north of town was weak, possibly because the downtown winds in this case were observed to be primarily from the south. (In agreement with this, the lowest temperature recorded was found on south Peger Road rather than in Creamer's Field).

Only a few traverses were carried out under fully overcast conditions, but 17 seems fairly typical. Overall heat island intensities were from 2°C to 3.5°C, and background temperatures north and south of town were similar. As the usual air drift from the north in the area is caused by radiative cooling on the hills to the north, the cloud cover, which would have reduced the radiative cooling substantially, may be directly responsible not only for the weak thermal gradients, but for the relatively uniform background temperatures as well.

Seasonal Variations

Seasonal variations in the intensity of the heat island can be traced both to surface changes (e.g., dry snow, wet snow, bare ground, dormant or growing vegetation) and to major changes in the pattern of insolation. The effect of changes in the day length and solar elevation angle during the period of continuous dry snow cover will be considered first, followed by the influence of breakup (snow melt) and the variation in solar radiation during the period when the ground is snow-free.

The Dry-Snow Season--

Thawing temperatures and even rain are possible in any month of the year in Fairbanks, but are highly unusual from late October through early March. The months of November through February and sometimes March are characterized by a complete cover of dry snow which is an excellent insulator in the outlying areas, but is normally partially removed and the remainder compacted in the city area. Traverses 1-23 and 28-38 were carried out under these conditions. There is some increase in snow depth through each period.

The solar radiation regime shows marked changes through the season of dry snow. Table 4 shows that day length in the November-February period varies from 3 hours 42 minutes to about 10 hours, with maximum solar elevation (approximately the angle above the horizon of the sun at noon) varying from 1°44' to around 16°. Since the intensity of sunlight on a horizontal surface is proportional to the sine of the elevation angle (neglecting the effect of the atmosphere) the intensity of the noon-hour solar radiation varies by almost an order of magnitude. When the doubling of the day length is also taken into account, it is not surprising that the possible daily total solar radiation varies by about two orders of magnitude.

During December and much of January, there is so little incoming solar radiation that the daily thermal cycle is lost in random temperature changes. Temperature changes are due to changes in the air (including cloudiness) several thousand meters up or to changes in the efficiency of wind mixing rather than to any regular daily changes, and if these upper air conditions stay constant for several days a near-steady state may develop at the ground. Under these circumstances, neither the albedo nor the thermal properties of

TABLE 4. DAY LENGTH AND MAXIMUM SOLAR ELEVATION AT FAIRBANKS (64°50'N) AS A FUNCTION OF TIME OF YEAR. ALL TIMES BASED ON 150°W MERIDIAN TIME (ALASKA STANDARD TIME).

Date	Sunrise Time	Sunset Time	Length of Day	Maximum Solar Elevation
Jan. 21	9:11	14:55	5:44	5°05'
Feb. 21	7:30	16:42	9:12	14°20'
March 21	5:49	18:10	12:21	25°10'
April 21	3:55	19:47	15:52	36°45'
May 21	2:09	21:30	19:21	45°12'
June 21	0:59	22:48	21:49	48°37'
July 21	2:13	21:40	19:27	45°48'
Aug. 21	3:56	19:50	15:54	37°33'
Sept. 21	5:31	17:57	12:26	25°10'
Oct. 21	7:02	16:09	9:07	14°45'
Nov. 21	8:47	14:27	5:40	5°25'
Dec. 21	9:59	13:41	3:42	1°44'

the surface are of major importance except during a rapid change from one type of weather to another. Earlier and later in the winter season, however, the diurnal cycle is well developed and the effects of the removal, discoloration and compaction of snow become quite important.

As a very rough first-order approximation, suppose we approximate the daily variation in the radiation balance by a sinusoidal variation in the heat conducted through the surface of the substrate. In this case, it is not too difficult to show that if the energy flux cycle has the same amplitude in all substrates, the amplitude of the thermal cycle will vary as the inverse square root of the product of the conductivity, the density and the specific heat ($1/\sqrt{c\rho k}$). Table 5 lists these properties for various building materials and for snow of various degrees of compaction. It should be kept in mind that the actual temperature variation will depend on albedo as well as thermal properties and variation of the incoming radiation. The values in the table are probably most useful in estimating relative cooling rates immediately after sunset, or after a sudden change in the incoming thermal infrared radiation. It is interesting to note that dry snow packed (and dirtied) by vehicular traffic has thermal properties surprisingly similar to those of concrete or asphalt, while a fresh snow surface is capable of extremely rapid response to changing radiative conditions.

Two sets of traverses were carried out specifically to obtain information on the dependence of the heat island on the time of day. Traverse sets 16A, B and C and 22A, B and C each include one traverse in the warmest part of the day, one a short time after sunset and one just before sunrise. The cooling rates between the early-afternoon and late-afternoon traverses of set 22 are particularly impressive, with the Creamer's Field temperature dropping by 14°C. while the downtown area cooled by only 5°C. The traverse vehicle was always on asphalt or firmly packed snow, although the surroundings of the roads varied greatly, so the difference between the city and background cooling rates is probably greater than that recorded.

The importance of the substrate at this time of year is clearly evident in the thermal infrared imagry of Figures 26 and 27. Both figures are from the March 4 flight. The lightest and warmest areas (other than open water areas such as the Chena River) are heavily travelled roads where the surface is asphalt or asphalt covered with clear ice. Parking lots and lightly travelled roads generally had a veneer of packed snow, giving them a much higher albedo. This leads to a lower daytime temperature which in turn is reflected in lower 5:00 a.m. temperatures. Figure 26 shows some particularly interesting effects, such as the "scribbled" looking area on the left side of the large parking lot below the round building in the upper center. This appearance, which is common in accessible open areas in the vicinity of the city, can only be attributed to snow machine tracks. Albedo is little affected by a single snow machine pass, and these tracks, which are conspicuous in infrared images from 1000 feet elevation, would not be detectable in visible light. Finally, the low-level inversion itself is visible in the

TABLE 5. THERMAL PROPERTIES OF VARIOUS SUBSTRATES FOUND IN THE FAIRBANKS AREA. (SNOW AT -20°C.) $1/\sqrt{c\rho k}$ IS PROPORTIONAL TO THE AMPLITUDE OF THE THERMAL CYCLE WITH A GIVEN ENERGY-BALANCE CYCLE

Substance	Density, ρ $g\ cm^{-3}$	Specific Heat, c $cal\ gm^{-1}\ {}^{\circ}C^{-1}$	Thermal Conductivity, k $cal\ sec^{-1}\ cm^{-1}\ {}^{\circ}C^{-1}$	$1/\sqrt{c\rho k}$
moist sandy clay	1.78	.33	.0022	28
brick masonry	1.7	.20	.0015	44
concrete	2.3	.20	.0022	31
asphalt	2.2	.20	.0036	25
snow, freshly fallen	.1	.468	.00018	345
snow, average undisturbed	.2	.468	.00036	172
snow machine track	.4	.468	.00097	73
snow, packed by auto traffic	.8	.468	.00400	26

mottled or patchy bright areas at either end of the parking lot. The bright spots are tree tops which are in higher and warmer air.

Figure 27 shows several thermal features related to heat release due to human activity directly rather than through surface modification. The most notable of these is the Chena River, which under natural conditions, as is visible in other images upstream from any addition of waste water, would be the coldest area in the image. Instead, waste water from Fort Wainwright, added upstream from this image, maintains a warm channel through the area crossed by traverses. Cooling water dumped by the Municipal Utilities System (MUS) power plant at the point where the entire river becomes a conspicuous bright band keeps the river well above natural temperatures for several kilometers. There are no bridges in the warmest area, but the effect of the river on air temperatures on the downwind bank must be considerable --

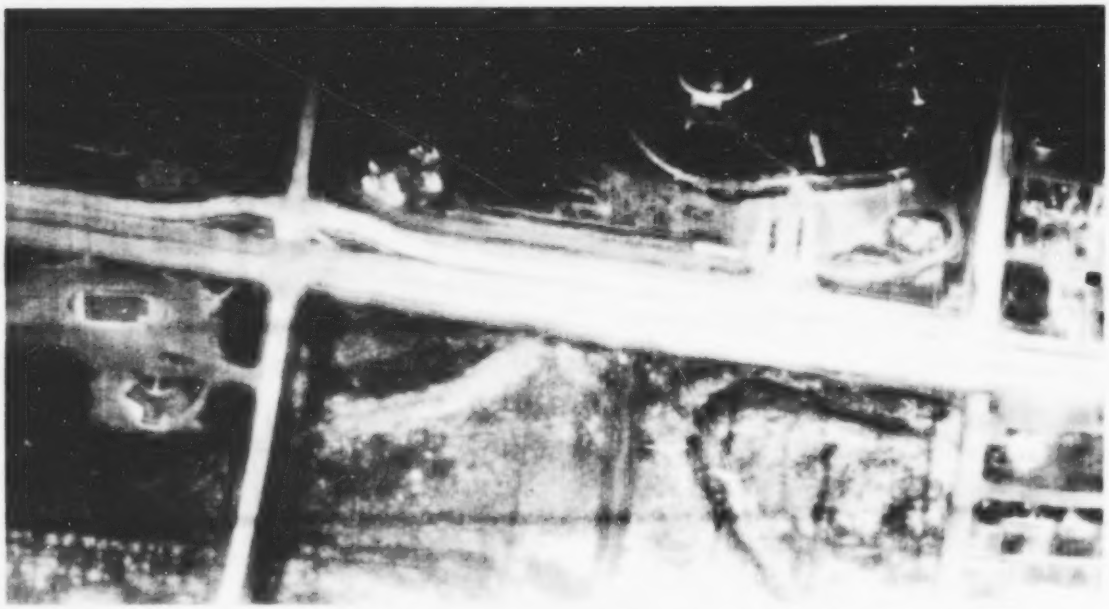

Figure 26. Thermal infrared imagery of the Alaskaland (AL) area, 0500 March 4, 1975. The general gradient of density from light at the bottom to dark at the top is an artifact of processing and should be ignored (Photo courtesy of U.S. Army 172nd MID(AS) and Cold Regions Research and Engineering Laboratory).

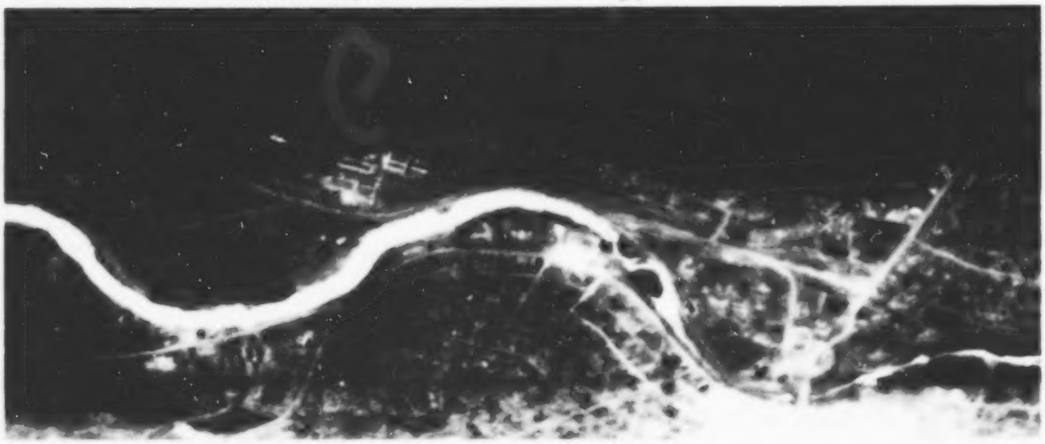

Figure 27. Thermal infrared image of part of downtown Fairbanks, about 5 a.m. on a clear March morning. Note the importance of the river as a heat source, especially downstream of the Municipal Utilities System power plant near the center of the photo. The general gradient of density from light at the bottom to dark at the top is an artifact of processing and should be ignored (photo courtesy of U.S. Army 172nd MID(AS) and Cold Regions Research and Engineering Laboratory).

especially when ambient temperatures are in the -40°C. range and the river is unfrozen. (The effect of the open water on ice fog in the same area has been discussed by Benson (1970) and by Ohtake (1970).) The general warmth of the city core is indicated by the bright haze just south of the Chena River bridge. The bright line extending south and then southeast from the MUS plant to the city core is due to a buried steam line. Thus the infrared images document both the increased thermal lag of disturbed surfaces and the direct addition of heat.

In summary, the daytime heat island during the dry-snow season becomes progressively weaker as the insolation increases. On the basis of thermograph records the mid-day heat island is essentially gone by late March. The nighttime heat island changes very little. The greatest heat islands observed occur in the evening hours, late in the dry-snow season or in the earliest part of the melting season (Table 3).

Snowmelt--

The snowmelt season is defined as the period when water is present in both liquid and solid phases in sufficient quantity that the latent heats of freezing and thawing are a non-negligible part of the energy balance. In Fairbanks this normally includes most of April, at least the latter part of March, and on occasion a few days in early May or late February.

During the earliest stages of snowmelt, air temperatures generally remain below freezing and solar radiation is of primary importance. Melting in undisturbed areas is confined to the immediate vicinity of south-facing, near-vertical dark surfaces -- e.g., the trunks of isolated trees. South-facing berms or cuts left by snow-removal equipment and darkened by vehicle exhaust or sanding operations are also subject to very early melt, as is snow in some locations on buildings. There is little or no runoff at this stage, and water is present in the liquid phase during the warmest part of the day only. The primary effect of this preliminary melting is to decrease the albedo of the snow surface still further, especially in areas where the snow is dirty.

Melting in flat areas occurs first in areas of dark ice and heavily soiled compacted snow -- i.e., on main roads. Reflected sunlight and reradiated thermal energy from buildings may accelerate the melting process in town, with the result that the downtown area has a considerable amount of running water in the daytime hours while snow -- even on roads --away from the city remains dry. The latent heat of freezing in the evening causes an effective increase in the specific heat which retards cooling even more than in the dry-snow season. Maximum daily 2 m air temperatures at this stage of melting may range from slightly below to slightly above freezing. Figure 28 shows an example of daily temperature variations early in this part of the melting season, while daily minimum temperatures at several locations are compared in Figure 29.

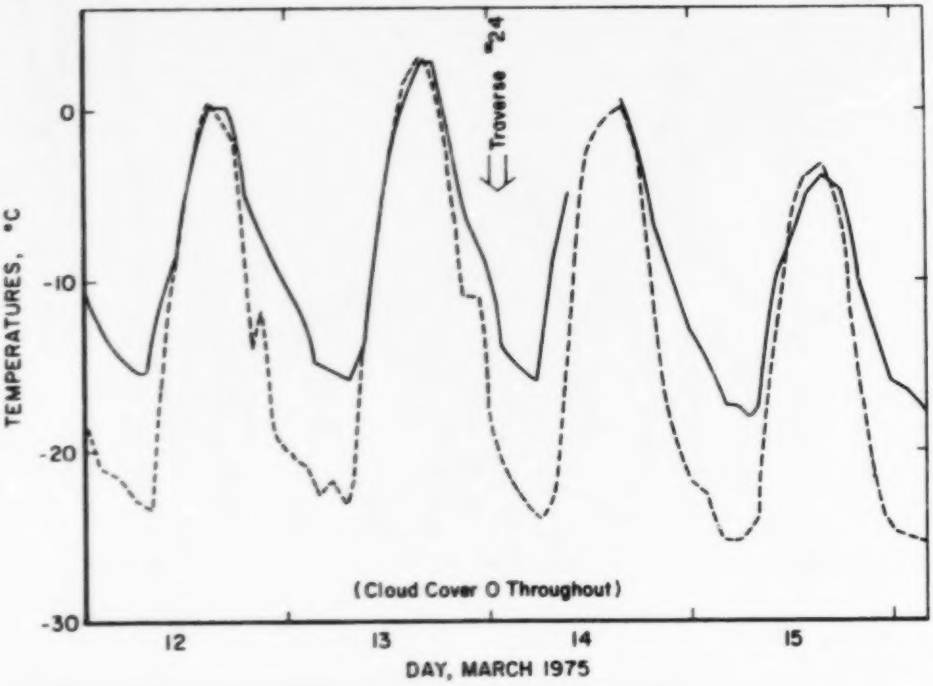

Figure 28. An example of daily temperature variations in town (solid line, thermograph CL) and at Creamer's Field (dashed line

It may seem puzzling that air temperatures can exceed freezing in the outlying areas without the snow surface temperature reaching the melting point. How is solar energy being transferred to the air? The widespread occurrence of trees, especially of low-albedo spruces, is probably the explanation. Solar energy is transferred to the air via trees at heights somewhat higher than the snow surface and an inversion is maintained very close to the ground. Advection of above-freezing air may be involved later in the season, but seems unlikely in itself to account for the pronounced daily peaks in Figure 28.

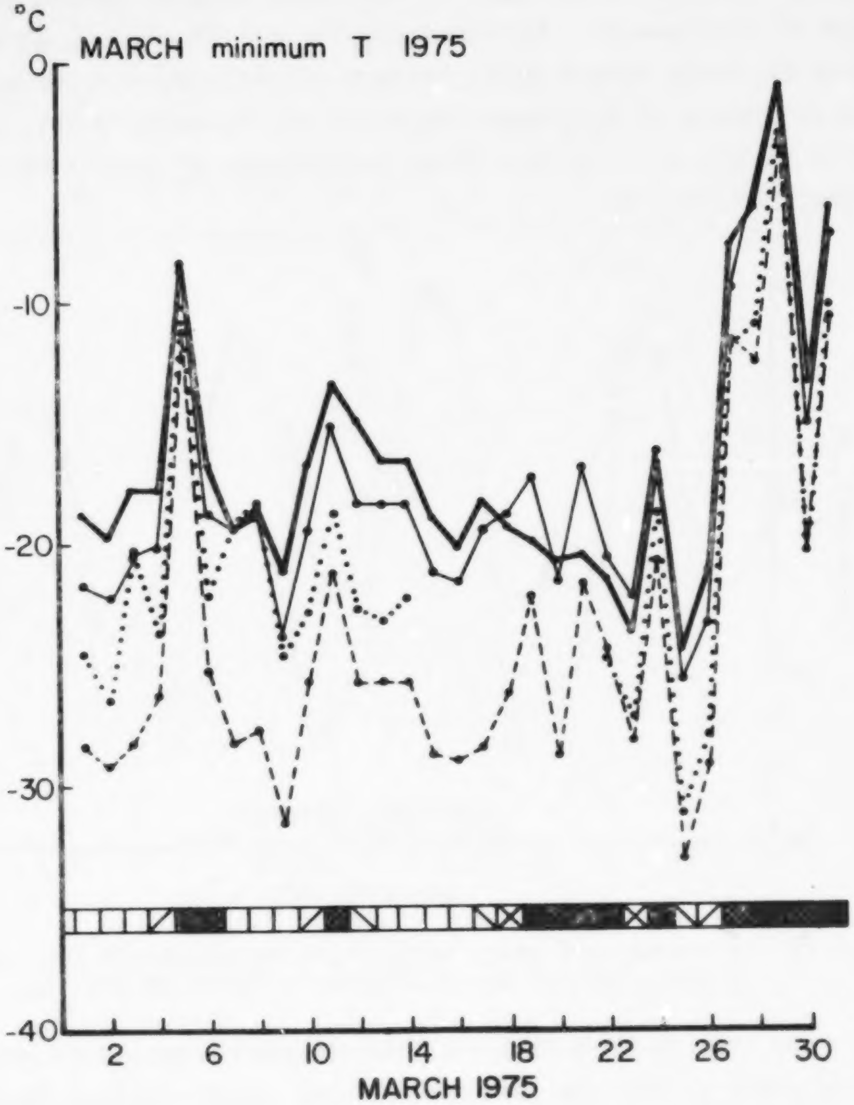

Figure 29. Comparison of daily minimum temperatures at four locations in March. Heavy solid line is site CL (downtown), light solid line is the official weather service temperature recorded at the airport, (WS), dashed line is Creamer's Field (CF) and dotted line is Peger Road (PR), both outlying stations. Squares show sky conditions, with open squares for clear skies, black squares for complete overcast and intermediate shading for intermediate conditions. Slant of shading indicates increasing (up to right) decreasing (down to right) or constant (crossed lines) cloudiness.

The major features of interest in Figure 28 are (1) the similarity of daytime temperatures in city and country; (2) the difference between city and country in evening cooling rates, and (3) the amplitude of the background temperature cycle -- as much as 27°C on the 13th and 14th. Note that traverse 24 (Figure 23) was carried out that night.

Snowmelt is a positive-feedback process even in undisturbed areas. The albedo of snow decreases when it becomes wet. Also, dirt in the snow remains as a concentrate at the snow surface, further lowering the albedo. This feedback process operates most strongly in city areas where the snowpack is dirtiest. Thus the downtown area becomes free of snow long before the outlying areas for a variety of reasons. The heat island and the dirtiness of the snow cause an earlier start to snowmelt, the contained dirt makes the feedback process more effective, and snow removal in the winter leaves less snow to be melted in the spring.

Given the right weather conditions, the city core could become snow-free while the outlying areas still had dry snow. More often, there is at least a short period with wet snow in both areas, followed by a period when the city is snow-free but the outlying areas still have a substantial snow cover. (Figure 30 and most of the vertical-incidence photographs previously presented). Note that at this time the albedo of the city is approximately that of deciduous forest - less than that of snow-covered fields, but greater than that of dense spruce forest. Figure 31 shows how the daily temperatures varied a few days after the photograph in Figure 30 was taken. In comparing this figure with Figure 28, it is apparent that both the extreme daily temperature variations and the contrast between the city and country cooling rates have diminished greatly. Furthermore, the presence of wet snow in the outlying areas but not in town has resulted in the daytime temperatures again being higher in the city. This difference again disappears as the snow cover melts fully.

The Summer Season--

Summer is here defined as the period between the completion of snowmelt and the re-establishment of the snow cover in fall. True darkness at night occurs at the very beginning of this time period (unless snowmelt is concluded very late) and from mid-August onward. The days are normally shorter than the nights by the time the snow cover is established in October. Once

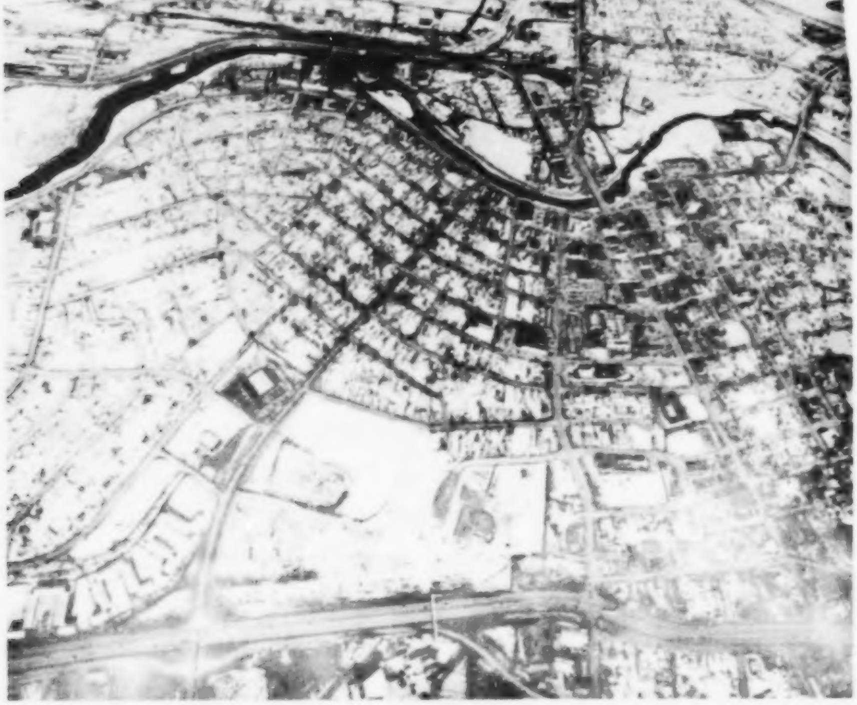

Figure 30. Oblique aerial photograph of Fairbanks, Alaska, looking north, taken during the snowmelt season, April 21, 1975. Note the lack of snow on roads and in the city core area just south of the wider bridge (Cushman Street). For comparison with Figure 2, the broad E-W highway near the bottom of the figure is Airport Road and the road bordering the snowcovered field at the top is College Road. The Creamer's Field thermograph is at the end of the side road north near the west edge of the subdivision roads south of College Road.

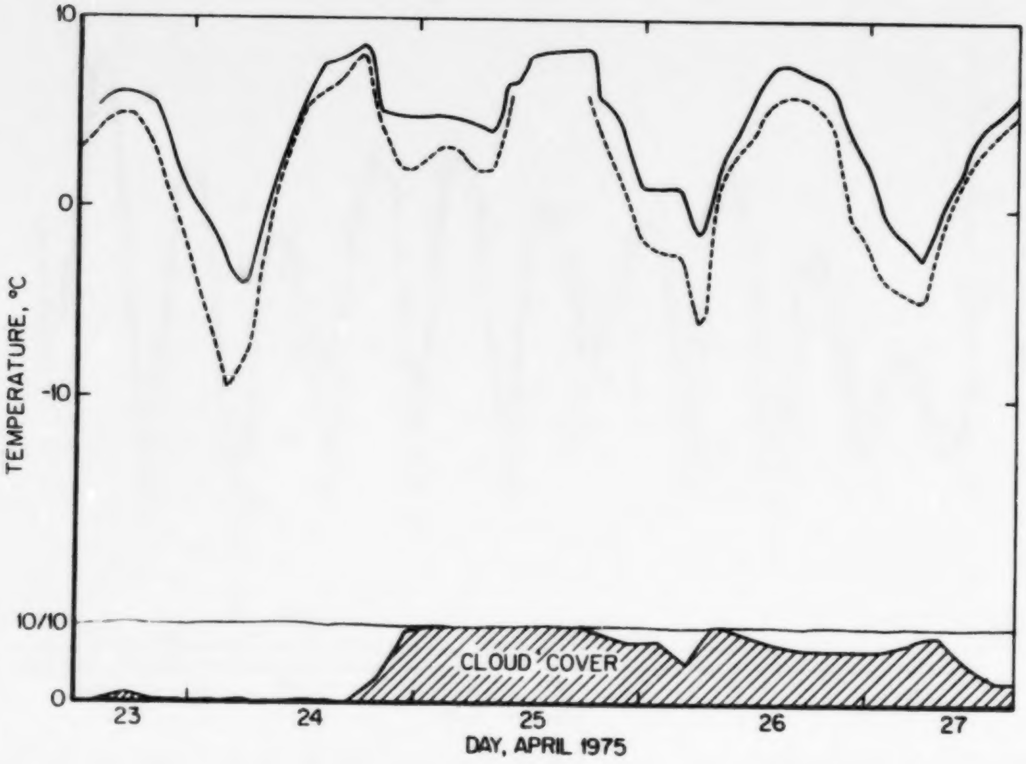

Figure 31. An example of daily temperature variations in town (solid line) and at Creamer's Field (dashed line) quite late in the snowmelt season. The curve at the bottom of the fiture gives cloud cover in tenths.

the snow cover is well established, temperatures rarely increase to the point that melting occurs, and the summer season as defined here is followed immediately by the dry-snow season.

Aside from day length, there is little difference in summer between Fairbanks and any other city of similar size and wind conditions. Anthropogenic heating is only about half of its winter maximum (see Section 8), but a marked diurnal cycle greatly increases the effect of the thermal substrate, while the lack of snow cover allows differences in evaporation and evapotranspiration to be felt. On clear nights, a heat island of up to 8°C develops, but daytime temperatures rarely show much difference between city and country temperatures.

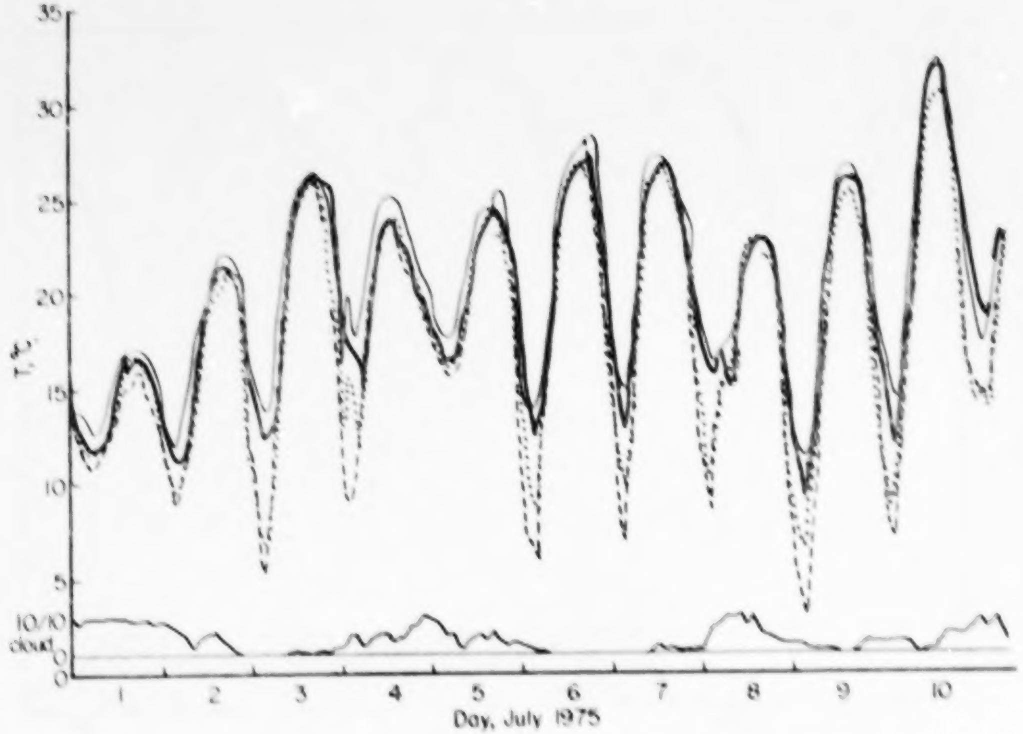

Figure 32. Temperatures and cloud cover during a relatively clear period in early July, 1975. Stations are the same as Figure 29.

Figure 32 shows an example of summer temperature variation during the time period when the sun drops only a few degrees below the horizon. The insolation at this time is very close to being a full sine wave, and the temperature wave follows this sine curve rather closely. The amplitude of the summer temperature wave is somewhat less than it was in March, even though the amplitude of the variation in incoming radiation is much larger; this is probably due to the change in substrate from snow to grass. The fact that the night is too short to allow even an approach to the radiative equilibrium temperature may also play a part.

A set of thermal infrared imagry flown on a summer night in 1970 (Figure 33) shows several points of interest including the following: 1. The dependence of nighttime temperature on very slight differences in elevation is clearly visible in Creamer's Field, at the top of the picture. The fact that the lowest-lying areas show up as bright spots within the darker swales suggest that stagnant, very shallow water was present in these areas. Such

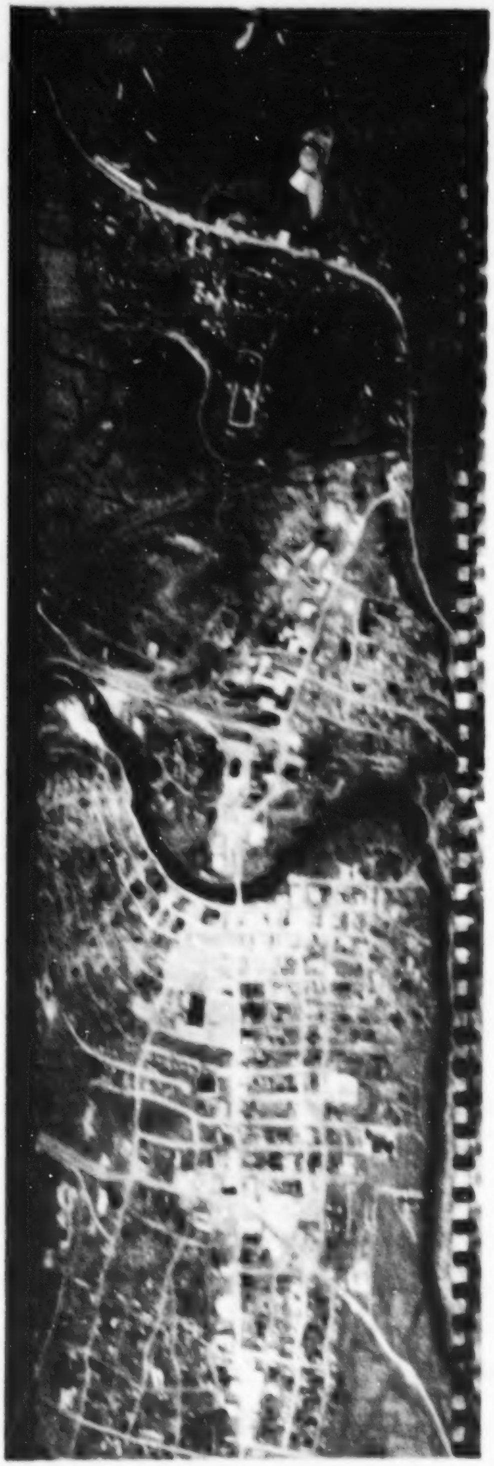

Figure 33. Thermal infrared imagery of the Fairbanks area in summer. Site CF is at the top edge. This scene was dated to approximately summer 1970 largely on the state of completion of the intersection of Airport Road and Cushman Street, near the lower edge.

water would be relatively cool by day, but would retain the day's heating longer at night than would the land surface. Deeper water, as in the Chena river and the gravel pit just below the first residential area, is colder than the land even at night. 2. The downtown area appears warmer than its surroundings primarily because of the very large fraction of area covered by artificial surfaces. In the original, it is possible to discern the pattern in which cars were parked in parking lots during the day, as these areas of pavement were shaded and were not heated to the same extent as were the traffic lanes. 3. The influence of the power plant on the Chena river, although still visible where the river runs out of the picture to the left, is vastly reduced from its effect in winter.

Ground Inversion Strength--

A number of traverses were carried out with thermistors mounted at .5 m as well as 2 m. The resulting data on near-ground inversion strength gave rise to the following generalizations:

1. Visible exhaust plumes were almost invariably associated with strong temperature gradients. When cars passed the traverse vehicle from either direction and their visible plumes reached the right front corner of the traverse vehicle, the result was an immediate shift toward less stable conditions - changes of 1°C/1.5 m (67°C/100 m) were normal. Exhaust plumes from stationary vehicles produced superadiabatic lapse rates if the plumes stayed low (e.g., if a light wind were present) or produced apparent inversions if the exhaust plumes were rising. It appears that the heat contained in an auto exhaust plume is sufficient to insure mixing through at least the first 2 m of the atmosphere.

2. On streets with heavy traffic and ice fog, but with the traverse vehicle not being obviously affected by a distinct plume, the vertical gradient was zero within the limits of our measurements. (Isothermal and adiabatic conditions could not have been distinguished from each other).

3. On streets with moderate to heavy ice fog but without appreciable traffic, inversions of as much as .5°C/1.5 m (33°C/100 m) in town or almost 1°C/1.5 m (67°C/100 m) out of town were observed.

4. On one occasion the car crossed a heavily traveled road (Airport Road) while itself running on a very lightly traveled road (Peger Road) with fog conditions approximately constant. An inversion of approximately 1°C/1.5 m (67°C/100 m) on the lightly traveled road changed immediately to a weak normal lapse across the heavily traveled road; in addition, the 2 m temperature increased by 2°C. If the lapse rates on and off of Airport Road were assumed constant up to the intersection temperature, the temperature disturbance due to traffic would have extended to a height of 5 m; in fact, both the normal lapse and the inverson probably decreased in intensity with height, in which case the disturbance extended to some height above 5 m.

5. Away from the fog, an inversion of 1°C/1.5 m (67°C/100 m) up to an extreme of 3°C/1.5 m (200°C/100 m) was normally observed. Maximum inversions were found on gentle slopes or extended flat areas; low temperature hollows (e.g., Ballaine Lake) were more nearly isothermal. Presumably air drainage produced isothermal cold pools in hollows. Slope inversions may reflect very shallow cold-air drainage in progress.

6. The maximum normal lapse rate observed from the moving car was approximately 1°C/1.5 m (67°C/100 m) in the downtown core area in heavy traffic. When the car was stationary with lights off, values as high as 6°C/1.5 m (400 times adiabatic) were observed. Since this was a night run, the thermistors were probably giving a reasonably accurate picture of the temperature distribution in the immediate vicinity of an idling car, especially under heavy ice fog conditions when thermal radiation from the engine compartment would be transferred via the suspended ice crystals to the air.

7. Horizontal temperature "waves" with more or less sinusoidal temperature changes with peak-to-trough amplitude of about 1°C and wavelength of the order of two long city blocks were observed with weak inversions (.5C/1.5 m) or with zero lapse rates.

Summary of Results

The overall strength of the Fairbanks heat island appears to be strongly tied to the strength of the low-level inversion in the undisturbed surroundings. The large values found for the maximum heat island intensity of this relatively small city are due to the well known fact that Fairbanks inversions are among the strongest and most persistent in the world (Benson, 1970).

SECTION 6

THE THREE-DIMENSIONAL HEAT ISLAND

MEASUREMENTS

Aircraft Observations

Four clear-night surface traverses were accompanied by helicopter flights, and one, by an instrumented fixed wing aircraft. FAA regulations did not allow us to fly at less than 300 feet (∿90m) over Fairbanks, and the two flights under ice fog conditions were further hampered by poor visibility.

Instrumentation on the helicopter flights consisted of a thermistor mounted on the side of the Pitot tube on the nose of a Bell 206 B Jet Ranger helicopter. The thermistor output was recorded on a battery-operated recorder. After the first flight, a small pressure transducer was hooked into a second battery recorder, in order to provide precise documentation of height changes. An experimenter in the back seat of the helicopter kept both recorders running and noted location on the temperature chart. A second experimenter rode up front as navigator. So long as the helicopter maintained forward motion the thermistor was well ahead of the rotor wash, but when descents were made to check lapse rates in outlying areas the speed sometimes dropped to the point that the thermistor showed a sharp rise in temperature as it was hit by the rotor wash. Such events were easy to identify on the chart record.

The major problem encountered was in getting good altitude control. Because of the very steep inversions and occasional step-like temperature structure in the Fairbanks area (Holmgren et al, 1975), it was important to know the exact height at which measurements were being carried out. On the first flight, most of the runs across town ended 50 to 75m higher than they began, and only two runs had usable data. For this reason a pressure transducer was added to the instrumentation on the remaining flights. The transducer-recorder combination was calibrated against a high precision barometer; pressure measurements were transformed to heights by using the hydrostatic equation and observed temperatures.

The fixed-wing observations were made from a Cessena 180 with thermistor attached to a wing strut. The flight coincided with Traverse 8, and observations were made at 320m, 470m, 780m and 1250m above the ground. Observations were attempted at 170m, but had to be discontinued because of dangerously low horizontal visibility due to ice fog at that level. Figures 19 and 40 were taken during this flight.

Hill-Slope Measurements

Previous work by the authors (Benson and Bowling, 1975) has shown that 2m temperatures on hill slopes are quite close to free-air temperatures at the same elevation, although this is not always the case for measurements taken on hill tops. As the initial stage in almost every traverse was a descent from the road in front of the Institute to the main road in the flats, 60m lower, we automatically have the background inversion on most traverses.

Tethered Balloon Observations

Information on the background lapse rate is available from an earlier project. Investigation of the surface inversions at Fairbanks using an acoustic sounder included a number of ascents with a tethered 3.2 m^3 balloon at a fixed site. This balloon was shaped so that it ascended nearly vertically and it carried apparatus for detailed profiling of the boundary layer (Holmgren et al, 1975). The ascents were made at a location north of College Road, marked A in Figure 2. Information on temperature, windspeed and pressure were telemetered to the ground station, while wind direction was obtained from the balloon orientation. Wind direction was not always available from nighttime ascents.

CO Concentrations

As CO is emitted primarily at street level, stable air should be reflected in a variation of CO levels with height. This was checked by comparing 30 minute CO measurements at three heights with those measured at the same site by the Fairbanks North Star Borough. The site is downtown, less than a block east of the Second Avenue - Cushman Street heat core. The Borough intake is located at 3m elevation, and instantaneous CO concentrations were obtained using a Beckman 315 BL infrared absorption analyzer. The instantaneous sampling was interrupted briefly to analyze our 30 minute bag samples, collected at 10 cm, 1m, and roughly 12 m (building top height), so all analyses were carried out using the same instrument.

RESULTS

The background lapse rate is known to be highly variable. Step-like temperature profiles are common (Figure 34), with layers of constant temperature or even normal lapse rates being separated by thin layers with extremely

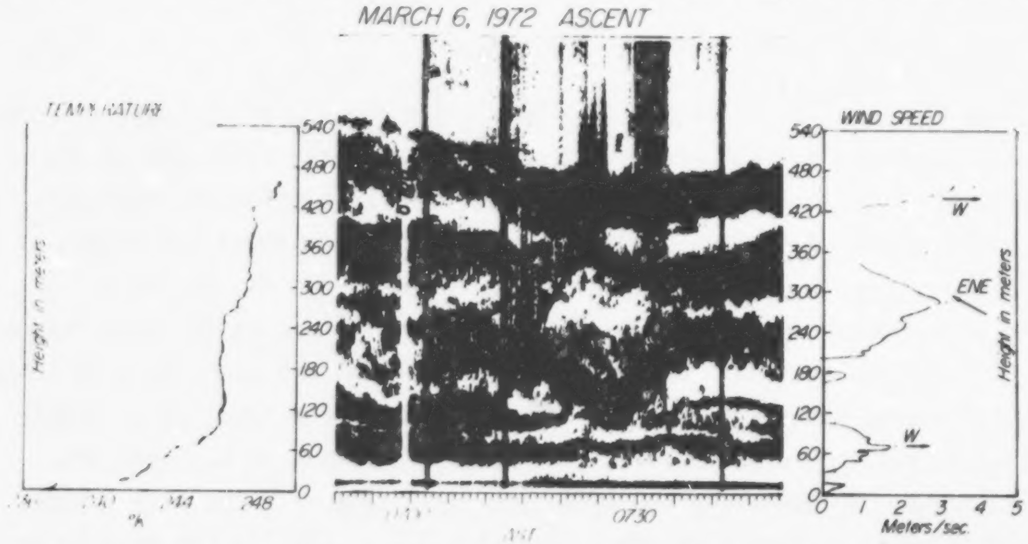

Figure 34. Vertical profiles of temperature, acoustic sounder backscatter and wind velocity in a relatively undisturbed area (from Holmgren et. al. 1975).

strong inversions. Strong ground inversions with isothermal conditions and wind speeds of 6-9 m $\sec^{-1}$ above 20 to 30 meters have also been observed, as have isothermal conditions near the ground with strong capping inversions several tens of meters aloft. On occasion a uniform inversion may reach to 100 m or more, as appeared to be the case during traverse 24.

Lapse rates in the lowest 90 m of the atmosphere in the city have had to be inferred from ground temperatures and the consistent lack of variability of CO concentrations with height. CO concentrations were identical at 10 cm, 1m, 3m and 12m in the city core under background inversion conditions, so good mixing and an adiabatic lapse rate to 12m are indicated.

As pointed out in the methods section of this chapter, the temperature in front of the Geophysical Institute, 60m above the elevation of the flats on which the town is sited, is a good approximation to the free-air temperature at that height. Thus the difference between the temperature at the Geophysical Institute and that at the cold background sites can be taken as the mean background inversion over the first 60 m, $T_B(60) - T_B(0)$. If the heat island intensity, $\Delta T(0)$, for each traverse is compared with this value for the same traverse, it is found that the equation

$$\Delta T(0) = 1.6 + .75\,(T_B(60) - T_B(0)) \qquad (1)$$

predicts the heat island intensity within 1.5°C for all but 3 cases (Figure 35). Considering the complexity and variability of the structure of the background inversion, the fit of the points must be considered excellent.

It is possible to use (1) to make some deductions about the height of the crossover point of the Fairbanks heat island - that is, the height at which the temperature is the same over the city as it is at the same height over undisturbed terrain. We assume that the lapse rate over the city center will not exceed the adiabatic rate. Then if the ground level city temperature is $T_c(0)$, the city temperature at a height z will be no lower than $T_c(0) - .01z$, .01°C/m being the adiabatic lapse rate. If the city temperature at 60 m is in fact given by $T_c(60) = T_c(0) - .01z$, it can readily be shown that the heat island at 60 m, $\Delta T(60)$, is given by

$$\Delta T(60) = 1 - .25\,(T_B(60) - T_B(0)) \qquad (2)$$

For $\Delta T(60) \geq 0$, i.e., for $(T_B(60) - T_B(0)) \leq 4°C$, the assumption of an

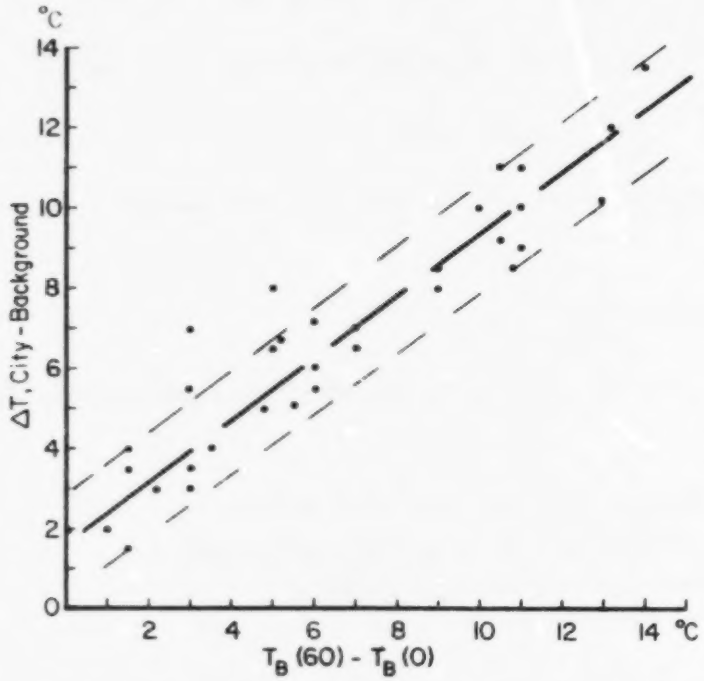

Figure 35. Comparison of heat island intensity and approximate 60 m inversion strength (Geophysical Institute temperature minus the same background temperature used in computing the heat island intensity).

adiabatic lapse rate over the city is not unreasonable and we can safely say that for a 60-meter inversion of 4°C or less, the heat island normally extends to above 60m.

For a 60-meter inversion of more than 4°C, (2) predicts a negative heat island at 60 m. This would represent convective overshoot and, while it may occur over a limited height range, Eq. (2) should not be considered to have any precise physical meaning for $(T_B\ (60) - T_B\ (0)) > 4°C$. If, however, we assume that the background lapse rate, γ, is constant at least to 60m and given by $\gamma = -(T_B\ (60) - T_B\ (0))/60$, we can define a crossover height. Let $\Delta T\ (z)$ be the heat island intensity at height z. We have the city temperature at z, $T_c\ (z) = T_c\ (0) - .01z$, and the background temperature at z, $T_B\ (z) = T_B\ (0) - \gamma z$. So

$$\Delta T(z) = (T_c\ (0) - .01z) - (T_b\ (0) - \gamma z). \qquad (3)$$

But $T_c(0) - T_B(0) = \Delta T(0) = 1.6 + .75\,(T_B(60) - T_B(0))$

and $(T_B(60) - T_B(0)) = -60\gamma$ from the definition of γ, so

$$\Delta T(z) = 1.6 - 45\,\gamma - (.01 - \gamma)z. \tag{4}$$

The crossover is defined by $\Delta T(Z) = 0$, so the crossover height Z, is given by

$$Z = (1.6 - 45\gamma) / (.01 - \gamma) \tag{5}$$

Representative values of Z for several values of γ are summarized in Table 6 and Figure 36.

TABLE 6. DEDUCED CROSSOVER HEIGHT, Z, AS A FUNCTION OF UNIFORM BACKGROUND INVERSION STRENGTH IN °C/100 m.

γ, °C/100m	Z, m
0	160
-1	102
-2	83
-5	64
-10	55
-15	52
-20	50
-30	49

If the values of z in Table 6 are compared with those calculated for a constant lapse rate in Section 9, the heights deduced during the stronger inversions are found to be too high relative to the fairly well substantiated value of z = 60m for $(T_B(60) - T_B(0))$ equal to 4°C. These stronger inversions are already known not to be constant with height, so the lack of agreement is no surprise. No detailed calculations have been made for more realistic lapse rates, as possible forms are too numerous. However, a concave-upward shape (steepest inversion near the ground) gives the best qualitative agreement between the theoretical and observed data. Figure 37 illustrates both the basis for the calculation and the effect of a non-constant background lapse rate.

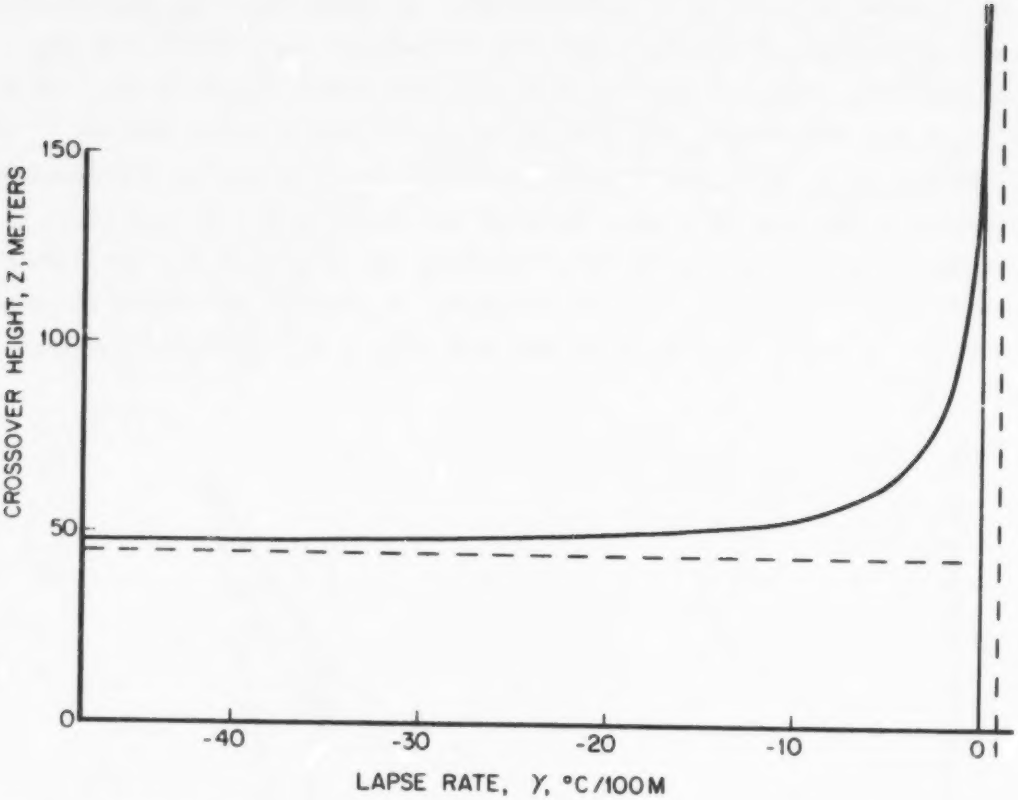

Figure 36. Plot of crossover height against inversion strength based on empirical relationship between heat island intensity and 60 m inversion and assumed constant background lapse rate. Assymptotic approach to Z - 45 m for strong inversions is physically unrealistic and indicates probable non-constant background lapse rates for these conditions.

The discussion to this point has assumed an adiabatic lapse rate above the city core. Although a superadiabatic lapse rate is unlikely on theoretical grounds, a stable lapse rate is quite possible, especially if any substantial fraction of energy transfer to the air is due to elevated sources (e.g., building walls, windows, elevated stacks). Thus the calculations to this point (allowing for modification under strong inversion conditions, see Figure 37) give a lower limit for the vertical extent of the heat island. An upper limit must come from the aerial traverse data. The aircraft measurements in every case showed that, at the lowest level sampled over the city, temperatures were above those at the ground, so that inversions, probably with bases above ground level, were present. In addition, city temperatures at levels accessible by aircraft were not measurably above those over the background areas, e.g., $\Delta T(z) = 0$ when z is the lowest flight level: 90 m under clear-sky conditions, and 170m in the one dense-fog case sampled. For the clear-sky case, then, the lapse rate within the city can be bracketed by an adiabatic lapse rate to around 50m with an inversion above that level as one extreme case, and by a weak inversion from the ground to at least 90m as the other extreme (Fig. 37). A near-adiabatic lapse rate to around 50m with an inversion at higher levels seems the most likely solution over the heat island core.

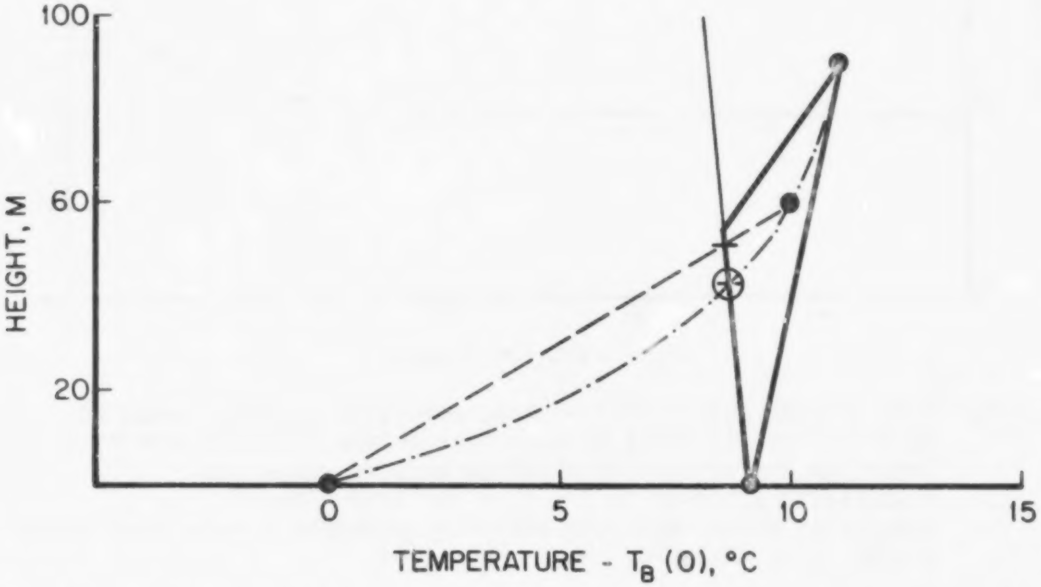

Figure 37. Limiting values for city lapse rate. Heavy dots are measured temperatures; light line is the adiabatic lapse rate over the city; dashed line is the background temperature profile assuming a constant lapse rate to 60m; dash-dot line is a more realistic background temperature profile. Cross shows calculated crossover height, circled cross, a more realistic value. The true city temperature profile must lie within the triangle formed by the heavy solid lines.

Measurements in clear weather above 90m showed an apparent influence of the city to and above that level, even though there was a 1°C to 6°C inversion between 2m and 90m over the city center. Both turbulence and wave-like temperature fluctuations differed in and out of town. Turbulence was encountered only over the city area, and was frequently associated with temperature fluctuations (breaking gravity waves) in situations when no such fluctuations were encountered over background areas. Flights during which temperature waves (always without detectable turbulence) were encountered in the background areas generally had relatively steady temperatures over the city. It appears in these cases that relatively low-level convection in the city may be acting either to influence the amplitude or stability of pre-existing waves or to generate waves where they did not previously exist. In the latter case (Figure 38) the wavelength in the west part of the east-west wave train appears similar to the distance between intersections on Airport Road, while the eastern section was over a loop of the Chena River. In each case, stronger than normal heating near the ground could have excited deeper than normal convective mixing which in turn could generate upper waves in somewhat the same way as a cumulus tower may form a pileus or scarf cloud by coherent lifting of stable air.

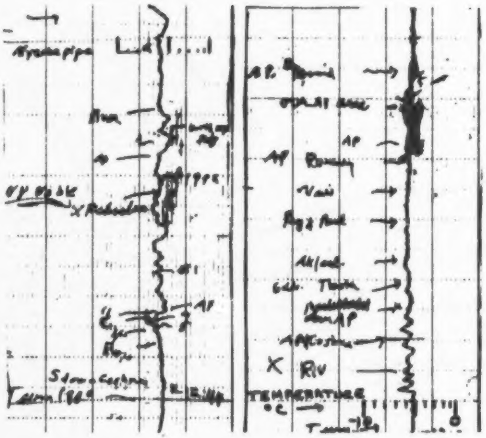

Figure 38. Thermistor traces across town during Traverse 23 at an elevation of 90m. Left side - North to South and return along Cushman Street; right side - East to West along the line of Airport Road.

The lowest aerial traverse height used in constructing cross sections of temperature above the city during traverses 24 and 29 showed sharp temperature gradients across the city. The colder ground areas north of the city had substantially higher temperatures aloft than did the background areas to the south, which were warmer near the ground. This was at first also interpreted as being due to coherent lifting of upper, stable air layers by convective activity lower down in the city air. Attempts to consider the amount of lifting which would be necessary in specific cases, such as Traverse 24 (Figure 39), together with the realization that while ground level winds were generally from the north, winds at flight level were more often from the east, made this hypothesis untenable in its original form. As both cases with definite gradients aloft showed gradients in surface background temperature of opposite sign, we suggest that the difference is due to more effective turbulent mixing of heat down to the ground in the southern area, which is relatively exposed to east winds (note topography on Figure 2). If this is the case, the position of the sharp gradient over the city is fortuitous.

The horizontal visibility above the city was significantly impeded during both aerial traverses with ice fog. During traverse 29, with moderate ice fog, the helicopter was in ice fog at an elevation of 90m, although the visibility was not so low as to terminate the measurements. An attempt to

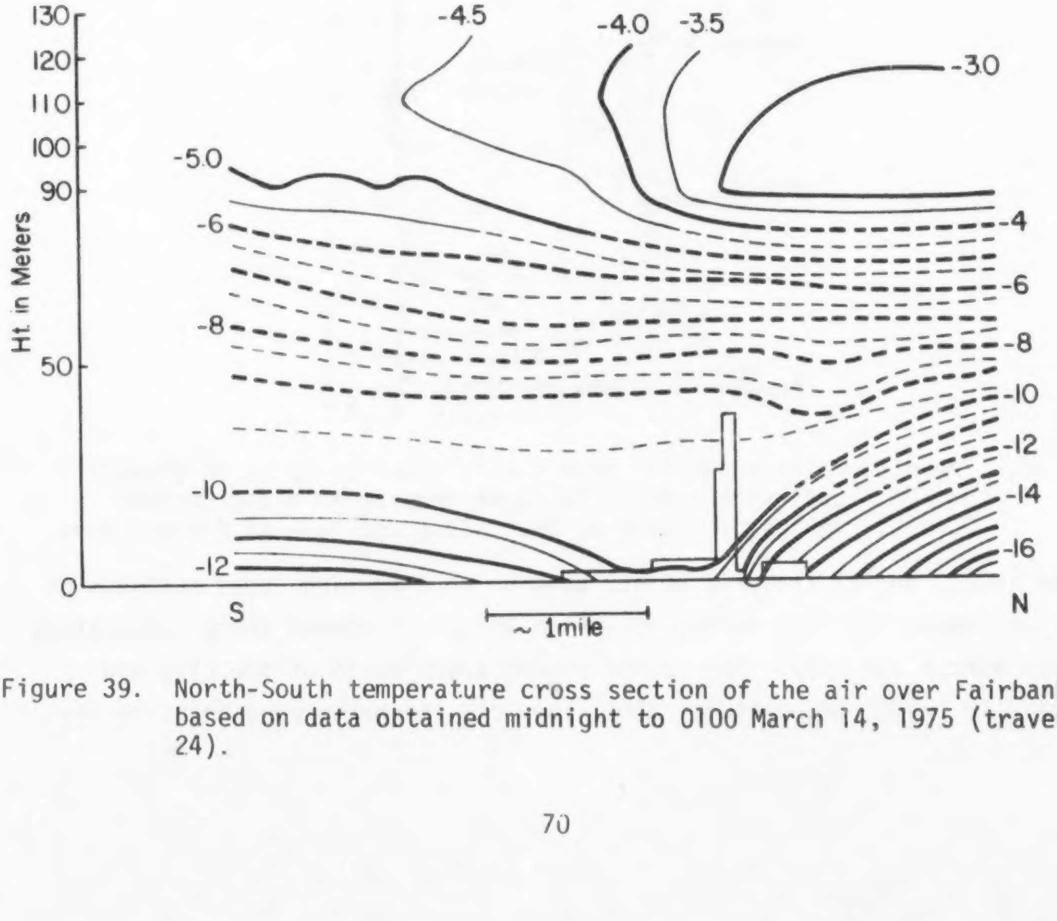

Figure 39. North-South temperature cross section of the air over Fairbanks, based on data obtained midnight to 0100 March 14, 1975 (traverse 24).

measure temperatures at 170 m during dense ice fog, however, had to be terminated due to dangerously low visibility (traverse 8). Large-scale vertical mixing to the flight levels seems unlikely, as the measured temperatures aloft were still higher, if only by 1°C in 29 and 2°C in 8, than any observed at the ground. The spread of major plumes (e.g., those from power plants) is known to produce fog layers aloft which at times blend with the ground-based fog over the southwestern (downwind) part of town, and the aircraft were probably in plume-derived fog. However, there is other evidence for an increase in the depth of vertical mixing during ice fog. SO_2, which is emitted primarily from elevated stacks, shows tremendously enhanced ground-level concentrations under ice fog conditions (Holty, 1973); while CO, which is primarily from ground-level sources, decreases at ground level under the same conditions. The combination of SO_2 and CO trends strongly indicates increased mixing depths during ice fog, as predicted by Bowling (1970). The major difference from this earlier prediction is that mixing is now known to take place over the city even when skies are clear.

In summary, a normal lapse rate or very weak inversion probably extends to at least 50m within the city, the height increasing as the background inversion weakens and/or ice fog develops. Temperature disturbances at higher elevations exist, but are not connected simply with the low-elevation heat island. With clear skies and no ice fog, the primary effect of the heat island on the air above 90m height is on air motion, which in turn may lead to temperature differences between the air over the city and its surroundings.

SECTION 7

THE WIND FIELD

MEASUREMENTS

Fixed Anemometers

Two anemometers are routinely operated in the area, one at the National Weather Service (WS in Fig. 2) and one operated by the Fairbanks North Star Borough on the south bank of the Chena River (B in Fig. 2). Observations were available at hourly intervals from the Weather Service, but their instrument normally did not record winds of less than 1 m sec^{-1}. The data from the Borough instrument were available only as output from a computer program which produced "average" hourly winds. During the second year of the study we added three more instruments. These consisted of a Lamprecht wind-run recorder installed at Peger Road (PR on Fig. 2), and two Gill propeller-vane anemometers, one at Creamers Field (CF on Fig. 2) and one at North Slope Batteries, (N on Fig. 2).

Hand-held Anemometers

During traverses 17 and 20, wind speeds were measured throughout the area by six to ten volunteers with small, hand-held anemometers. The anemometers, which had starting speeds of a few cm sec^{-1}, were fabricated in the Geophysical Institute Shop. Records from an earlier series of measurements carried out by Benson and Weller in the late 60's were also available. The primary difficulty with this technique was in scheduling. Traverse 17 was run under an overcast sky and 20 was run under a stratocumulus layer which was breaking up and re-forming in a thoroughly erratic manner. The earlier observations were made under light ice fog conditions in 1969-70.

These studies demonstrated that the horizontal scale of some major wind shears was less than the spacing we could hope to obtain with any reasonable number of point observations. This, of course, affected the fixed anemometers as well. The information obtained was worthwhile in demonstrating this variability, as well as providing some data on very low wind speeds, especially in the northern part of the area.

Plume Drift Directions

Power plant stack plumes are generally visible from observation sites above the ice fog, and have previously been used to deduce wind directions above fog top height. Some caution is necessary in interpreting this type of data as differences in wind directions indicated by two or more plumes which do not reach quite the same height may be due to vertical shear. This must be considered even when only high stack plumes are used (Figure 40).

At temperatures between -20°C and -30°C moist plumes from heating plants in single-story buildings and from vehicles were generally visible. Low-level wind directions inferred from the direction of these plumes were recorded as opportunity offered on traverses or while experimenters were driving around in the area for other purposes. Although the effects of time and space could not be clearly separated in observations of this sort, certain patterns did show repeatedly enough to be useful.

A broader scale view is possible using time-lapse photography of plumes. This technique has been used experimentally in the Fairbanks area for more than ten years. The power plant plumes are clearly visible in area-wide shots, but resolution of low-level house plumes required a telephoto lens and a rather limited field of view. Vehicle plumes were not generally visible.

Plume observations, whether direct or via time-lapse photography, are possible only over a very limited range of conditions. Small plumes rarely have enough condensation to be visible at temperatures above -20°C, and below -30°C the plumes tend to be lost in a thickening layer of ice fog. Nevertheless, plume observations are one of the best currently available methods of observing the wind field, as opposed to the wind at individual points.

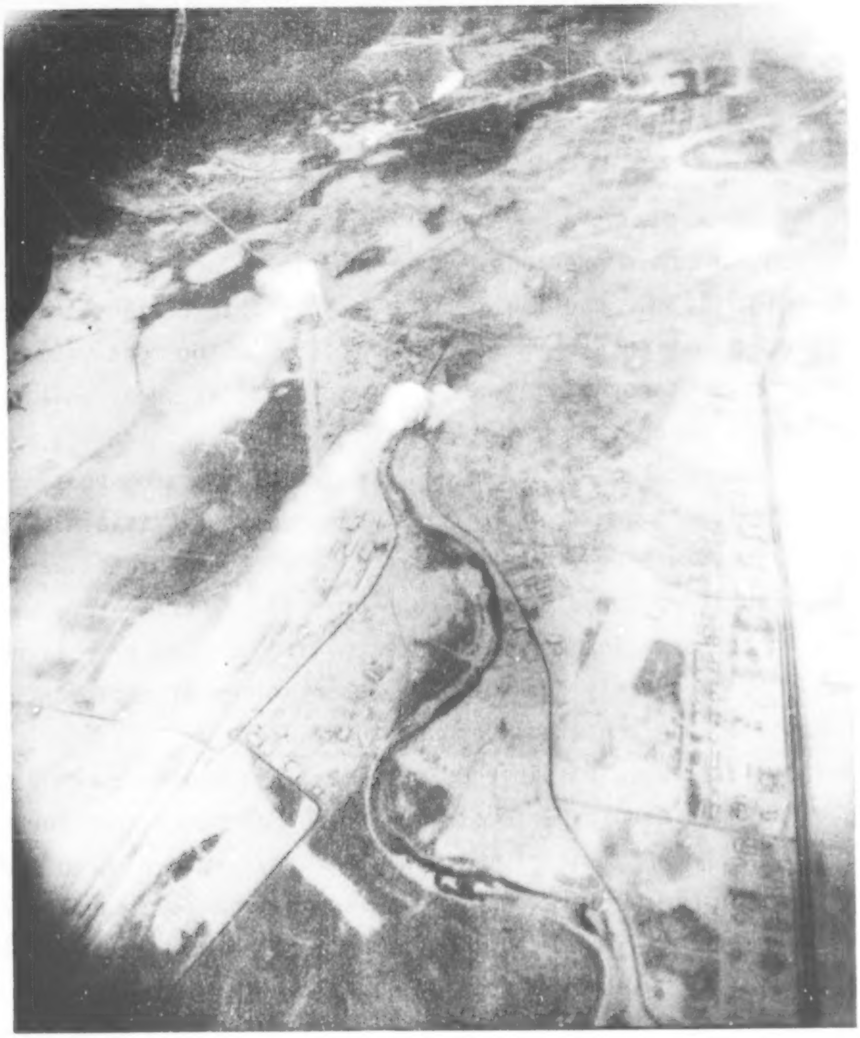

Figure 40. Photo of Fairbanks area, looking east, taken 3 January 1975 with a temperature of -42.5° measured at the city core. East, west, and north winds may be observed to affect plumes emitted at different levels.

RESULTS

Point Measurements

Winds measured in Fairbanks tend to be either several m sec^{-1} and fairly consistent in direction or under 2 m sec^{-1} and extremely erratic. The first case is associated with relatively good dispersal conditions and slight heat islands and is of no particular interest with regard to this study. The second case can be illustrated by a day's records from our three anemometer sites (Figure 41). Figure 42 illustrates for comparison a few possible sets of wind directions which give coherent areal flow patterns, or which persist for an hour or more on the wind record. There were also two periods in which relatively uniform northeasterlies prevailed. As the spacing between stations was 5 to 7 km, air moving at the observed speeds would have taken 2 hours or more to travel between stations. Apparent patterns which last for less than 2 hours are probably due to local eddies or waves (this includes most of the available observations).

The particular day shown in Fig. 41 was selected because the combination of low wind speeds and sufficient constancy of wind direction at individual sites allowed the 15 minute averages to be defined. Many days with low wind speeds had winds so unstable in direction that no readable plot could be made.

Simultaneous measurements at several points using hand-held anemometers provided additional data on wind fluctuations, as well as some suggestions of wind fields, although not under the best sky conditions. The mean wind field from Traverse 17 was shown in Figure 25; Figure 43 shows the wind fields from two different measuring intervals during Traverse 20. The two stations near College Road in Figure 43 are of particular interst, as they maintained virtually a 180° shear for the entire 40 minutes of measurement. The record from the southeastern station (Joy School) includes a notation that when wind speed dropped, the direction would change temporarily from WSW to NNW. Evidently some sort of kilometer-scale shear or local eddy was maintaining itself with relatively slight shifts in position for almost an hour in this area.

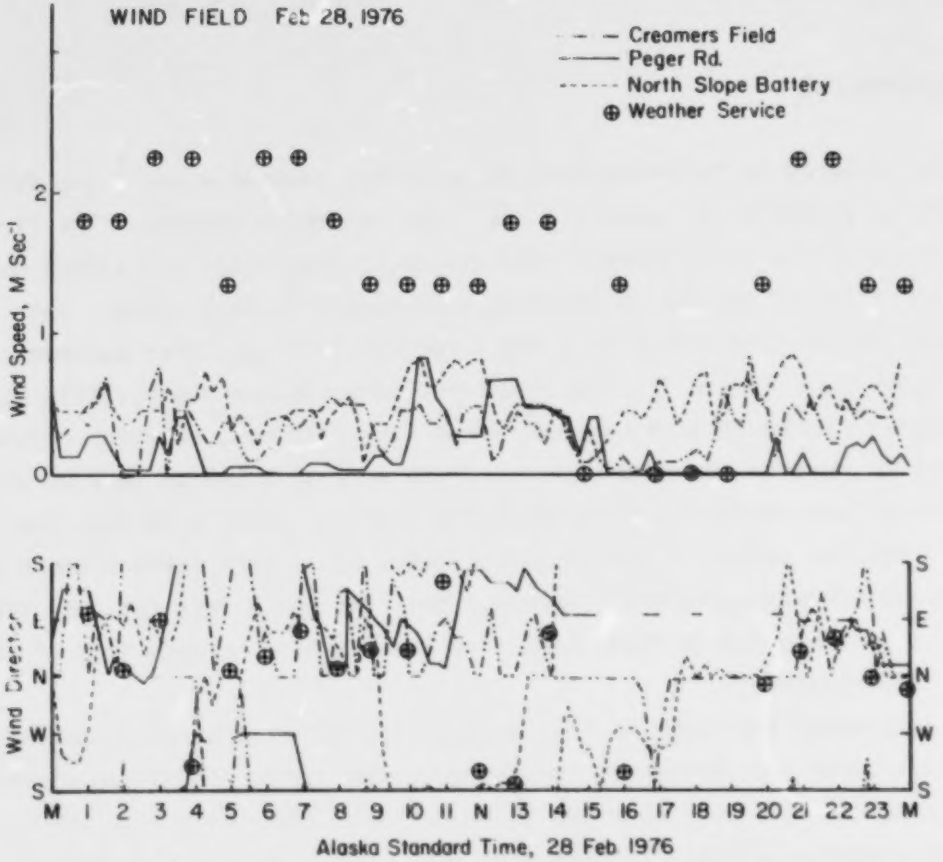

Figure 41. (above) Comparison of winds at three sites through the course of a day.

Figure 42. (below) Suites of wind directions for various simple wind fields for comparison with Figure 41. Wind measuring sites coded same as Figure 41.

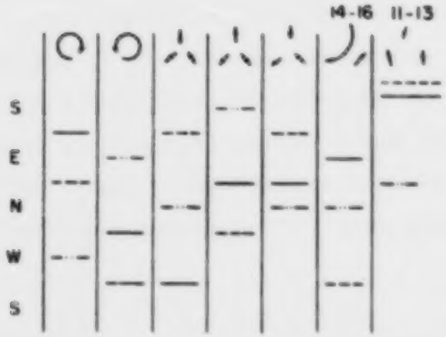

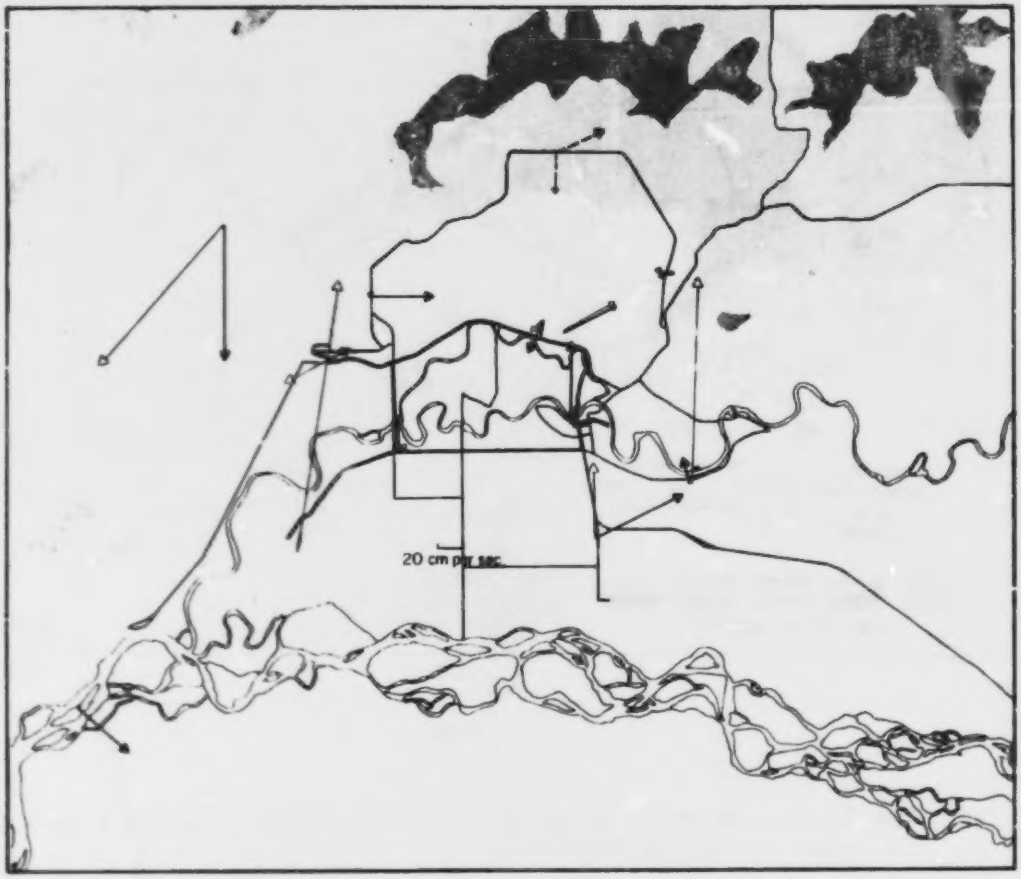

Figure 43. Wind vectors for 2 two-minute measuring periods during Traverse 20 (0900-1000 8 February 1975). The lengths of solid arrows indicate measured wind speeds; dashed arrows indicate that only wind direction was available. Filled arrowheads-0925; open arrowheads 1000.

Figure 44 shows near-surface (2m) wind roses representing wind directions and strengths measured during four periods of light ice fog, when the stratification of the atmosphere is stable and the surface air flow pronounced. All four ice fog events occurred during the winter of 1969-70. As can be seen, the wind speeds and therefore the diffusion processes close to the ground are low. The flow of air is determined by the local topography and results from gravitational downslope (katabatic) drainage of cold air, produced by radiative cooling of the surface. River and stream valleys, even if small, thus clearly become channels draining air downslope, as can be seen from Figure 44. The slope angles of either valley or hillslope determine the

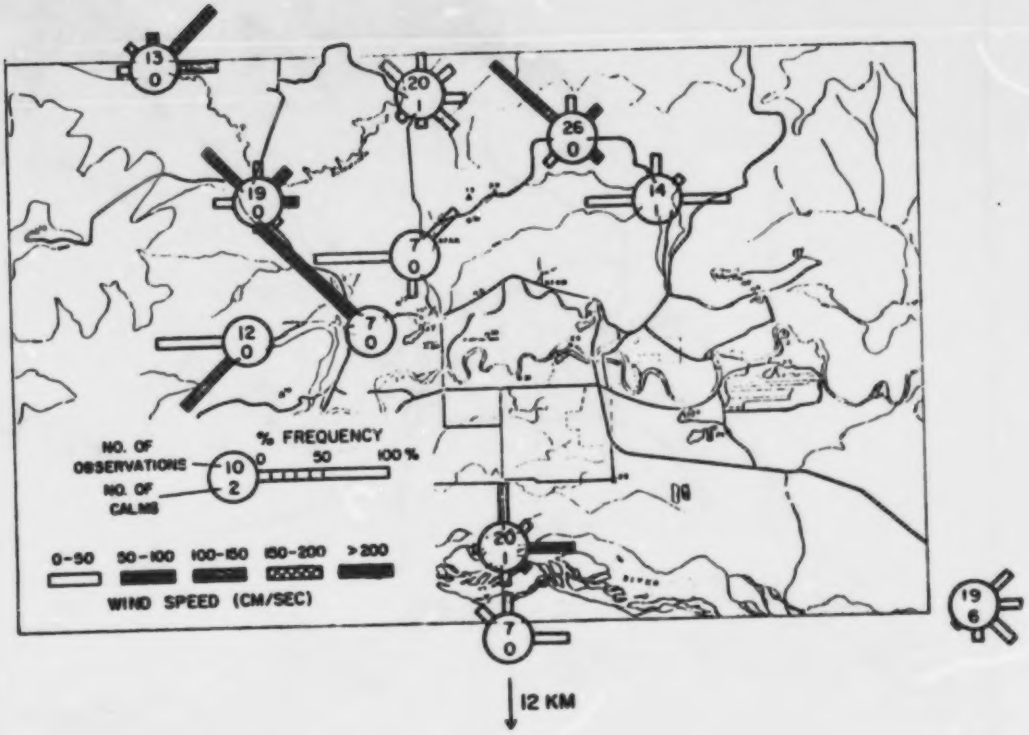
13
0
20
1
26
0
14
1
19
0
7
0
7
0
12
0
20
1
7
0
19
6
NO. OF OBSERVATIONS
NO. OF CALMS
% FREQUENCY
0
50
100%
10
2
0-50
50-100
100-150
150-200
>200
WIND SPEED (CM/SEC)
12 KM

Figure 44. Low level wind roses at sites in the Fairbanks area for 4 periods of light ice fog in 1969-1970.

wind speed: strong winds are generated on steep slopes; weak winds on relatively flat terrain. Frictional effects resulting from high surface roughness probably also affect the wind speeds.

Winds are generally less than 0.5 m sec^{-1} (1 mph), but occasionally on steeper slopes or in well-defined stream channels they reach or exceed 1 m sec^{-1} (2 mph).

The mean wind speed near the surface in Fairbanks and surroundings during periods of ice fog is approximately 0.5 m sec^{-1} (1 mph). If this wind speed were uniform, an air parcel near the surface could be expected to travel about 40 km day^{-1} down the Tanana valley. However, the problem is more complex because of the oscillation of low level air over the city which reduces the net value of 40 km day^{-1} to a significantly lower value.

Vertical and Small-Scale Horizontal Shears

Both the acoustic sounder and plume observations have confirmed the existance of substantial wind shear in the vertical. Figures 34 and 40 document the types of vertical wind structures likely to occur. In addition, we have observed cases in which plumes from idling vehicles and those from nearby single-story buildings have indicated substantial (180°) wind shear between about 1 m and 4 m.

Horizontal shears are indicated by 180° wind shifts indicated by plume directions over distances of 100m along roads. Small-scale convergences are sometimes indicated by vehicle plumes--in one case, plumes from cars idling in parking lots on opposite side of College Road converged on the road.

Time lapse movies and visual observations of house plumes have documented both organized and apparently chaotic variability in wind direction in space and time. In one striking case, a 180° change in wind direction was observed to propagate back and forth along a row of houses several times. Presumably a gravity wave was responsible.

It should be emphasized that observation of wind shears through plume observations requires a good deal of luck--plumes must be present on both sides of a shear zone, the temperature and humidity conditions must be such that the plumes are visible, and an observer must be present who recognizes the significance of the plume directions.

There is other evidence that periodic motions exist regularly and frequently in the lower atmosphere over Fairbanks. Benson (1970) observed and photographed waves at the upper boundary of the ice fog layer and speculated on the wind shear and diffusion processes at this boundary. Wilson and Fahl (1969) defined the characteristics of the waves and identified them as atmospheric gravity waves. Using infrasonic pressure transducers, they found the mean periodicity to be approximately three minutes and the mean pressure, temperature and orbital wind speed amplitudes were 15 microbars, 0.5°C and 0.2 cm sec^{-1}, respectively.

A long period motion of air has also been observed by measuring temperature oscillations on the slopes of hills which surround Fairbanks on three sides. These temperature variations have periods of roughly 20 minutes. Benson (1970) and Haurwitz (1973) have interpreted them as internal seiches in the pool of cold air confined by the local topographic features.

The Low-Level Horizontal Wind Field

It is possible to organize the data we have gathered according to the following working hypotheses:

We consider that the low-level wind field at a particular time is due to the interaction of a number of driving mechanisms, each of which tends to produce its own pattern of winds. Observations generally show a combination of two or more of the patterns discussed. The eight most important patterns are:

1. Uniform wind direction at relatively high speeds.
2. Strong winds south of town, stagnation further north.
3. Northward penetration of gravity drainage down the Tanana River.
4. Gravity drainage from the local hills.
5. A back eddy from the Tanana drainage.
6. Covergence toward the heat island.
7. Gravity waves.
8. Local wind shears.

(1) Uniform wind direction at relatively high speeds. Pattern 1 is associated with weak-inversion or neutral lapse rates and probably represents low-level penetration of geostrophic winds. It gives good dispersion conditions and little heat island. The geostrophic wind probably has a major influence on the relative importance of the other wind fields, even when penetration to the ground does not occur.

(2) Strong winds south of town, stagnation further north. A modified version of pattern 1, which we will call pattern 2, has high wind speeds in the southern part of the Fairbanks area with relatively stagnant air in the more sheltered areas farther north. Pattern 2 can cause a major breakdown of air quality forecasts, as the Weather Service Office at the airport is frequently in the southern, high-wind zone while the major part of Fairbanks is in the northern, stagnant zone. The windy area is normally much warmer than the stagnant area, especially if skies are clear. This results in a "one-sided" heat island, such as was observed in Traverse 38 (Figure 24).

(3) Northward penetration of the gravity drainage down the Tanana River. This may almost be considered a special case of pattern 2, as it is unlikely to occur without reinforcement from easterly geostrophic winds aloft. So far as the heat island and dispersion conditions are concerned, the effects are similar to (2), but may be weaker.

(4) Gravity drainage from the local hills. In broad scale, the combination of topography and Coriolis acceleration tends to give very weak east to southeast winds in the northeast part of the Fairbanks area (along the Steese Highway), weak northerly flow near the University, and weak northeasterly flow southwest of town. Observations of wind directions along College Road in near-calm conditions generally confirm this mechanism (but see also patterns 5 and 8). Observations along Airport Road are less consistent, probably due to more interference from other patterns. On a finer scale, hillside areas with different slopes, aspects, and elevations will tend to produce air of different temperatures which would be expected to move out over the basin at different heights. Observed "low speed jets" moving in different directions at different heights (Holmgren et al., 1975) could be due to this mechanism.

(5) Back Eddy from the Tanana River drainage. This pattern, with a clockwise eddy, was observed by Benson and Weller in the late 1960's and described by them in an unpublished report to ARCO and to Earth Resources Company in 1970. Their data were given in Figure 44, and their summary figure of the wind structure is included here as Figure 45. The north to south component of flow in this pattern would act to reinforce the same component in (4), while the sense of rotation in the two cases is opposed. Combination of the two patterns could give eddies in either or both directions superimposed on a general drainage flow from the north.

(6) Convergence toward the heat island. Southerly components were observed on several occasions along Airport Road while air flow on the College Road section was northerly. Also, the simultaneous wind measurements taken on January 25 (under nearly calm but cloudy conditions) show convergence on the city center from all

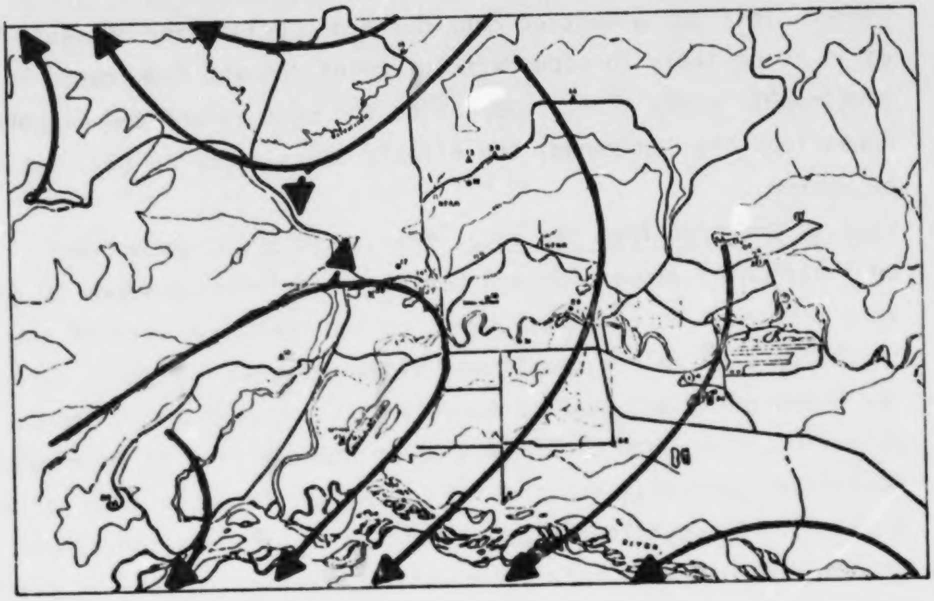

Figure 45. Surface flow pattern for ice fog deduced from the data in Figure 44.

directions. The interaction between this pattern and (3) is of particular interest with regard to the proposed industrialization of the North Pole area, which is located in the Tanana air drainage upstream of Fairbanks. Although the undisturbed air drainage down the Tanana Valley would normally carry pollutants well south of Fairbanks, convergent flow toward the city from the south could carry pollutants back northward into the city core.

The six patterns discussed so far are reasonably stationary in time and have a broad spatial scale. Unfortunately for purposes of measurement, they are complicated by the presence of at least two types of small-scale and/or time-dependent wind fields with local speeds comparable to (2) through (6) above (0.2 to 2.0 m sec^{-1}). These are listed as (7) and (8) below.

(7) Gravity waves. Waves with periods of 2-3 minutes and wavelengths of several hundred meters are well known from infrasonic and acoustic sounder records (Fahl, 1969; Holmgren et al., 1975) and are probably responsible for the usual "ocean wave" appearance of the upper boundary of the ice fog layer as seen from hilltop

locations (Benson, 1970). Several 180° wind shifts in succession were at times observed along Airport Road with wavelengths compatible with a gravity wave orign. Time lapse photography of several house plumes south of the University also suggested wind fluctuations of gravity wave orign, and some rhythmic fluctuations of temperature along traverses and on thermograph records (Benson, 1970) may be due to the same mechanism. Longer period gravity waves are believed to be associated with seiche oscillations between Chena Ridge and Birch Hill (∿ 30 minute period) and between Chena Ridge and the Salcha Bluffs area (∿ 4 hour period) (Haurwitz, 1973). These long-period standing waves do not seriously interfere with wind measurements, although they could be of considerable importance in pollutant transport. This is especially true of the 4-hour wave with respect to effluents from the North Pole area. The high-frequency traveling waves, however, introduce considerable confusion into both wind and temperature records. All of the gravity wave phenomena are probably dependent primarily on the geostrophic winds aloft for excitation.

(8) Local wind shears. This category is rather poorly understood. Its existence is based primarily on an observation of a 180° horizontal wind shear over a distance of less than a kilometer and remaining stationary for at least an hour (Figure 43). Certain temperature measurements (e.g., persistent cold and warm spots not obviously controlled by topography and not constant in position from day to day) are also best explained by some sort of channeled air drainage. Most of these observations (including the measured wind shear) were made along College Road, which frequently is nearly paralleled by an isothermal line in a zone with a strong horizontal temperature gradient. The observations may indicate: (a) kilometer-scale eddying; (b) wind shear across a micro-scale cold front upwind of the heat island, possibly with miniature wave cyclones; (c) shear between regions controlled by different wind patterns (1) through (6); (d) a very low level vertical wind shear on a slightly sloping interface. Other explanations are undoubtedly possible. The phenomenon is of interest with respect to mechanics of air flow

into the heat island from the north and because of possible interference with measurements of the regional wind field. Wind observations along a traverse cannot distinguish between (7) and (8), so the relative importance of these two patterns is unknown.

Radiation conditions, regional winds aloft, and surface pressure gradients probably combine to control the relative importance of the different factors.

In addition to the horizontal patterns described, vertical shears are extreme. In one photographically documented case, (Figure 40) the upper stack plumes were under the influence of a strong east wind, lower level plumes from the same power plant were being driven by a west wind, and plumes from 2-story apartment buildings and a school were going south. All three plumes were within an exceptionally deep (200 m) ice fog layer.

In summary, air movement in the Fairbanks basin is controlled by a number of competing driving mechanisms. As a result, the observed wind field is highly variable in both horizontal and vertical space and in time.

SECTION 8

FAIRBANKS ENERGY-USE INVENTORY

The energy-use inventory concentrated on four energy sources: coal, gasoline, fuel oil, and imported electricity. Locally generated electricity (plus the waste heat released in the course of generation) was included in the coal and fuel oil figures. The area covered is approximately that of the Fairbanks North Star Borough; roughly 75% of the Borough population lives in Fairbanks and most of the remaining 25% work and/or shop there.

ELECTRICITY

Electricity is imported 164 km from the mine-mouth plant at Healy by the Golden Valley Electric Association (GVEA). GVEA figures for electricity produced at Healy since the plant opened in February 1968 are given in Table 7 and may be seen in terms of the area's commercial electrical generation in Figure 46. Like most in this section, this figure is cumulative, i.e., the top line gives the total GVEA and Municipal Utilities generation, the next line down gives total GVEA production, etc.

COAL

Coal is imported from Healy via the Alaska Railroad (ARR), which provided us with monthly figures from mid-1967 to the present. In addition, monthly consumption figures since 1964 were obtained from all of the coal-fired power plants in the area--GVEA, Municipal Utilities System (MUS), the University heating plant (U of A), and the two plants on Fort Wainwright. These are shown in Figure 47. Comparison of the railroad and power plant totals on a

TABLE 7. ELECTRICITY IMPORTED TO FAIRBANKS (IN MILLIONS OF KWH).

	1968	1969	1970	1971	1972	1973	1974	1975
Jan.	0	6.4	16.3	16.2	17.0	17.3	17.3	18.6
Feb.	4.2	6.3	12.6	15.4	11.3	15.1	16.2	16.8
Mar.	6.6	6.2	13.0	16.9	14.4	9.8	16.4	18.4
Apr.	6.2	5.8	11.0	14.2	15.9	14.8	12.3	17.1
May	3.2	7.7	8.9	11.1	10.2	14.1	15.4	11.5
June	7.6	6.5	5.2	0	11.2	12.1	14.4	15.5
July	7.1	6.5	9.7	9.0	11.4	13.0	13.9	16.1
Aug.	3.9	7.2	10.6	12.3	13.6	13.8	14.7	14.7
Sept.	4.4	7.8	11.9	11.6	9.4	10.0	10.5	11.5
Oct.	6.0	9.6	13.3	15.0	15.6	12.6	17.8	17.6
Nov.	0.7	12.7	12.2	16.1	16.1	16.7	18.0	17.7
Dec.	8.4	14.6	15.3	14.6	15.0	17.1	17.3	18.0
Year	58	97	140	153	161	166	184	194

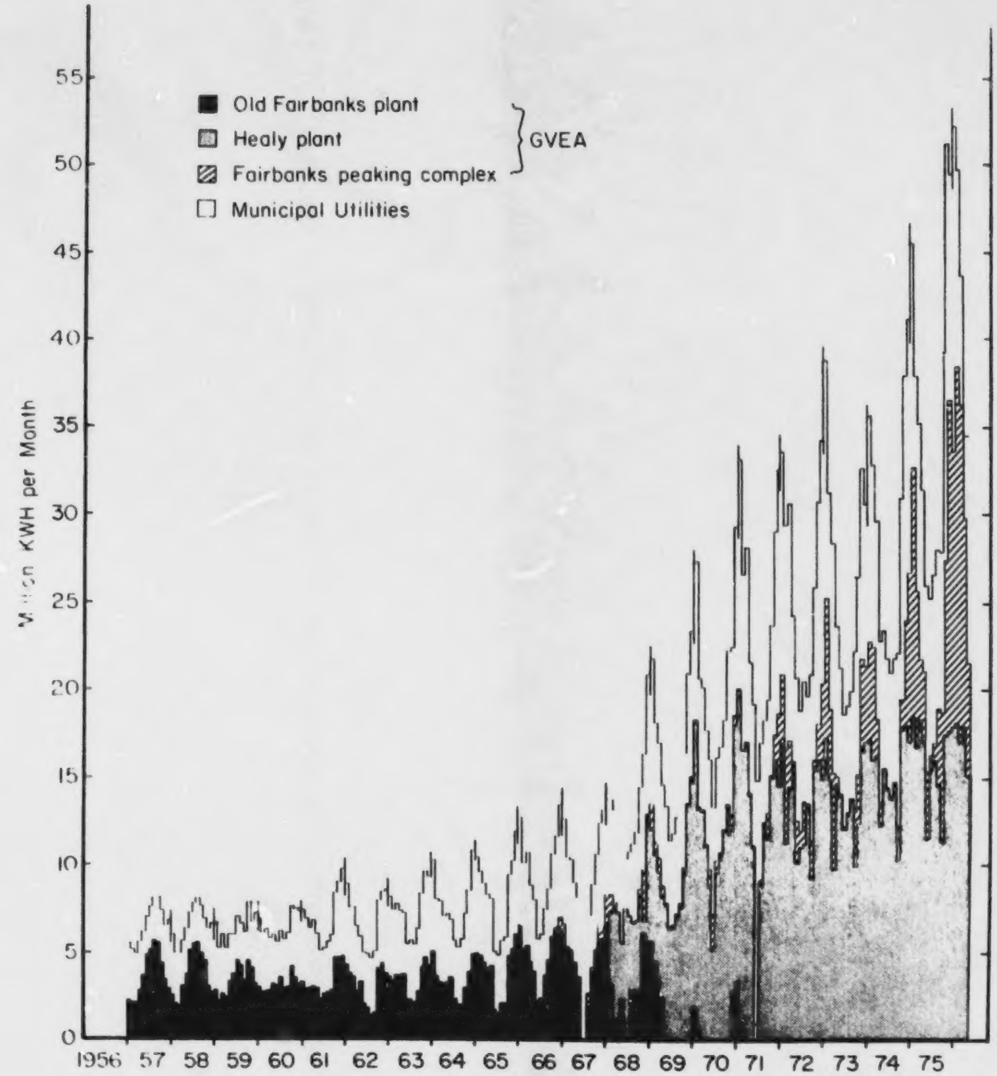

Figure 46. Commerical electricity production as a function of time in and for the Fairbanks area.

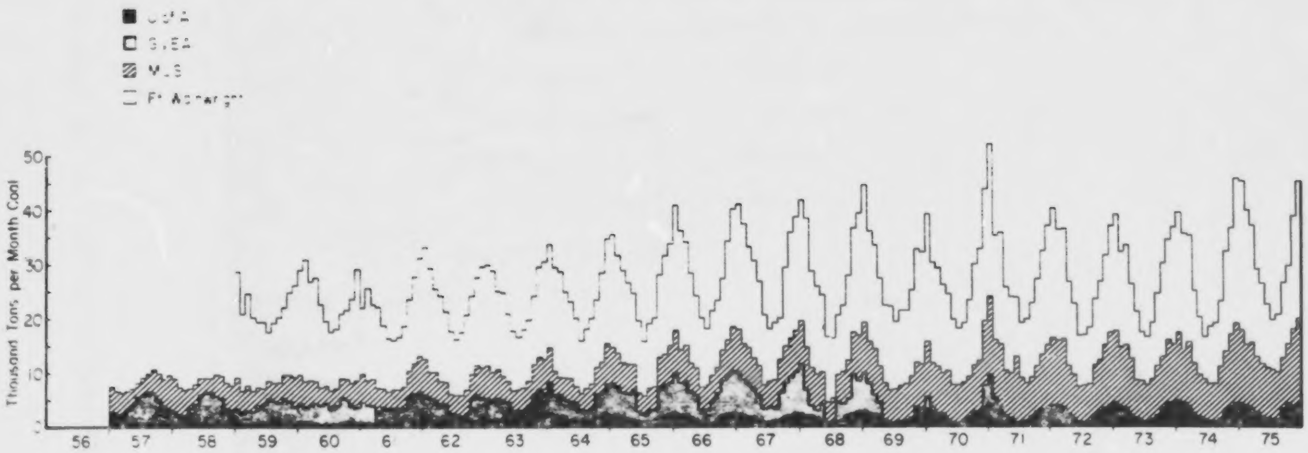

Figure 47. Cumulative coal consumption by power plants in the Fairbanks area in thousands of tons.

monthly basis showed many months with more power plant use than railroad imports. However, comparison of yearly totals allows some estimate of how the residual, which includes home heating and probably some waste, has changed over the course of the study.

The power plant coal consumption has remained quite constant. GVEA ceased coal-fired generation in the Fairbanks area in 1971, shortly after the Healy plant became fully operational, but MUS increased its capacity at about the same time. Home heating has always accounted for a relatively small fraction of the coal use, the greatest value being 72 x 10^3 tons (≈ 20% of the total) during Benson's (1970) study. As Table 8 shows, the residential coal use has since dropped to less than 1% of this amount. Table 9 shows the monthly breakdown of use by the various power plants for the last two years, and Figure 47 shows this breakdown back to 1957.

To avoid the effects of stockpiling on monthly data in the final sum of monthly coal use given in Table 10 and used for the total energy use, the power plant use for each month was multiplied by the ratio of the yearly ARR imports to the yearly power plant consumption. This slightly overestimates summer consumption.

GASOLINE

Gasoline consumption figures for the Fourth Judicial District (which includes most of Alaska north of the Alaska Range) were obtained from the Alaska Department of Revenue. These were broken down by highway, marine, and aviation use, but not by area within the District. Luckily, a large percentage of the population and most of the road mileage are in the Fairbanks area. Alaska Railroad imports to Fairbanks were around 75% of the District's taxable sales, and this figure was used to estimate the Fairbanks area gasoline use. (Tax figures were used rather than Alaska Railroad figures because it was felt they would follow monthly fluctuations more accurately.)

Figure 48, which shows both the adjusted Fairbanks area use from the tax data and the Alaska Railroad imports, shows the much greater month-to-month consistancy of the tax data. Marine use (which is a small fraction of the total) was included with highway gasoline. Aviation gasoline is consumed over a much wider area than is highway gasoline. Since most bush flights in

TABLE 8. FAIRBANKS AREA COAL USAGE BY YEAR IN THOUSANDS OF TONS

	Alaska Railroad Imports	Power Plant Use	Residual (Home Heating)
1959	292.6	243.2	49.4
1960	283.4	281.6	1.8*
1961	322.0	256.8	65.2
1962	350.7	278.2	72.5
1963	334.5	284.5	50.0
1964	----	302.6	----
1965	Records	316.1	----
1966	Destroyed	348.6	----
1967	----	350.8	----
1968	384.7	338.5	46.2
1969	366.5	335.0	31.5
1970	349.7	335.1	14.6
1971	364.3	354.3	10.0
1972	335.2	331.9	3.3
1973	331.6	331.0	0.6
1974	347.7	347.0	0.7
1975	393.1	378.9	14.2

* This figure is obviously not the correct one for residential use, and probably represents a sharp decrease in stockpiling in the area.

TABLE 9. MONTHLY POWER PLANT COAL USE BREAKDOWN IN 10^3 TONS - 1974 AND 1975

	MUS	%	UofA	%	Ft. Wainwright	%	Total
1974 J	12.6	32	4.7	12	22.1	56	39.3
F	10.1	28	4.3	12	21.2	60	35.6
M	11.9	34	3.6	10	19.6	56	35.1
A	9.5	38	2.2	9	13.3	53	25.0
M	7.9	39	1.6	8	10.7	53	20.2
J	7.4	45	1.2	7	8.0	48	16.6
J	6.8	37	1.1	6	10.5	57	18.4
A	6.8	36	1.1	6	11.2	58	19.1
S	9.6	42	1.4	6	12.1	52	23.1
O	10.8	34	3.0	9	18.5	57	32.3
N	13.4	37	3.7	10	19.5	53	36.5
D	14.8	32	4.3	9	26.7	58	45.8
1974 Year:	121.5	35	33.2	10	193.3	55	347.0
1975 J	13.1	29	4.4	10	27.6	61	45.1
F	11.4	29	3.7	9	24.7	62	39.9
M	11.9	32	3.5	9	21.6	58	37.0
A	10.0	35	2.6	9	16.0	56	28.7
M	9.5	36	1.8	7	14.8	57	26.2
J	9.2	41	1.5	7	11.6	52	22.3
J	8.9	46	1.4	7	9.2	47	19.5
A	8.5	42	1.4	7	10.4	51	20.3
S	9.1	34	3.4	13	13.9	53	26.4
O	11.1	38	4.1	14	14.3	48	29.6
N	13.7	35	4.0	10	21.1	55	38.8
D	15.7	35	4.2	9	25.3	56	45.1
1975 Year:	132.3	35	36.0	10	210.6	55	378.9

TABLE 10. TOTAL COAL USE IN THE FAIRBANKS AREA, UNITS 10^3 TONS

	1967	1968	1969	1970	1971	1972	1973	1974	1975
Jan.	46	47	49	41	54	40	39	39	47
Feb.	42	44	39	31	37	37	32	36	42
Mar.	37	33	37	30	37	37	33	35	38
Apr.	34	29	30	27	27	27	26	25	30
May	30	28	25	25	25	23	21	20	27
Jun.	23	19	24	21	25	17	17	17	23
Jul.	20	19	21	18	20	17	17	18	20
Aug.	22	23	23	20	21	18	19	19	21
Sep.	23	25	23	24	24	24	25	23	27
Oct.	33	32	28	31	28	27	30	32	31
Nov.	40	42	36	34	34	32	34	37	40
Dec.	43	45	35	46	39	37	37	46	47
Year:	394	385	366	350	364	335	332	348	393

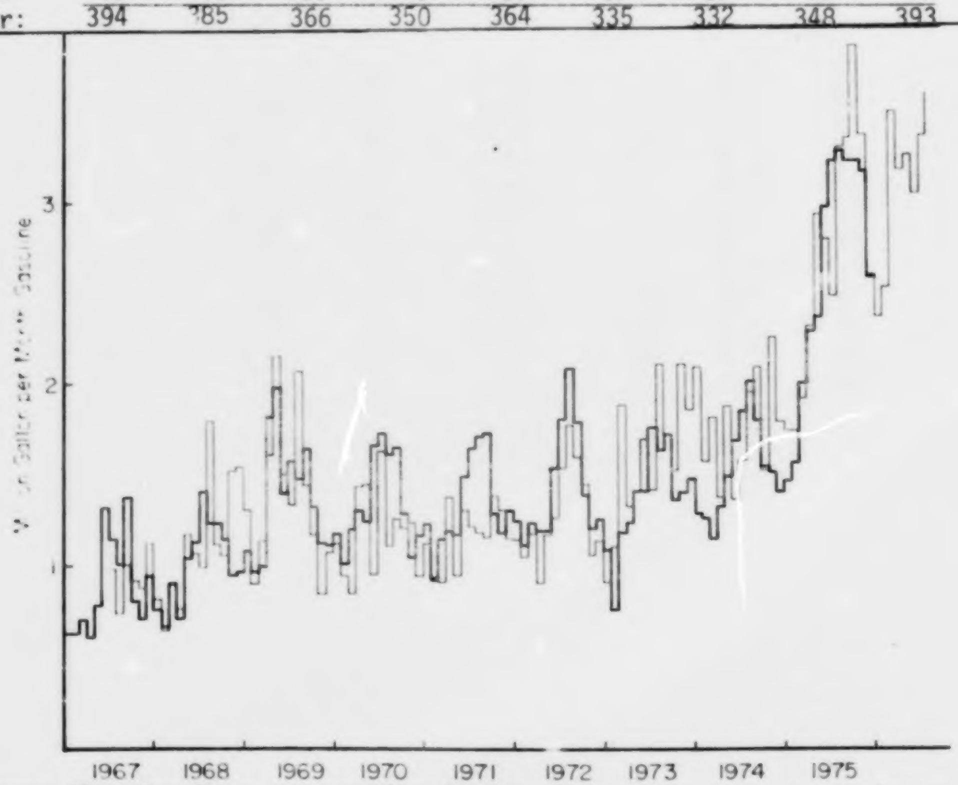

Figure 48. Gasoline consumption in the Fairbanks area. Heavy line-adjusted tax data; light line-Alaska Railroad imports

the interior have Fairbanks as one terminus, 10% of the total aviation use was assigned to the Fairbanks area. Both the raw data for the Fourth Judicial District and the adjusted total for the Fairbanks area (0.75 x highway and marine + 0.10 x aviation) are shown in Table 11. Note that while electricity and coal consumption are overwhelmingly dominated by winter heating and lighting requirements, gasoline consumption has a clear summer peak. A much weaker and less consistent midwinter peak probably reflects the lower mileage per gallon (due in part to increased idling) at temperatures below about -25°C.

Gasoline data from periods before 1967 had been destroyed before we requested it. However, Benson (1965, 1970) had earlier obtained values for gasoline imports to Fairbanks from 1957 through 1964. His Figure 4 (which is not cumulative) is here reproduced as Figure 49. Note that the full vertical scale on this figure is equivalent to the first scale division on Figure 48.

ICE FOG: LOW TEMPERATURE AIR POLLUTION

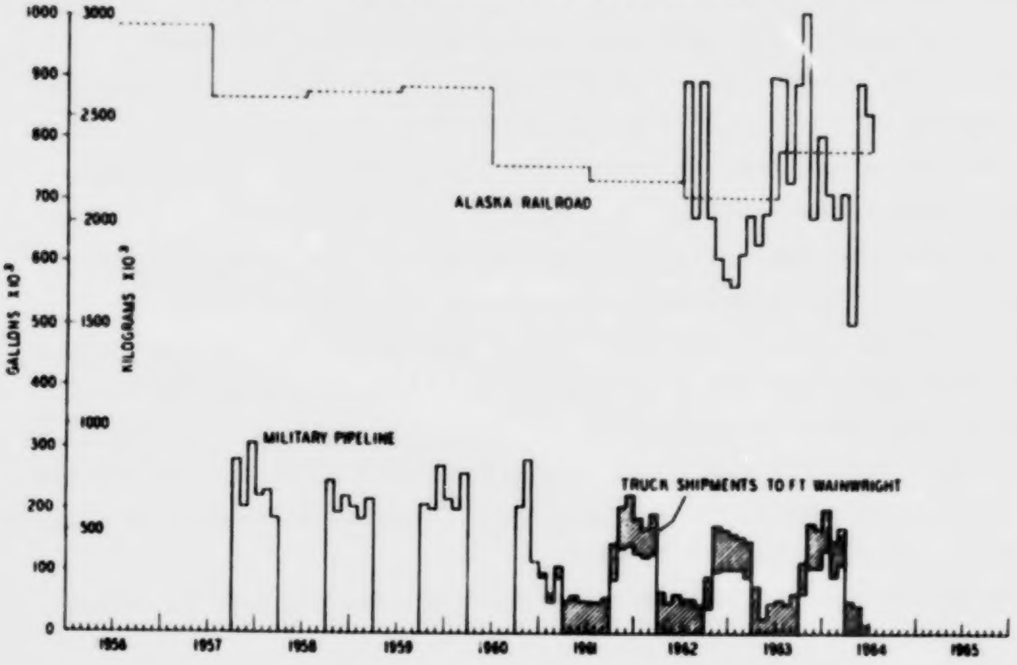

Gasoline imported to Fairbanks and Ft. Wainwright.

Figure 49. Gasoline imported to Fairbanks and Fort Wainwright prior to 1965 (not cumulative).

FUEL OIL

Fuel oil is imported both by the Alaska Railroad (ARR) and by truck. ARR data were obtained without difficulty, but figures for total truck shipments were unobtainable. Yearly total figures from the Federal Energy Administration for 1974, compared with ARR data, made it clear that truck shipments could not be ignored. Total fuel oil consumption was therefore calculated from data on use rather than imports.

Fuel oil is used as a motor fuel, as a heating fuel for buildings, and for electricity generation (primarily as peaking power). Sources of data were: the Alaska Dept. of Revenue for highway and marine diesel consumption in the Fourth Judicial District; the eight fuel oil companies currently operating in Fairbanks for heating oil; and GVEA, MUS, and Fort Wainwright for power generation oil use.

Diesel fuel is used primarily for trucks and heavy equipment and has a substantially greater role than gasoline in long-distance transport. Furthermore, the use of diesel fuel outside of the Fairbanks area increased greatly during both the initial transport of material to the North Slope in 1969-70 and the actual construction of the Alaska Pipeline. We estimated that under normal conditions (e.g., 1967), 60% of the diesel fuel for motor
We also assumed that the ratio of diesel to gasoline use in the Fairbanks area had a ceiling which was estimated from the greatest ratios of tax figures observed in normal years. Table 12 shows these ratios year by year; the ceiling ratio was set at 0.4. The years 1970, 1971, 1974, and 1975 were adjusted to this ratio by multiplying the basic 60% figure by 0.4 divided by the calculated ratio for that year. The multiplier figures for the fraction of the total diesel use in the Fourth Judicial District assumed to be consumed in Fairbanks are also given in Table 12.
use would be consumed in the Fairbanks area (approximately a 50 km radium).

TABLE 11. FAIRBANKS AREA GASOLINE CONSUMPTION (THOUSANDS OF GALLONS). SEE TEXT FOR EXPLANATION OF ADJUSTMENT.

Month	Air	Marine & Highway	Adjusted Total	Air	Marine & Highway	Adjusted Total	Air	Marine & Highway	Adjusted Total
	1967:			**1970**:			**1973**:		
J	104	825	629	148	1557	1883	121	1440	1092
F	109	825	630	162	1333	1016	101	1000	760
M	155	925	709	357	1574	1216	127	1556	1180
A	166	792	611	369	1694	1307	139	1639	1243
M	204	1019	785	322	1628	1253	200	1858	1414
J	310	1723	1323	442	2164	1667	438	1818	1407
J	311	1492	1150	298	2275	1736	342	2304	1762
A	263	1321	1017	277	2118	1616	397	2137	1642
S	191	1824	1387	281	2172	1657	695	2221	1735
O	91	1072	813	124	1705	1291	157	1789	1357
N	61	933	706	89	1392	1053	148	1869	1417
D	111	1242	943	68	1552	1171	176	1957	1485
Y	2076	13994	10703	2935	21165	16167	3039	22229	16976
	1968:			**1971**:			**1974**:		
J	91	1001	760	57	1644	1239	171	1704	1295
F	80	877	666	64	1242	938	99	1671	1263
M	115	1205	915	85	1518	1147	182	1520	1158
A	150	934	715	153	1569	1192	281	1734	1329
M	140	1376	1046	137	1551	1177	391	1939	1493
J	263	1480	1136	332	1950	1496	568	2177	1690
J	309	1836	1408	364	2154	1652	656	2391	1859
A	314	1617	1244	310	2245	1715	654	2608	2021
S	267	1620	1242	317	2275	1738	664	2312	1800
O	255	1500	1151	121	1711	1295	381	2013	1548
N	181	1247	953	72	1568	1183	387	1974	1519
D	279	1255	969	43	1744	1312	357	1841	1416
Y	2444	15947	12205	2054	21172	16084	4792	23883	18391
	1969:			**1972**:			**1975**:		
J	218	1412	1081	49	1657	1248	187	1932	1468
F	431	1237	971	66	1482	1118	267	2051	1565
M	538	1261	1000	100	1643	1242	494	2602	2001
A	797	1377	1830	160	1563	1188	2224	2755	2289
M	1042	1432	1984	175	1555	1184	337	3113	2370
J	627	1782	1399	372	2008	1543	555	3898	2979
J	537	2033	1578	522	2352	1816	503	4245	3234
A	410	1916	1478	477	2732	2097	547	4306	3284
S	327	2156	1650	367	2345	1795	442	4255	3235
O	197	1747	1330	211	1823	1388	344	4261	3230
N	101	1491	1128	133	1596	1210	248	4189	3167
D	178	1471	1121	107	1672	1265	186	3428	2590
Y	5403	19315	15027	2736	22429	17095	6323	41032	31406

TABLE 12. RATIO OF TAXED YEARLY SALES OF DIESEL OIL TO THOSE OF GASOLINE FOR THE IV JUDICIAL DISTRICT. SEE TEXT FOR EXPLANATION OF THE MULTIPLIER

	Fourth J. D. Diesel/Gasoline	Multiplier for Diesel
1967	0.27	.60
1968	0.24	.60
1969	0.36	.60
1970	0.63	.40
1971	0.48	.50
1972	0.25	.60
1973	0.21	.60
1974	0.82	.30
1975	1.3	.20

Figures obtained from the Alyeska Pipeline Company confirm that their fuel use out of Fairbanks from 1968-1975 was about 60% of the total fuel taxed in the Fourth Judicial District for that period. However, it is not known how this fuel was broken down between taxed fuel, fuel on which taxes were refunded, and non-taxed fuel. (Much of the Alyeska use was off State roads.) Nor are records available for Alyeska subcontractors. Taking all this into consideration, the multipliers are probably about right, although the results could easily be off by 20 to 30%. This uncertainty is most serious during the summer months, when motor fuel consumption peaks and heat and power requirements are at a minimum. During the winter months, motor fuel is usually a small fraction of the total fuel oil consumption.

Power plant consumption of fuel oil occurs primarily at the Fairbanks peaking complex of GVEA, for which GVEA provided monthly data back to the opening of the complex in 1964. MUS has some diesel generating capacity, and figures were obtained from MUS beginning in 1967 for months in which oil use exceeded 10,000 gallons. MUS use in other months was figured at 5,000 gal/mo, but this is small relative to the uncertainty in motor use. Fort Wainwright also uses relatively small amounts of oil. The Fort Wainwright figures prior to 1975 were actually for total diesel imports via the military pipeline. Data for 1975 were actual power plant consumption figures. The two sets of data agree quite well, although the pipeline data probably have poorer time resolution.

Heating oil is the largest fraction of the total area-wide oil combustion on a yearly basis and in all seasons except summer. Eight companies are currently selling heating oil in the Fairbanks area. Three of these (including the largest single dealer) supplied us with complete or nearly complete monthly sales in gallons from 1967 through 1975. Of the remainder, two supplied 1974 and 1975 monthly data, one supplied 1975 monthly data, one (the smallest) supplied its 1975 yearly data, and one (apparently the second smallest) was only able to provide data for August and September of 1976. The 1975 monthly totals are therefore based primarily on real data and are probably accurate to within 2% or about 20,000 gal/month. Monthly data for the companies and months when real data were not available were reconstituted by taking the ratio of available monthly sales figures to those of the largest company for the same months and assuming the ratio held constant. Where enough monthly data were available to show a difference in the form of the annual curve, this was retained in the reconstruction. One company started operations in 1972, and their figures for 1972 and 1973 were reconstituted by assuming a linear increase in the fraction of sales from 0 in June 1972 to the observed fraction in Janaury 1974. It must be recognized that the figures for heating oil become steadily less reliable as they go back in time; however, the three companies for which accurate data are available throughout account for about 50% of the total.

Table 13 and Figure 50 show the monthly breakdown of fuel oil use since 1967.

Fuel oil data from prior to 1967 had been destroyed by some sources, but again the Benson (1970) figures are available from 1957 through 1964. Benson's Figure 5 is reproduced as Figure 51. Again, this is not a cumulative figure. Note that the full vertical scale on this figure is equivalent to the first scale division on Figure 50.

TABLE 13. FAIRBANKS AREA FUEL OIL CONSUMPTION, UNITS OF 10^3 GALS.
SEE TEXT FOR DATA SOURCES AND ADJUSTMENTS

		Taxed (Motor) Fuel	Adjusted Motor Fuel	Heating Oil	Power Plants			Total	ARR
					Military	MUS	GVEA		
1967	J	126	75	1252	101	53	37	1518	
	F	147	88	1125	105	26	6	1350	
	M	257	154	792	97	5	2	1050	
	A	264	158	607	46	5	6	822	
	M	250	150	415	34	5	1	605	
	J	586	352	258	21	5	0	636	
	J	472	283	215	13	5	0	516	314
	A	440	264	209	13	5	62	553	304
	S	497	298	506	13	39	13	869	847
	O	295	177	766	46	54	34	1077	781
	N	173	104	936	42	49	73	1204	1005
	D	257	154	1322	34	179	80	1769	1066
	Y	3765	2259	8406	563	430	314	11972	
1968	J	[illegible]	100	1339	50	280	126	1895	1309
	F	197	118	1169	21	79	56	1443	978
	M	323	194	809	71	23	5	1102	940
	A	124	74	685	0	12	2	773	1228
	M	325	195	379	4	11	5	594	694
	J	846	508	384	8	5	0	905	582
	J	486	292	258	8	5	3	566	262
	A	406	243	306	13	5	1	568	572
	S	351	210	618	8	5	1	842	907
	O	280	168	827	21	18	21	1055	1069
	N	177	106	1173	13	53	209	1554	1877
	D	124	74	1514	8	138	18	1752	1996
	Y	3806	2283	9452	227	634	451	13047	12414
1969	J	102	61	2076	8	176	111	2432	1463
	F	306	184	1427	17	98	43	1769	891
	M	502	301	985	4	44	60	1394	509
	A	1053	632	870	13	16	43	1574	1611
	M	1090	654	454	8	5	9	1130	1715
	J	625	375	443	0	5	9	832	1079
	J	515	309	261	8	5	10	593	637
	A	495	297	535	8	42	11	893	1313
	S	655	393	662	63	35	10	1163	1445
	O	796	478	767	8	57	29	1339	1581
	N	487	292	1426	21	98	395	2232	1787
	D	341	204	1254	8	169	13	1648	1829
	Y	6965	4179	11160	168	750	743	17000	15860
1970	J	269	107	1768	8	216	0	2099	2592
	F	429	172	1473	17	104	11	1777	1361
	M	835	334	1061	4	78	6	1483	2220
	A	1601	640	951	17	64	11	1683	1959
	M	1069	427	487	4	42	44	1004	1727
	J	1319	527	427	4	33	163	1154	589
	J	1290	516	346	4	30	51	947	713
	A	1438	575	579	4	46	11	1215	971
	S	1687	675	725	4	42	16	1462	1155
	O	1206	482	845	4	5	26	1362	1291
	N	966	386	1224	4	5	59	1678	1230
	D	1380	552	1715	147	17	33	2464	1711
	Y	13488	5395	11601	223	682	432	18333	17519

(continued)

Table 13. (Continued)

		Taxed (Motor) Fuel	Adjusted Motor Fuel	Heating Oil	Power Plants			Total	ARR
					Military	MUS	GVEA		
1971	J	946	473	2006	8	5	40	2532	1846
	F	738	369	1797	4	11	4	2185	1600
	M	1574	787	1426	8	15	16	2252	1356
	A	673	336	1071	4	5	3	1419	1407
	M	251	125	769	8	5	21	928	967
	J	628	314	276	4	5	86	685	967
	J	2766	1383	237	3	5	21	1649	822
	A	1338	669	489	4	29	10	1201	840
	S	507	253	655	4	85	123	1120	1495
	O	396	198	811	3	5	19	1036	2186
	N	185	93	1468	5	5	158	1729	1583
	D	231	116	1946	6	5	492	2565	1313
	Y	10233	5116	12951	62	180	992	19301	16382
1972	J	111	67	1910	6	31	590	2604	1138
	F	181	109	1681	3	5	576	2374	1125
	M	427	256	1473	4	32	289	2104	1308
	A	429	257	1064	3	15	9	1348	1591
	M	363	218	623	6	5	277	1129	1052
	J	654	393	397	3	5	105	903	649
	J	822	493	346	8	5	107	959	519
	A	701	421	451	4	66	5	947	1344
	S	979	587	820	4	20	208	1639	1496
	O	560	336	1064	4	16	74	1494	1410
	N	293	176	1565	4	5	248	1998	1416
	D	156	93	1671	8	5	670	2447	2393
	Y	5645	3387	13065	58	260	3158	19928	15441
1973	J	374	224	2591	8	33	1053	3909	1400
	F	139	83	1854	8	5	525	2475	1998
	M	100	60	1485	8	5	640	2198	1221
	A	110	66	1001	8	5	44	1124	702
	M	455	273	715	8	5	5	1006	793
	J	602	360	422	8	5	9	804	1316
	J	700	420	466	13	104	13	1016	777
	A	738	443	688	8	133	22	1294	963
	S	606	364	806	13	13	315	1511	830
	O	544	326	1372	8	5	398	2109	1885
	N	254	153	1933	13	14	619	2732	1813
	D	264	159	2278	8	98	585	3128	1414
	Y	4878	2927	15610	113	425	4227	23302	15112
1974	J	312	94	2549	8	25	681	3357	1710
	F	487	146	2638	17	29	770	3600	1376
	M	1758	528	1908	8	5	236	2685	2155
	A	808	242	1235	8	5	145	1635	742
	M	1056	317	716	21	5	26	1085	1203
	J	1752	525	658	13	11	4	1211	923
	J	2024	607	590	13	13	25	1248	872
	A	1867	560	917	13	236	67	1793	960
	S	2376	713	1004	21	47	197	1982	1063
	O	2339	702	1782	38	36	170	2728	1524
	N	2066	620	2106	42	5	620	3393	1902
	D	2823	847	2585	34	5	1047	4518	2033
	Y	19668	5900	18688	235	422	3986	29231	16463
1975	J	2279	456	3391	54	104	1686	5691	3401
	F	2991	598	2572	19	46	1008	4243	2495
	M	4250	850	2018	22	12	1069	3971	2618
	A	4361	872	1769	17	66	485	3209	2730
	M	4008	802	927	0	8	467	2204	2748
	J	4640	928	925	0	4	88	1945	1432
	J	3959	792	803	0	2	89	1686	1149
	A	4966	993	992	0	5	474	2464	1735
	S	5780	1156	1443	24	4	829	3456	1768
	O	5994	1199	2105	24	23	1159	4510	3863
	N	5267	1253	3284	36	24	2018	6615	3650
	D	3986	797	3322	41	89	1781	6030	4229
	Y	53420	10684	23550	237	385	11152	46008	31818

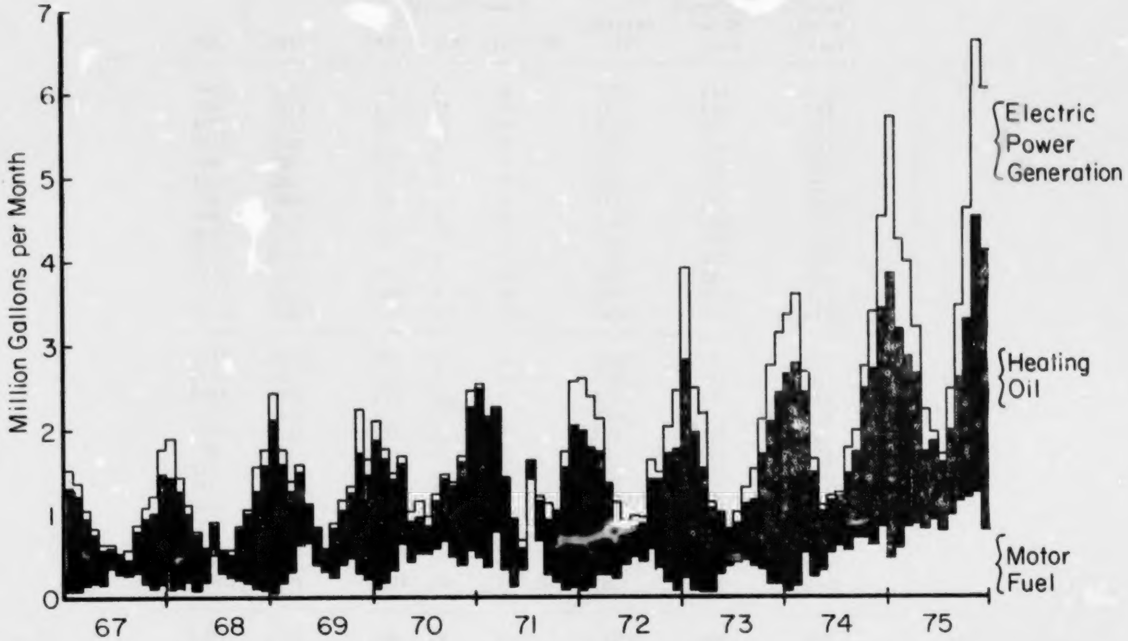

Figure 50. Cumulative fuel oil use in the Fairbanks area.

TOTAL ENERGY

The total energy derived from these fuels was calculated in terms of million KWH/month. Healy electricity was included as generated. Figures obtained from Ft. Wainwright indicated that coal as delivered (including dirt, non-coal matrix, snow, etc.) had an energy content of about 3500 KWH/ton, which was used to convert coal consumption to total energy production. (Note that this includes waste heat; actual electricity generation runs closer to 1000 KWH/ton.) The conversion factors for oil and gasoline were both based on heats of combustion of 10^7 cal/kg, which gave 34.8 KWH/gal for gasoline and 38 KWH/gal for fuel oil. The resulting total energy use for the Fairbanks area is given in Table 14, together with mean monthly temperatures. The conversion factors given above were used on the data from Tables 7, 10, 11, and 13 to arrive at the data of Table 14 which applies to most of the Fairbanks North Star Borough. The data from Table 14 are plotted in Figure 52. Note that the monthly mean temperatures are plotted inverted to facilitate comparison with fuel use.

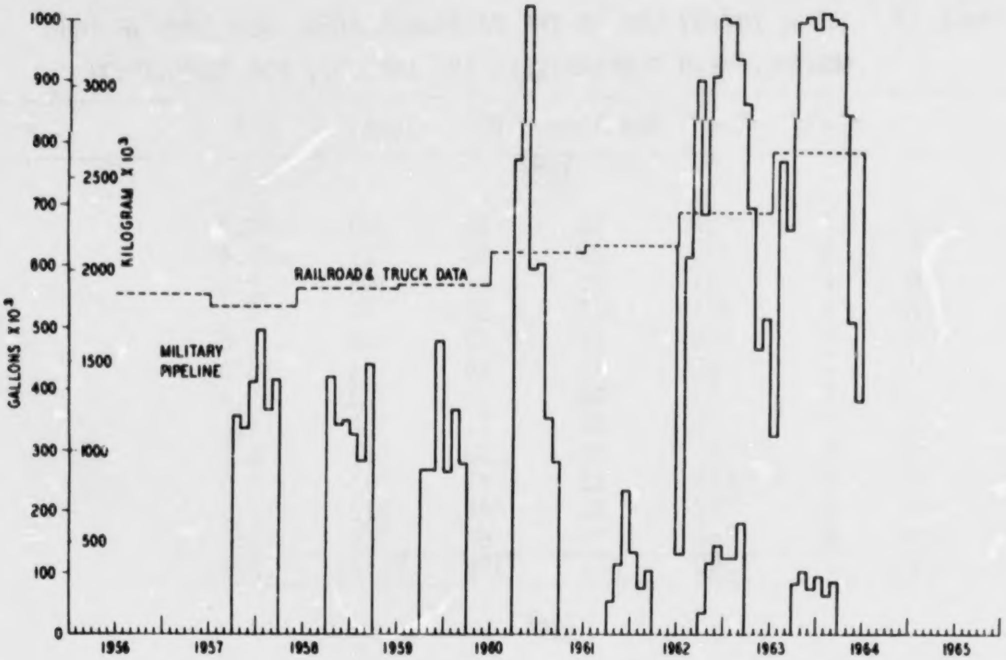

Fuel oil imported to the Fairbanks area. All fuel tanks at Ladd AFB were filled by the Air Force before the base was turned over to the Army, resulting in abnormally high monthly rates near the end of 1960.

Figure 51. Fuel oil imported to the Fairbanks area prior to 1965 (not cumulative).

BREAKDOWN OF ENERGY USE

Per capita energy use was calculated for five months--January, June, and December of 1971 and June and November of 1975. The population of the Fairbanks North Star Borough from 1969 through 1972 was 45,000 ± 1,000, and 45,000 was used for the 1971 months. By 1975, the population was estimated (by the Borough) at around 65,000. The resulting per capita energy consumptions for summer and winter are shown in Table 15. Although there is an apparent increase in per capita energy use from 1971 to 1975, the increase is almost entirely in transport use. This is probably the least reliable portion of the energy inventory and the portion most susceptible to systematic errors associated with pipeline construction, so the increase shown should not be taken too seriously.

TABLE 14. TOTAL ENERGY USE IN THE FAIRBANKS AREA, MILLIONS OF KWH
MONTHLY MEAN TEMPERATURES ARE INCLUDED FOR COMPARISON

	Healy	Coal	Gasoline	Oil	Total	$\overline{T}$°C
			1967			
J	0	163	22	58	243	-26.2
F	0	148	22	51	221	-21.6
M	0	131	25	40	196	-12.3
A	0	121	21	31	173	- 0.2
M	0	106	27	23	156	7.6
J	0	82	46	24	152	16.6
J	0	72	40	20	132	15.5
A	0	76	35	21	132	14.6
S	0	80	48	33	161	8.2
O	0	116	28	41	185	- 4.0
N	0	142	25	46	213	-12.5
D	0	154	33	67	254	-18.6
Y	0	1390	372	455	2217	- 2.8
			1968			
J	0	166	26	72	264	-23.9
F	4	152	23	55	234	-20.6
M	7	114	32	42	195	-10.7
A	6	102	25	29	162	- 1.6
M	3	96	36	23	158	- 8.6
J	8	65	40	34	147	15.3
J	7	64	49	22	142	18.8
A	4	82	43	22	151	14.7
S	4	88	43	32	167	6.0
O	6	111	40	40	197	- 5.5
N	1	145	33	59	238	-16.5
D	8	155	34	67	264	-27.6
Y	58	1341	425	496	2320	- 3.6
			1969			
J	6	171	38	92	307	-32.6
F	6	136	34	67	243	-21.9
M	6	128	35	53	222	-12.1
A	6	104	39	60	209	2.3
M	8	85	41	43	177	9.6
J	7	84	49	32	172	18.2
J	6	74	55	23	158	15.2
A	7	80	51	34	172	9.9
S	8	80	57	44	189	9.5
O	10	97	46	51	204	1.1
N	13	125	39	85	262	-17.1
D	15	122	39	63	239	-15.6
Y	97	1283	523	646	2549	- 2.8

(continued)

Table 14 (Continued)

	Healy	Coal	Gasoline	Oil	Total	$\bar{T}$°C
			1970			
J	16	143	41	80	280	-26.8
F	13	110	35	68	226	-13.3
M	13	106	42	56	217	- 6.2
A	11	95	45	64	215	0.0
M	9	89	44	38	180	11.0
J	5	72	58	44	179	14.4
J	10	65	60	36	171	16.9
A	11	69	56	46	182	13.8
S	12	85	58	56	211	4.9
O	13	109	45	52	219	- 7.3
N	12	119	37	64	232	-11.9
D	15	160	41	94	310	-23.2
Y	140	1224	563	697	2624	- 2.2
			1971			
J	16	187	43	96	342	-35.4
F	15	127	33	83	258	-20.3
M	17	128	40	86	271	-18.6
A	14	93	41	54	202	- 3.0
M	11	85	41	35	172	8.5
J	0	85	52	26	163	17.4
J	9	69	57	63	198	16.1
A	12	71	60	46	189	13.4
S	12	82	60	43	197	7.0
O	15	98	45	39	197	- 2.3
N	16	117	41	66	240	-17.5
D	15	132	46	97	290	-21.0
Y	153	1275	560	733	2721	- 4.5
			1972			
J	17	141	43	99	300	-26.9
F	11	128	39	90	268	-23.4
M	14	128	43	80	265	-19.3
A	16	94	41	51	202	- 6.2
M	10	80	42	43	175	8.5
J	11	59	54	34	158	15.2
J	11	60	63	36	170	18.0
A	14	64	73	36	187	14.9
S	9	83	62	62	216	4.5
O	16	94	48	57	215	- 2.9
N	16	111	42	76	245	-13.9
D	15	130	44	93	282	-19.0
Y	61	1174	595	757	2687	- 4.1

(continued)

Table 14 (continued)

	Healy	Coal	Gasoline	Oil	Total	$\bar{T}$°C
			1973			
J	17	137	38	149	341	-27.9
F	15	113	26	94	248	-18.6
M	10	117	41	84	252	-11.2
A	15	92	43	43	193	1.8
M	14	75	49	38	176	10.3
J	12	61	49	31	153	15.8
J	13	58	61	39	171	16.7
A	14	67	57	49	187	12.8
S	10	86	60	57	213	8.5
O	13	105	47	80	245	- 3.8
N	17	120	49	104	290	-18.1
D	17	129	52	119	317	-19.6
Y	166	1160	574	885	2786	- 2.8
			1974			
J	17	137	45	128	327	-27.0
F	16	125	44	137	322	-27.7
M	16	123	40	102	281	-13.6
A	12	87	46	62	207	1.6
M	15	71	52	41	179	10.8
J	14	58	59	46	177	14.8
J	14	64	65	47	190	17.5
A	15	67	70	68	220	15.1
S	11	81	63	75	230	10.8
O	18	114	54	104	290	- 5.9
N	18	128	52	129	327	-17.4
D	17	160	49	172	398	-24.1
Y	184	1217	640	1111	3152	- 3.8
			1975			
J	19	163	51	216	449	-26.4
F	17	145	54	161	377	-19.6
M	18	135	70	151	374	-10.8
A	17	104	80	122	323	- 0.9
M	12	95	82	84	273	12.0
J	16	82	104	74	276	17.4
J	16	71	113	64	264	20.2
A	15	74	114	94	297	13.4
S	12	96	113	131	352	7.7
O	18	107	112	171	408	- 4.5
N	18	140	110	251	519	-22.2
D	18	164	90	229	501	-26.8
Y	194	1378	1093	1748	4413	- 3.4

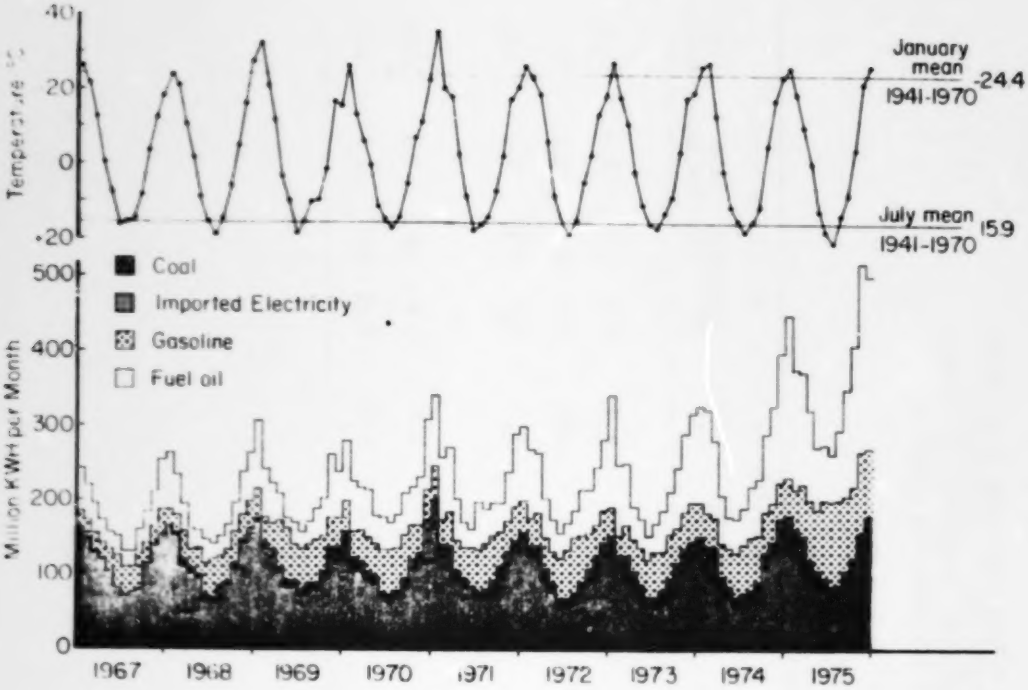

Figure 52. Total cumulative energy use in the Fairbanks area broken down by fuel type and compared with mean monthly temperatures.

An additional breakdown of total energy use for 1973-75 is given in Table 16, in which mobile sources (taxed motor fuel), dispersed stationary sources (heating oil and electricity), concentrated stationary sources, and the military base are listed separately. The first two categories are self-explanatory. Concentrated sources were the MUS and GVEA power plants. (The U. of A. plant is primarily a heating plant, and its entire output was included in the dispersed power.) Comparison of generation and fuel consumption figures for the major utilities gave approximately 9 KWH/gal of diesel oil and 1000 KWH/ton of coal. The remaining energy is mostly dissipated locally in stack gases (from oil-fired plants) and in cooling water released to the Chena River (from coal-fired plants) although MUS does have some steam lines to the downtown area. Using the previous total energy contents of the two fuels, the waste heat for the two fuels separately was calculated at 29 KWH/gal of oil and 2500 KWH/ ton of coal. The total waste heat, however, was calculated as energy content of fuel minus the electrical energy generated.

TABLE 15. AVERAGE POWER CONSUMPTION PER PERSON (INCLUDING WASTE HEAT) IN THE FAIRBANKS AREA FOR 3 WINTER AND 2 SUMMER MONTHS. JANUARY 1971 WAS INCLUDED BECAUSE OF THE RECORD LOW MONTHLY TEMPERATURE: DECEMBER 1971 AND NOVEMBER 1975 SHOULD BE APPROXIMATELY COMPARABLE.

			Total Energy		Breakdown by fuels: all in KWH person^{-1}							
						Power Plant			Transport			
	$\bar{T}$,°C	Population (thousands)	Consumption 10^3 KW	KW/ person	Electricity (Healy)	Coal	Oil	Heating Oil	Oil	Gas	Total Stationary	Total Mobile
Jan 1971	-35.4	45	460	10.2	0.5	5.6	0.05	2.3	0.5	1.3	8.4	1.8
Dec 1971	-21.0	45	390	8.7	0.4	3.9	0.6	2.2	0.1	1.4	7.1	1.5
Nov 1975	-22.2	65	721	11.1	0.4	3.0	1.7	2.7	1.0	2.3	7.8	3.3
June 1971	17.4	45	226	5.0	0	2.6	(0.1)	0.3	0.4	1.6	3.0	2.0
June 1975	17.4	65	383	5.9	0.3	1.8	0.07	0.75	0.75	2.2	2.9	3.0

TABLE 16. BREAKDOWN BY POINT OF RELEASE OF ENERGY USED IN THE FAIRBANKS AREA. ALL FIGURES IN MILLION KWH PER MONTH OR YEAR

	Mobile			**Dispersed Stationary**					**Concentrated** (power plant waste heat)			**Military**
	Oil	Gasoline	Total	Oil	Healy Elec.	Local Elec.	UofA	Total	Oil	MUS Coal	Total	
1973												
J	9	38	47	98	17	22	15	152	31	33	66	75
F	3	26	29	70	15	16	12	113	15	28	43	61
M	2	41	43	56	10	19	12	97	19	29	47	64
A	3	43	46	38	15	9	7	69	1	26	29	48
M	10	49	59	27	14	7	5	53	0	17	17	45
J	14	49	63	16	12	7	4	39	0	18	19	32
J	16	61	77	18	13	6	3	40	3	17	22	32
A	17	57	74	26	14	6	5	51	4	18	25	37
S	14	60	74	31	10	12	7	60	10	23	33	47
O	12	47	59	52	13	14	12	91	12	24	35	60
N	6	49	55	73	17	16	15	121	18	29	49	65
D	6	52	58	87	17	14	15	133	20	27	50	76
Y	112	572	684	592	166	147	112	1017	135	291	434	642
1974												
J	4	45	49	97	17	18	16	148	20	31	52	77
F	6	44	50	100	16	17	15	148	23	25	49	75
M	20	40	60	73	16	14	13	116	7	30	37	69
A	9	46	55	47	12	11	8	78	4	24	28	47
M	12	52	64	27	15	8	6	56	1	20	21	38
J	20	59	79	25	14	7	4	50	0	18	20	28
J	23	65	88	22	14	7	4	47	1	17	17	37
A	21	70	91	35	15	7	4	61	9	17	28	39
S	27	63	90	38	11	12	5	66	7	24	31	43
O	27	54	81	68	18	13	11	110	6	27	32	67
N	24	52	76	80	18	20	13	131	18	33	51	70
D	32	49	81	98	17	24	15	154	31	37	67	96
y	224	640	864	710	184	158	114	1166	128	303	435	686
1975												
J	17	51	68	129	19	27	16	191	52	33	87	100
F	23	54	77	98	17	21	13	149	31	29	59	87
M	32	70	102	77	18	22	12	129	31	30	61	77
A	33	80	113	67	17	14	9	107	16	25	42	57
M	30	82	112	35	12	14	6	67	14	24	37	52
J	35	104	139	35	16	10	5	66	3	23	26	41
J	30	113	143	31	16	10	5	62	3	22	24	32
A	37	114	151	38	15	13	5	71	14	21	35	36
S	44	113	157	55	12	16	12	95	24	23	47	50
O	46	112	158	80	18	22	14	134	34	28	62	51
N	48	110	158	125	18	33	14	190	59	34	92	76
D	30	90	120	126	18	31	15	190	54	39	95	90
Y	405	1093	1498	896	194	233	126	1449	335	331	667	749

The military plants are heating as well as power plants, and their total output was simply calculated at 3500 KWH/ton of coal and 38 KWH/gal of fuel oil, fuel oil contributing less than 1 million KWH in most months.

During 1975, the energy use peaked at 519 million KWH per month in November (=720,000 KW or 1.03 x 10^{10} cal/min). The minimum energy use, in an unusually warm July, was 264 million KWH per month (=355,000 KW or 0.51 x 10^{10} cal/min). For practical computational purposes, the energy consumption in Fairbanks may be set at 10^{10} cal/min in a cold winter month and 0.5 x 10^{10} cal/min in a warm summer month.

PRODUCTION OF UNAVOIDABLE COMBUSTION PRODUCTS

Water vapor (H_2O) and carbon dioxide (CO_2) production are dependent on fuel consumed. Benson (1970) calculates that 1.38 kg of H_2O and 3.10 kg of CO_2 are produced for each kg of gasoline burned, 1.33 kg of H_2O and 3.13 kg of CO_2 are produced for each kg of fuel oil, and 0.68 kg of H_2O and 2.36 kg of CO_2 are produced for each kg of coal (as delivered). As a gallon of gasoline weighs 2.99 kg, a gallon of fuel oil weighs 3.36 kg and a ton of coal weighs 907.2 kg, the H_2O and CO_2 produced by complete combustion may be obtained by multiplying the numbers in Tables 8, 9, 10, 11, and 13 by the numbers in Table 17. Table 18 shows some representative calculations of CO_2 and H_2O for 1975. These values do not include H_2O release from activities other than fuel consumption.

TABLE 17. PRODUCTION OF H_2O AND CO_2 PER UNIT OF FOSSIL FUEL BURNED (COMPLETE COMBUSTION ASSUMED)

Fuel	H_2O (thousand kg)	CO_2 (thousand kg)
Coal (tons)	.617	2.14
Gasoline (thousand gallons)	4.13	9.28
Fuel Oil (thousand gallons)	4.47	10.52

TABLE 18. H_2O AND CO_2 (IN MILLIONS OF KG/MONTH) GENERATED BY FOSSIL FUEL COMBUSTION IN THE FAIRBANKS AREA IN 1975. MONTHLY TOTALS EXCLUDE COAL HEAT.

	Mobile		Oil Heat		Coal Heat		Power Plants		Total	
	H_2O	CO_2	H_2O	CO_2	H_2O	CO_2	H_2O	CO_2	H_2O	CO_2
J	8.1	18.4	15.2	35.7			36.1	115.9	59	170
F	9.1	20.8	11.5	27.1			29.4	96.5	50	144
M	12.1	27.5	9.0	21.2			27.7	90.8	49	140
A	13.4	30.4	7.9	18.6			20.2	67.2	41	116
M	13.4	30.4	4.1	9.8			18.2	60.8	36	101
J	16.5	37.4	4.1	9.7			14.2	48.7	35	96
J	16.9	38.3	3.6	8.5			12.4	42.7	33	89
A	18.0	40.9	4.4	10.4			14.7	48.5	37	100
S	18.5	42.2	6.5	15.2			20.1	65.5	45	123
O	18.7	42.6	9.4	22.1			23.6	75.8	52	141
N	18.7	42.6	14.7	34.6			33.2	104.9	67	182
D	14.3	32.4	14.9	35.0			36.4	116.8	66	184
Y	178	404	105	248	9	30	286	935	578	1616

SECTION 9

THEORY

INTRODUCTION

There are several empirical relationships between heat island intensity, ΔT_{max}, and the observed meteorological and geographical setting (Landsberg, 1974). Oke (1972) suggested two relationships; first, $\Delta T_{max} = \phi^{1/4}/4v^{1/2}$, where ϕ is population and v is mean wind speed. He also suggested that the maximum heat island in the case of no wind and no cloud cover is given by $\Delta T_{max} = 2.96 \log \phi - 6.41$. Ludwig (1970) placed more emphasis on lapse rate in the first 100 m,[*] with the equation $\Delta T_{max} = \phi^{1/4}\ (.0633-.298\ \frac{dT}{dp})$ where $\frac{dT}{dp}$ is the lapse rate in °C/mb. If all three equations are applied to the Fairbanks area (population 65,000) with an assumed temperature of -20°C, a surface pressure of 1000 mb, a 100 m inversion of 15°C ($\frac{dT}{dp} = -1.11$) and a wind speed of 1 m $\sec^{-1}$ we obtain:

$\Delta T_{max} = 4.0°C$ (Oke, v = 1)
$\Delta T_{max} = 7.8$ (Oke, clear and calm)
$\Delta T_{max} = 6.3°C$ (Ludwig)

The Fairbanks heat island observed in the present study with clear night skies, snow cover and light winds has very rarely been less than 10°C, and has on occasion been measured as 14°C. This discrepancy may be attributed to the fact that the combination of lapse rate, wind speed and per capita heat production at Fairbanks is completely outside the range for which the empirical models were developed. Indeed, these factors combined with the absence of solar radiation in winter make Fairbanks an ideal place to study certain aspects of the urban heat island.

---

[*] This refers to the difference in air temperatures measured at the ground and at an altitude of 100 m. The actual air temperature profile is often complex and involves stronger gradients in places as discussed later in the text.

Computer simulations have been carried out in considerably more detail (e.g., Leahey and Friend, 1971, Atwater and Pandolfo, 1975). However, these do not generally give the form of the dependence on such variables as population, wind speed and lapse rate, which is what we intend to do here. The approach used is similar to that of Leahey and Friend (1971).

Physically, the intensity of a heat island is determined by heat addition to the air by the substrate (which is strongly influenced by how long the air stays over the city, i.e., wind speed), by how this heat is distributed vertically and (if the air contains gasses or aerosols active in the thermal infrared) by increased radiative energy loss from the warmer air. Increased radiative loss from the substrate will influence the amount of heat available for transfer to the air, but will also be influenced by the substrate temperature, which is tied to the air temperature. We assume that in Fairbanks in winter, with very low H_2O content of the air, thermal radiation from the air need be considered only if fog (ice fog) is present. At zero background wind speed, no fog, and a fixed total energy loss from the substrate, the intensity of the steady-state heat island will be determined by a balance among three factors: Higher infrared radiative loss from the warmer city substrate (buildings, pavement, automobiles, and air-warmed natural surfaces), increased convective energy transfer from the substrate to the air, and air exchange with the surroundings induced by the horizontal temperature gradient around the city. If fog, other aerosols or gases with strong infrared absorption bands are present in quantity, the net radiative loss from the substrate will be partially or wholly absorbed by the local air. The upper part of the optically active layer will then re-radiate this energy away from the city. If the temperature at the top of this layer approximates the substrate temperature (as will normally be true for thin layers) the total radiative energy loss will be the same with or without fog, even though the mechanics of the energy loss differ somewhat. The background lapse rate, provided it is stable, would affect the length of time required to reach equilibrium but should have little effect on the equilibrium temperature in the zero-wind case. The zero-wind case, combined with fog, but neglecting the heat island circulation, was considered by Bowling (1970).

The case with wind but neglecting radiative cooling has been considered by Summers (1965). The basic assumption is that stable air moving over the urban surface is heated uniformly from below. The heating results in an adiabatic lapse rate reaching from the ground up to some height Z at which it intersects the undisturbed temperature profile. The amount of temperature change is determined by the requirement that the change in the thermal energy of the air column,

$\int_0^Z \Delta T(z)\rho c_p dz$, be equal to the energy added by the heating from below. (Here z is the vertical coordinate, ρ is the density of air and c_p is the specific heat at constant pressure of air.) This approach actually overestimates the heat island intensity, as it does not allow for the increased radiative energy loss from the warm city surface. Increased radiative loss from the air is neglected for the moment. Application of the Stefan-Boltzman law shows that at -20°C, the radiative energy loss increases by $.5 \times 10^{-2}$ cal cm^{-2} min^{-1} for each degree Celsius temperature increase.

In general, the input to the steady-state nighttime heat island is a fixed energy flux, h. The substrate temperature, T, at any point is determined by how this energy flux h, is partitioned between a part, q, which heats the air, and a part lost through radiative cooling. For any particular energy flow, h, from the substrate, there will exist an ideal radiative-equilibrium heat island intensity, ΔT_{re}, at which the increase in radiative loss over the city relative to the background is just balanced by the energy flux, h, through the substrate. $T_{re} = T_o + \Delta T_{re}$ is the radiative-equilibrium temperature at a point. It must be emphasized strongly that ΔT_{re} and T_{re} are limiting values which will be observed only under certain transient conditions (e.g., a local temperature maximum along a flow line). $T = T_{re}$ implies $q = 0$, and if this condition held area-wide in the presense of any cross-isotherm wind component, no heat island could exist. The energy balance for the city may be written as

$$h = \sigma T_{re}^4 - \sigma T_o^4. \qquad (6)$$

T_o is the background temperature, assumed to be in radiative equilibrium with the sky; i.e., $T_o = T_{re}$ for $h = 0$, and σ is the Stefan-Boltzmann constant, $\sigma = 8.132 \times 10^{-11}$ cal cm^{-2} min^{-1} °K^{-4}. The relationship of T_{re} to the observed temperature T, to q and to h is shown in Figure 53.

Normally the energy flux h will vary through a city. For any given point, then, an ideal radiative-equilibrium temperature T_{re} is defined from equation (6). T_{re} is the temperature at which h is entirely radiated away, and no energy is available for transfer into the air column at that point, i.e., the Lagrangian derivative* of the air temperature, $\frac{dT}{dt}$, would be equal to zero. If the air temperature at y is less than $T_{re}(y)$ (as will normally be the case when h is increasing along the wind) convective transfer will be active and may consume a substantial portion of the available energy $(q > 0)$. If the air temperature at y is greater than $T_{re}(y)$ (as may be the case where h is decreasing along the wind) radiative cooling will occur at the surface $(q < 0)$. The difference between T_{re} and T_o, i.e., ΔT_{re}, the radiative-equilibrium heat island, may be obtained by expanding $\sigma T_{re}^4 = \sigma(T_o + \Delta T_{re})^4$ as a polynomial: $\sigma T_{re}^4 = \sigma T_o^4 + f T_o^2 \Delta T_{re} + 6T_o^2(\Delta T_{re})^2 + 4 T_o(\Delta T_{re})^3 + (\Delta T_{re})^4$. It is then apparent that if $\frac{\Delta T_{re}}{T_o} \ll 1$, $\sigma T_{re}^4 \simeq \Lambda T_o^4 + 4 T_o^3 \Delta T_{re}$, so $\sigma T_{re}^4 - \sigma T_o^4 \simeq 4 T_o^3 \Delta T_{re}$. From (6) we then have

$$\Delta T_{re} \approx h/4\sigma T_o^3 \tag{7}$$

The maximum temperature measured in a particular heat island situation in any traverse along the mean wind should satisfy equation (7) for the value of h at that particular point. Figure 54 is a cross section through a hypothetical city in which h increases to a maximum and then decreases. The wind is assumed to blow from left to right over a city with its center and maximum heat input at y =R. Note that the core of the heat island is downwind of the maximum city heat input, and that $q = 0$ and $\Delta T = \Delta T_{re}$ at the heat island core.

An expression for the heat actually transferred to the air, q, may be obtained by using equation 7. To a good approximation,

---

*i.e., the derivative calculated moving with the air column.

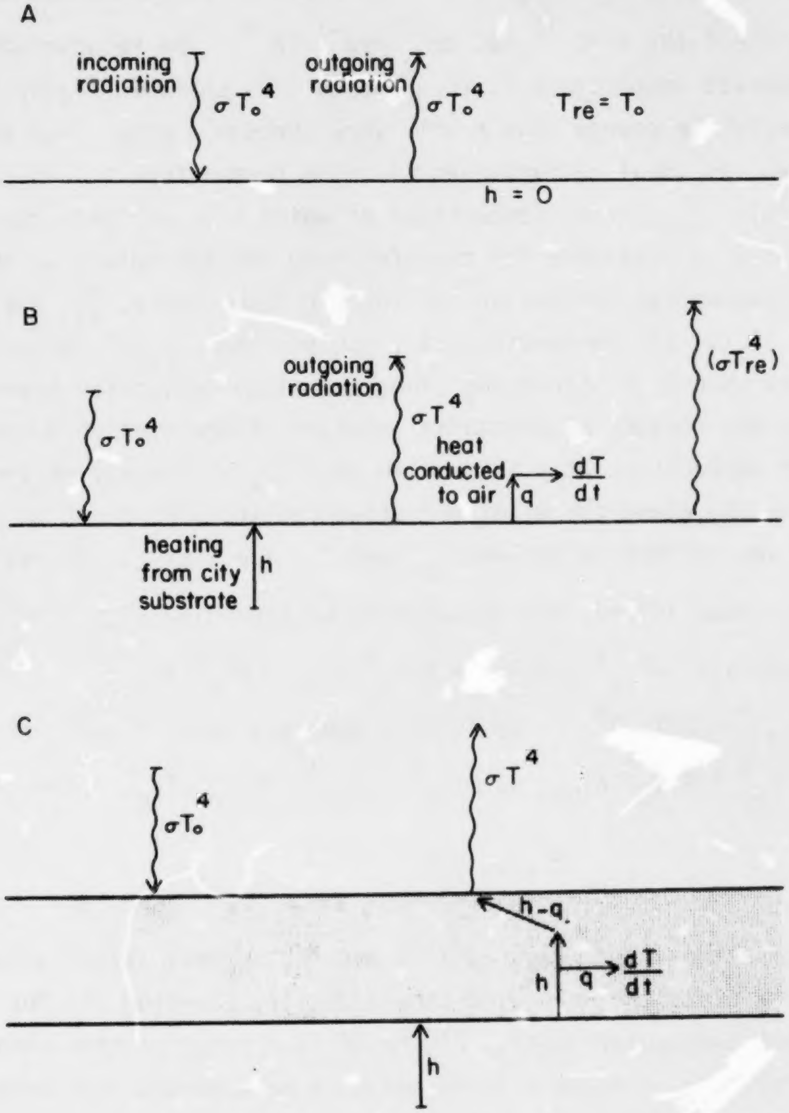
A
incoming radiation
σT_o^4
outgoing radiation
σT_o^4
$T_{re} = T_o$
h = 0
B
outgoing radiation
σT_o^4
σT^4
heat conducted to air
q
$\frac{dT}{dt}$
(σT_{re}^4)
heating from city substrate
h
C
σT_o^4
σT^4
h-q
h
q
$\frac{dT}{dt}$
h

Figure 53. Surface and fog-top energy balances for (a) clear background area; (b) clear city; (c) foggy city.

$$q = h - 4\sigma T^3 \Delta T, \qquad (8)$$

where ΔT is the difference between the temperature T measured at any point in the city, and the background temperature T_o. Note again that this ΔT is normally not ΔT_{re}, and that if $\Delta T = \Delta T_{re}$, $q = 0$.

Note that h includes all of the added heat due to the presence of the city - not only that added by human activity, but also that due to albedo differences, differences in the rates at which various substances respond to changes in their energy balances, and differences in the heat loss by evapotranspiration. Only changes in roughness are not included. Our calculations for Fairbanks will include only the man-made heating, because the other terms are believed to be small in Fairbanks in midwinter. In most climates they must be included.

In addition to neglecting the radiative effect, the previously mentioned empirical approaches neglect the possible influence of the form of the lapse rate. Thus a temperature profile which is isothermal to 90 m and capped by an inversion of 3° in 10 meters would not be expected to have the same effect as a 3° inversion in the lowest 10 meters with a 90 m isothermal layer above, even though both give identical 100 m lapse rates.

The purpose of this section is to consider theoretically two extensions of the Summers approach. The first to be considered will be the effect of the form of the lapse rate in the case where q, rather than h, is assumed to be known. Four types of temperature profiles will be considered: a simple linear profile, a logarithmic profile (inversion strength decreasing with altitude), a step function with sharp inversions separating regions of adiabatic lapse rate, and a capping inversion. The second extension involves including the radiative loss for a specific but not unreasonable case in which the equations can be handled analytically, followed by an examination of the functional dependence of the heat island intensity (measured at the city center) on population, population density, wind speed, inversion strength, and energy use per capita. The particular case considered is one in which the value of h increases linearly toward the center of a circular city and the initial lapse rate is constant with height. Many of the assumptions are similar to those of Leahey and Friend (1971), but they are applied to give an analytical result which allows consideration of the expected heat island as a function of such factors as population density.

All calculations are valid only upwind of the maximum heat island, i.e., for $q > 0$ at all points. The conditions for the radiative partition case are even more rigid, as this calculation is valid only for h increasing linearly. Downwind of the point at which q becomes 0 (i.e., where $\Delta T = h/4\sigma T^3$) if h is decreasing the substrate will be too warm for h to balance the radiative loss. If the air is clear the substrate will cool radiatively; if the air is optically active the radiation will take place from the mixed layer, as shown in Figure 54. In either case the ground level temperature will decrease downwind of the point at which q becomes 0.

The effect of the circulation induced by the heat island on the strength of the heat island is neglected throughout, although it may have considerable influence at very low wind speeds. Another assumption which must be kept in mind is that the lapse rate in the mixed layer is adiabatic, with the temperature at the base of the mixed layer being equal to that of the substrate. In actual fact, the substrate must be slightly warmer than the air and the lapse rate must be slightly superadiabatic for convective heat transfer to be possible. We here assume that the difference from the adiabatic case is small relative to the difference between the initial lapse rate and the adiabatic one. Thus the approach taken here is not applicable to initial lapse rates near the adiabatic.

Still another possible source of error is the assumption that the background temperature, T_0, is the radiative-equilibrium temperature. Heat island intensity is normally measured at 2 m, but the 2 m background temperature may be noticeably greater than that at the ground surface (up to about 5°C). As it is the ground surface which approaches, but normally does not reach, the radiative equilibrium temperature, the heat island strength predicted by the model will be slightly overestimated.

The calculations to be made assume partition of h into two fractions at the city surface. The radiative fraction is emitted directly from the substrate and lost to the system, while the conducted fraction, q, is conducted to the base of the atmosphere and then mixed convectively. Absorption and re-radiation by the atmosphere are considered negligible, and in the thin boundary layer being considered, this is a good approximation for clear air (i.e., with normal amount of CO_2 and H_2O as the only optically active

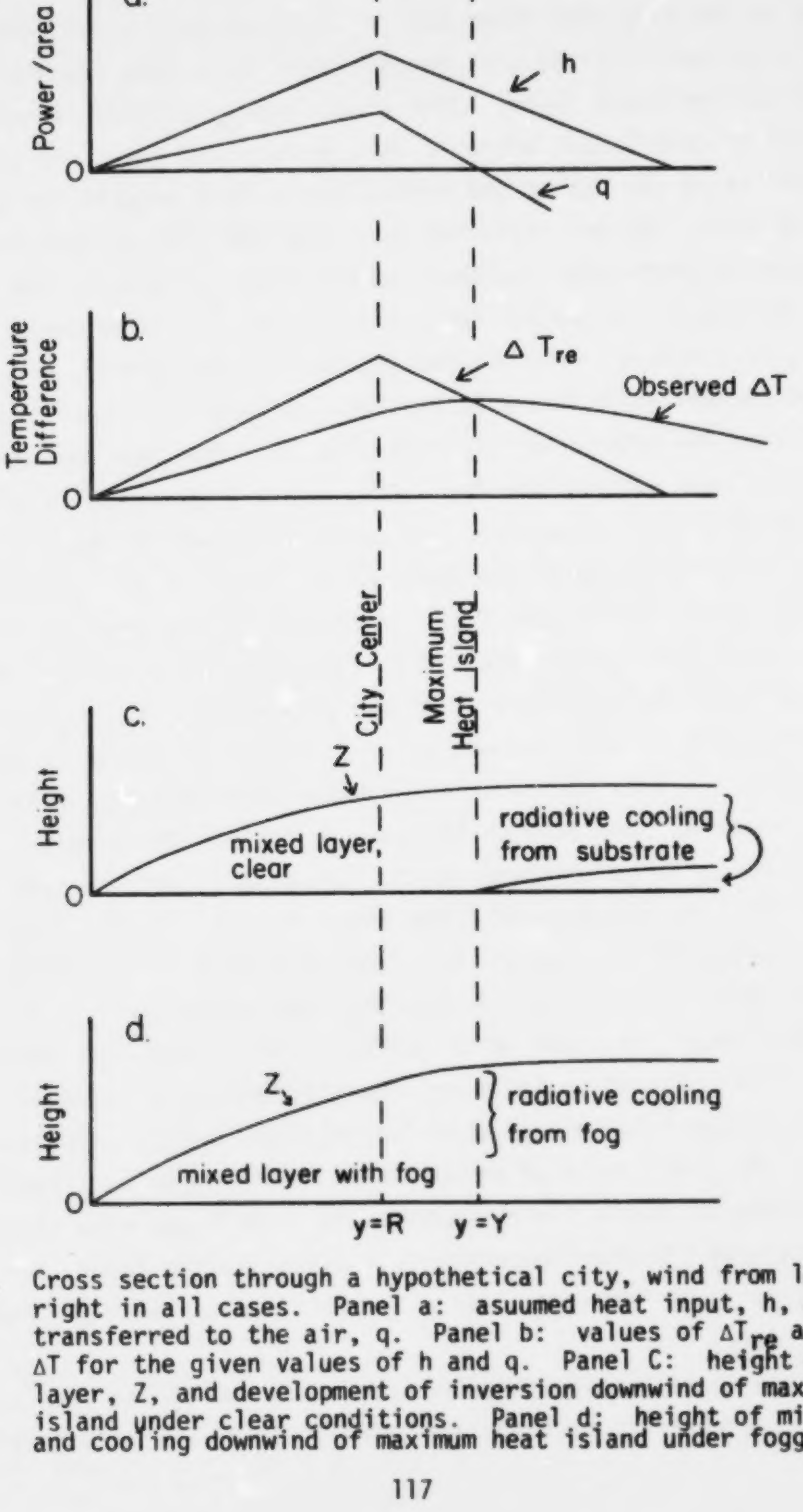
a.
Power /area
0
h
q
b.
Temperature Difference
0
ΔT_{re}
Observed ΔT
City Center
Maximum Heat Island
c.
Height
0
Z
mixed layer, clear
radiative cooling from substrate
d.
Height
0
Z
mixed layer with fog
radiative cooling from fog
y=R
y=Y

Figure 54. Cross section through a hypothetical city, wind from left to right in all cases. Panel a: asuumed heat input, h, and heat transferred to the air, q. Panel b: values of ΔT_{re} and observed ΔT for the given values of h and q. Panel C: height of mixed layer, Z, and development of inversion downwind of maximum heat island under clear conditions. Panel d: height of mixed layer, Z, and cooling downwind of maximum heat island under foggy conditions

components). In turbid air, and particularly in the extreme case of optically thick fog in the city with clear air in the background areas, the energy radiated from the substrate will be partially to totally absorbed in the lower part of the mixed layer. This excess energy will be transferred to the fog top by convection, where it will be radiated away. If the fog top (assumed to be at the top of the mixing layer) were exactly the temperature of the substrate, the net radiative loss from the city surface/mixing layer system would be unchanged, and thus the net heat addition to the system would be unchanged. In actual fact, a fog layer of finite depth heated from below must be slightly cooler at the top than at the bottom, as an adiabatic lapse rate becomes established in the fog. Because the top of the fog layer is cooler than the substrate, the radiative loss from the fog top is less than it would have been without the fog. This reduces the fraction of h which is lost by radiation and inceases q, the amount retained in the city air; the net result is an increase in the heat island intensity ΔT. However. we will neglect this affect and assume that the radiative loss from the city, and thus the energy available to heat the air, is the same with or without a fog.

In addition, the modification of the background lapse rate proceeds a little differently in the presence of fog. Figure 55 shows corresponding steps in the process of modification with and without a fog in the mixing layer. In each case the area on the diagram between the original and modified sounding is proportional to the added heat, and the heat added in the two cases is approximately the same. However, in the foggy case radiative cooling at the top, Z, will lead to a temperature below that of the unmodified sounding. In order to have the same energy gain in both the clear and the foggy cases the layer which suffers a net energy loss (horizontally shaded) must be balanced by increases (heavily vertically shaded) in the layer which enjoys a net energy gain (vertically shaded). This can only be done within the constraints of an adiabatic mixing layer by allowing the adiabatic layer to have a higher temperature. The foggy city is then predicted to have a higher temperature, a deeper mixing layer, and stronger vertical overturning than the clear one. This applies when the background area is not foggy.

Inability to find a fog-free area upwind of and at the same altitude as the city of Fairbanks is probably the primary reason why measurements of the

Fairbanks heat island showed the foggy heat island to be consistently less than the heat island under clear skies.

THE EFFECT OF THE FORM OF THE TEMPERATURE PROFILE

We now proceed to examine the effect of different forms of the lapse rate on the intensity of the heat island. For this purpose we will define a standard Cartesian coordinate system with z being the vertical coordinate

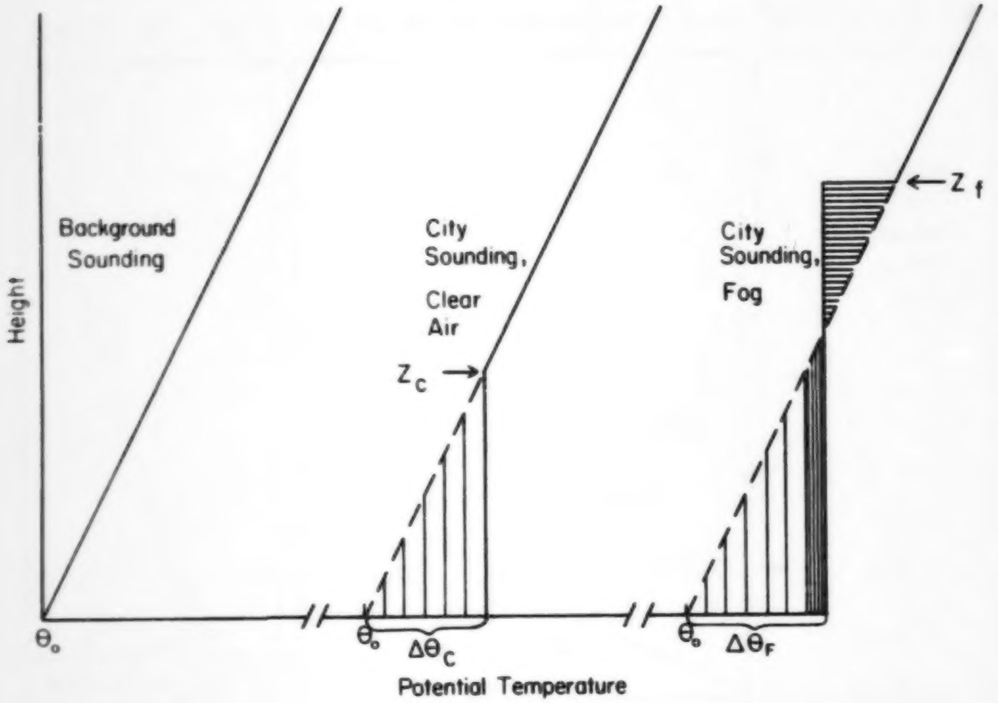
Height
Background Sounding
City Sounding, Clear Air
Z_c
City Sounding, Fog
Z_f
θ_o
θ_o
$\Delta\theta_C$
θ_o
$\Delta\theta_F$
Potential Temperature

Figure 55. City vs. background soundings for clear and city-fog cases. Both city soundings have had the same net heat addition.

and y being the coordinate along the wind, with the y axis running through the city core and the origin of the system being the upwind edge of the city. In order to simplify the calculation we will use the potential temperature $\theta(y,z)$ (neglecting the x coordinate). θ and T are related by $\theta(y,z) = \Theta + T(y,z) + .01\ z$, where z is in meters, T is in °C, and .01 is the adiabatic lapse rate, .01 $°K\ m^{-1}$. For our purposes, Θ is arbitrary, as we will be interested only in differences in θ. The heat island intensity at y is then given by $\Delta T = T(y,0) - T(0,0) = \theta(y,0) - \theta(0,0) = \Delta\theta$. Figure 56 and Table 19 are included to aid in the definition of the symbols to be used.

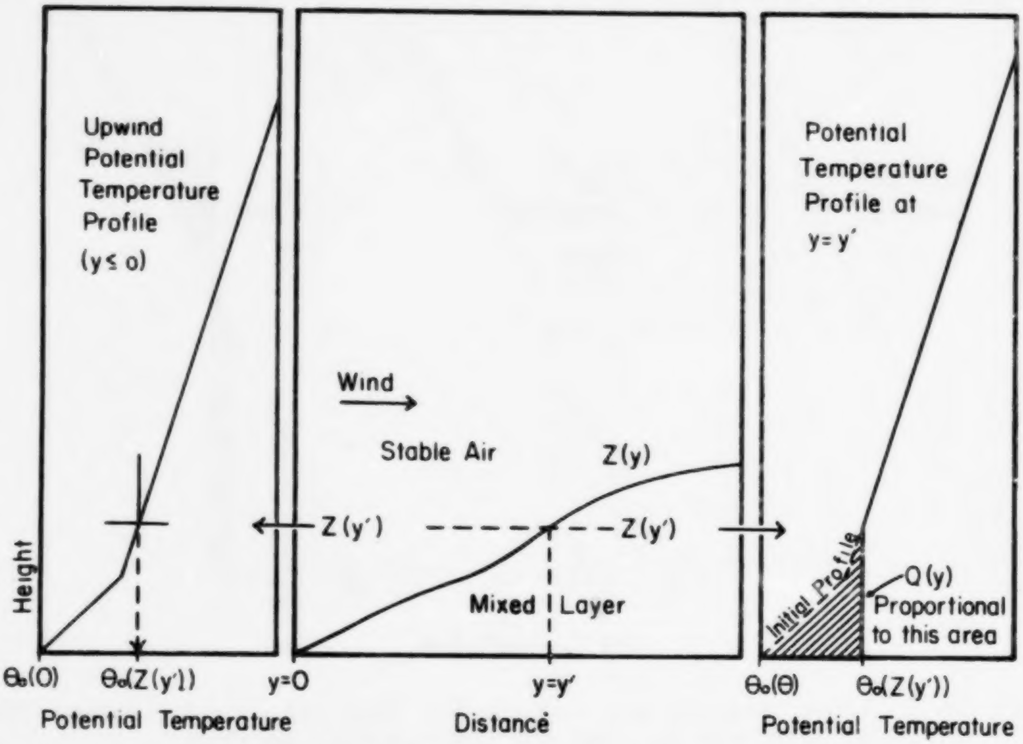

Upwind Potential Temperature Profile (y≤ o)
Height
$\Theta_0(0)$
$\Theta_0(Z(y'))$
Potential Temperature
Wind
Stable Air
Z(y)
Z(y')
Z(y')
Mixed Layer
y=0
y=y'
Distance
Potential Temperature Profile at y= y'
Initial Profile
Q(y) Proportional to this area
$\Theta_0(\Theta)$
$\Theta_0(Z(y'))$
Potential Temperature

Figure 56. Development of mixing layer as background air moves into the city. Left panel - background sounding. Center panel - cross section showing increase of Z (for non-uniform q) as air moves into city. Right panel - sounding at y = y' within the city. Shaded area = $(d-d_0)dz$ is equal to Q(y).

Let the undisturbed potential temperature as a function of height be $\theta(0,z)$, and the lapse rate be $\frac{d\theta_0}{dz} = \frac{\partial\theta}{\partial z}(0,z)$. Assume that heat is added only at the lower surface of the atmosphere, and that added heat is immediately mixed adiabatically, so that

TABLE 19. SYMBOLS USED

Variables:

$A = \dfrac{8\sigma^2 T_o^6}{\rho c_p}$ (energy length^{-1} temp^{-1} time^{-2})

$B = \Gamma/v$ (temp length^{-2} time)

c_p = specific heat of air at constant pressure

E = total energy released by heating

$h = h(y) = h(x,y)$, energy flux (energy area^{-1} time^{-1}) from the city surface

$G = \pi R^2/\phi$, area per person

P = atmospheric pressure

$q = q(y) = q(x,y)$ conductive energy flux from the city surface to the air

$Q(y) = \int_0^y \frac{q(y)}{\rho c_p v}\, dy$, the energy accumulated by a unit column of air traveling from $y = 0$ to y, divided by the volume heat capacity of the air.

T = temperature, usually in °K

T_o = background temperature

T_{max} = temperature at warmest part of heat island

T_{re} = radiative equilibrium temperature (eq 1)

$\Delta T = T - T_o$

R = radius of city

v = mean wind speed

x = horizontal coordinate perpendicular to the wind

continued

Table 19 (Cont.)

---

y = horizontal coordinate along the wind

Y = y-coordinate of the point of maximum temperature in the heat isalnd

z = height coordinate

$Z = Z(y)$ = mixing height; $Z(0) = 0$

$\gamma = \gamma(z)$ = potential lapse rate = $\frac{d\theta_o}{dz}$

$\gamma(Z) = \gamma(z) \Big|_Z$

$\theta = \Theta + T(y,z) + .01\ z$ = potential temperature

Θ = for our purposes, an arbitrary constant

ρ = air density

ϕ = population

Constants:

a = lapse rate at $z = 0$ in logarithmic profile

b = constant in logarithmic profile

C = height of base of capping inversion

J = rate of change of h along the wind

K = rate of change of q along the wind

m = ratio of heat island intensities with and without fog

z_i = layer limits in step function temperature profile

Γ = lapse rate for the linear temperature profile

γ_i = lapse rate in layer i in the step function and capping inversion temperature profiles

σ = Stefan-Boltzmann constant, = 8.132×10^{-11} cal cm^{-2} min^{-1} °K^{-4}.

$$\theta(y,z) = \theta(0,Z(y)) \qquad 0 \leq z \leq Z(y) \tag{9a}$$

$$\theta(y,z) = \theta(0,z) \qquad z > Z(y) \tag{9b}$$

$Z(y)$ is the mixing depth, and is determined as follows:

The wind is assumed to be along the y axis with speed v. The rate of heat release to the air per unit area by the substrate is $q(y)$, which gives an amount of heat addition $\frac{q(y)dy}{v}$ to a column of air with a unit basal area as it travels a distance dy. If Z is small enough that the density of air, ρ, does not vary too much with height, the energy per unit area involved in changing the height of the top of the mixed layer from $Z(y)$ to $Z(y+dy)$ is $\rho c_p\ Z(y)d\theta_y$, where $d\theta_y = \theta(0,Z(y+dy)) - \theta(0,Z(y)) = \left.\frac{d\theta_o}{dz}\right|_Z dZ(y)$, and c_p is the specific heat of air at constant pressure. If this is set equal to the added heat, $\frac{q(y)dy}{v}$, then

$$\left.\frac{d\theta_o}{dz}\right|_Z \rho c_p Z dZ = \frac{q(y)dy}{v}, \tag{10}$$

or

$$\left.\frac{d\theta_o}{dz}\right|_Z Z dZ = \frac{q(y)}{\rho c_p v}\, dy. \tag{11}$$

Since $Z = 0$ at $y = 0$,

$$\int_o^Z \left.\frac{d\theta_o}{dz}\right|_Z Z\, dZ = \int_o^y \frac{q(y)}{\rho c_p v}\, dy. \tag{12}$$

Let $\int_o^y \frac{q(y)}{\rho c_p v}\, dy = Q(y)$ (13)

and $\gamma(Z) = \left.\frac{d\theta_o}{dz}\right|_Z$. (14)

Then

$$\int Z\,\gamma(Z)dZ = Q(y). \tag{15}$$

We will consider four cases:

Case 1: linear profile

$$\theta_o(z) = \theta_o(0) + \Gamma\,z; \qquad \gamma(Z) = \Gamma = \text{const} > 0 \tag{16}$$

$$Q(y) = \int \Gamma\,ZdZ = \frac{1}{2}\,\Gamma\,Z^2 \tag{17}$$

$$Z(y) = \sqrt{\frac{2Q(y)}{\Gamma}} \tag{18}$$

The ground potential temperature = $\theta_o(Z) = \theta_o(0) + \Gamma Z$, so

$$\Delta T = \theta_o(Z) - \theta_o(0) = \Gamma Z = \sqrt{2\Gamma Q(y)}. \tag{19}$$

Case 2: logarithmic profile

$$\theta_o(z) = \frac{a}{b}\,\ell n\,(1+bz)+\theta_o(0); \qquad \gamma(Z) = \frac{a}{1+bZ} \tag{20}$$

(Physically, a is the initial lapse rate at z = 0; b is the inverse of the height at which the lapse rate is one half of that at the surface.)

$$Q(y) = \int \frac{aZ}{1+bZ}\,dZ = \frac{aZ}{b} + \frac{a}{b^2}\,\ell n\,\left(\frac{1}{1+bZ}\right) \tag{21}$$

In this case an analytic solution for Z, and thus for ΔT, is not practical. Results for a particular numerical case will be discussed below.

Case 3: step function profile

$$\begin{array}{lll} \theta_o(z) = \theta_o(0) + \gamma_1 z \Big|_{z \leq z_1} & & \gamma(z) = \gamma_1 \\ = \theta_o(z_1) \Big|_{z_1 \leq z \leq z_2} & & \gamma(z) = 0 \\ = \theta_o(z_1) + \gamma_3(z - z_2) \Big|_{z_2 \leq z \leq z_3} & & \gamma(z) = \gamma 3 \\ = \theta_o(z_3) \Big|_{z_3 \leq z \leq z_4} & & \gamma(z) = 0 \\ = \theta_o(z_3) + \gamma_5(z - z_4) \Big|_{z_4 \leq z \leq z_5} & & \gamma(z) = \gamma_5 \end{array} \quad (22)$$

z_1, z_2, etc., are heights of the tops and bases of the adiabatic layers.

For Z F z_1, $\int Z \gamma_1 \, dZ = Q(y)$ (23)

$$\gamma_1 \frac{Z^2}{2} = Q(y) \quad (24)$$

up to the y at which $Q(y) = \frac{z_1^2 \gamma_1}{2}$

At that point Z makes a discontinuous jump to z_2.

Then $Q(y) = \frac{\gamma_1 z_1^2}{2} + \int_{z_2}^{Z} \gamma_3 Z dZ$

$$= \frac{z_1^2 \gamma_1}{2} + \gamma_3\left(\frac{Z^2 - z_2^2}{2}\right) \text{ until } Z = z_3,$$

where $Q(y) = \frac{z_1^2\gamma_1}{2} + \frac{\gamma_3(z_3^2 - z_2^2)}{2}$, etc.

Between z_2 and z_3, for example,

$$Q(y) = \frac{z_1^2\gamma_1}{2} - \frac{z_2^2\gamma_3}{2} + \frac{Z^2\gamma_3}{2}$$

or

$$\frac{Z^2\gamma_3}{2} = Q(y) - \frac{z_1^2\gamma_1}{2} + \frac{z_2^2\gamma_3}{2}$$

and

$$Z = \sqrt{\frac{2Q(y) - \gamma_1 z_1^2 + \gamma_3 z_2^2}{\gamma_3}} \quad . \tag{26}$$

The heat island intensity, $\theta(0,Z) - \theta(0,0) = \Delta T$ is given by

$$\Delta T = \Delta\theta = \gamma_1 z_1 + \gamma_3 (Z - z_2). \tag{27}$$

Case 4: capping inversion

$$\begin{aligned} \theta_o(z) &= \theta_o(0) + \gamma_1 z \Big|_{0 \le z \le C} \qquad \gamma(Z) = \gamma_1 \\ \theta_o(z) &= \theta_o(C) + \gamma_2(z - C) \Big|_{C \le z} \qquad \gamma(Z) = \gamma_2 \end{aligned} \tag{28}$$

$\gamma_2 >> \gamma_1$; C is the height of the base of the capping inversion.

For $Z < C$, $Q(y) = \gamma_1 \frac{Z^2}{2}$ (29)

$$Z = \sqrt{\frac{2Q(y)}{\gamma_1}} \tag{30}$$

and $$\Delta T = \Delta\theta = \sqrt{2\gamma_1 Q(y)} \ . \tag{31}$$

For $Z > C$,

$$Q(y) = \gamma_1 \frac{C^2}{2} + \int_C^Z \gamma_2 Z dZ = \gamma_1 \frac{C^2}{2} + \frac{\gamma_2}{2} (Z^2 - C^2) \tag{32}$$

$$Z = \sqrt{\frac{2Q(y) + C^2(\gamma_2 - \gamma_1)}{\gamma_2}} \quad \text{(valid only for } Q(y) > \gamma_1 \frac{C^2}{2}\text{, which is automatic for } Z > C\text{)} \tag{33}$$

and $$\Delta T = \Delta\theta = C(\gamma_1 - \gamma_2) + \sqrt{\gamma_2[2Q(y) + C^2(\gamma_2 - \gamma_1)]}. \tag{34}$$

In order to compare the four cases with each other, with the Fairbanks case and with the empirical inversion model of Ludwig (1970), calculations were carried out for each of the four cases with the constants adjusted to give the same 100 m inversion for all four cases. The constants used were:

Case 1 $\Gamma = .1522$ °K m^{-1}
Case 2 $a = 1$ °K m^{-1}, $b = .2$ m^{-1}
Case 3 $z_1 = 10$ m, $z_2 = 45$ m, $z_3 = 55$ m, $z_4 = 89.56$ m
$\gamma_1 = \gamma_3 = \gamma_5 = .5$ °K m^{-1}
Case 4 $\gamma_1 = .01$ °K m^{-1}, $\gamma_2 = 1.432$ °K m^{-1}, $C = 90$ m

All four cases give a 15.22°K potential temperature inversion (= 14.22°C measured inversion) over the first hundred meters of the sounding. (This is quite a large inversion, but by no means unknown in Fairbanks, as shown in the discussion below. The use of .1522 is to give simple constants in the logarithmic case.) In addition, calculations were carried out for a 100 m potential temperature inversion of 4.6°K (3.6°C/100 m) for cases 1 and 2.*

---

*Case 1 $\Gamma = .406$, case 2 $a = 1$°K m^{-1}, $b = 1$ m^{-1}.

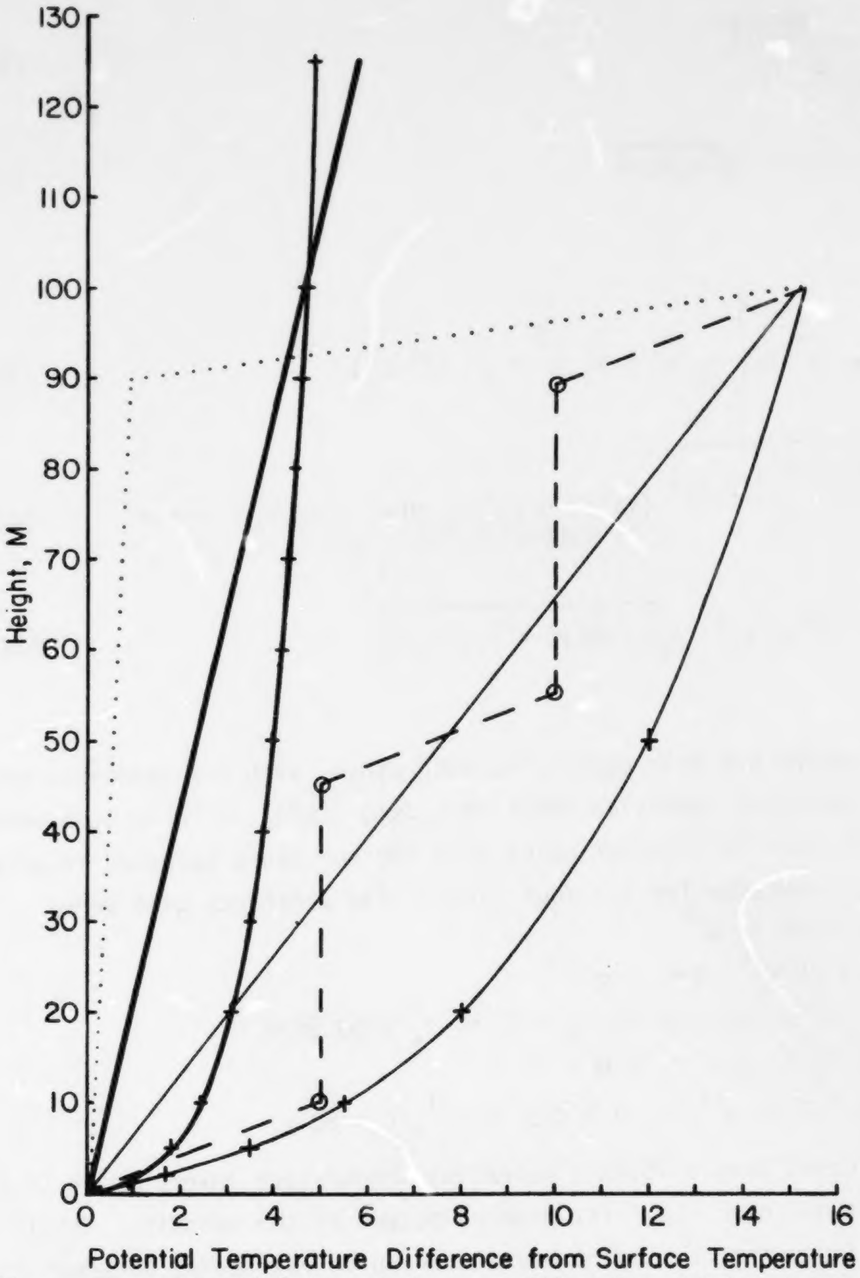

Figure 57. Potential temperature profiles for which calculations were made of mixing height and heat island intensity. Light lines - lapse rates with the 100 meter potential temperature difference equal to 15.22°C. Plain line - linear case; line with crosses - logarithmic case; dashed line - stepped case; dotted line - capping inversion case. Heavy lines - linear and logarithmic profiles for 100 meter potential temperature differences of 4.6°C (3.6C/100 m inversion).

The various initial soundings used are shown in Figure 57; the resulting heat island intensities and heights are shown in Figures 58 and 59. Note that the form of the sounding is of sufficient importance to outweigh a three-fold change in the lapse rate in some cases. A good deal of the scatter in Ludwig's (1970) plots is probably due to this kind of variation in the form of the lapse rate.

In order to compare these calculations with the Fairbanks case, we will consider two cases in which Fairbanks helicopter data were available - traverses 24 (14 March 1975) and 38 (26 Feb 1976). Table 20 gives the important temperatures for both cases.

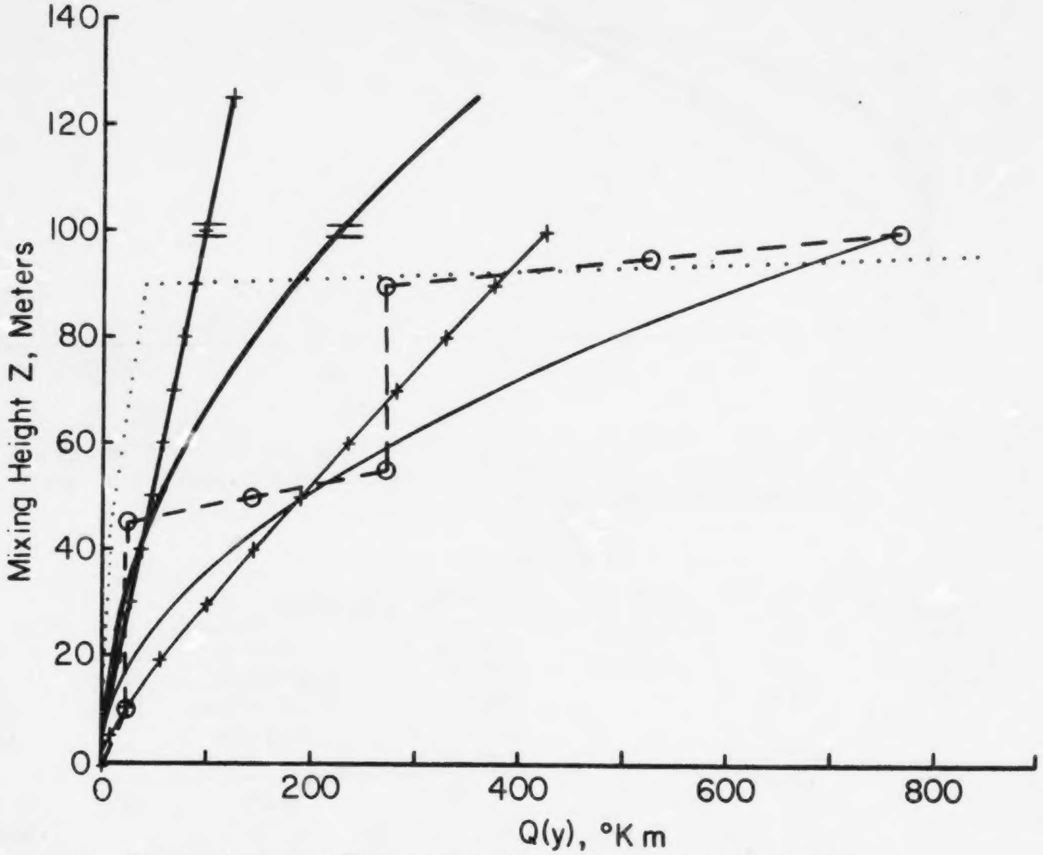

Figure 58. Mixing height, Z as a function of accumulated bottom heating Q(y), in °K m. Line types as in Figure 57. Short double lines indicate the 100 m level.

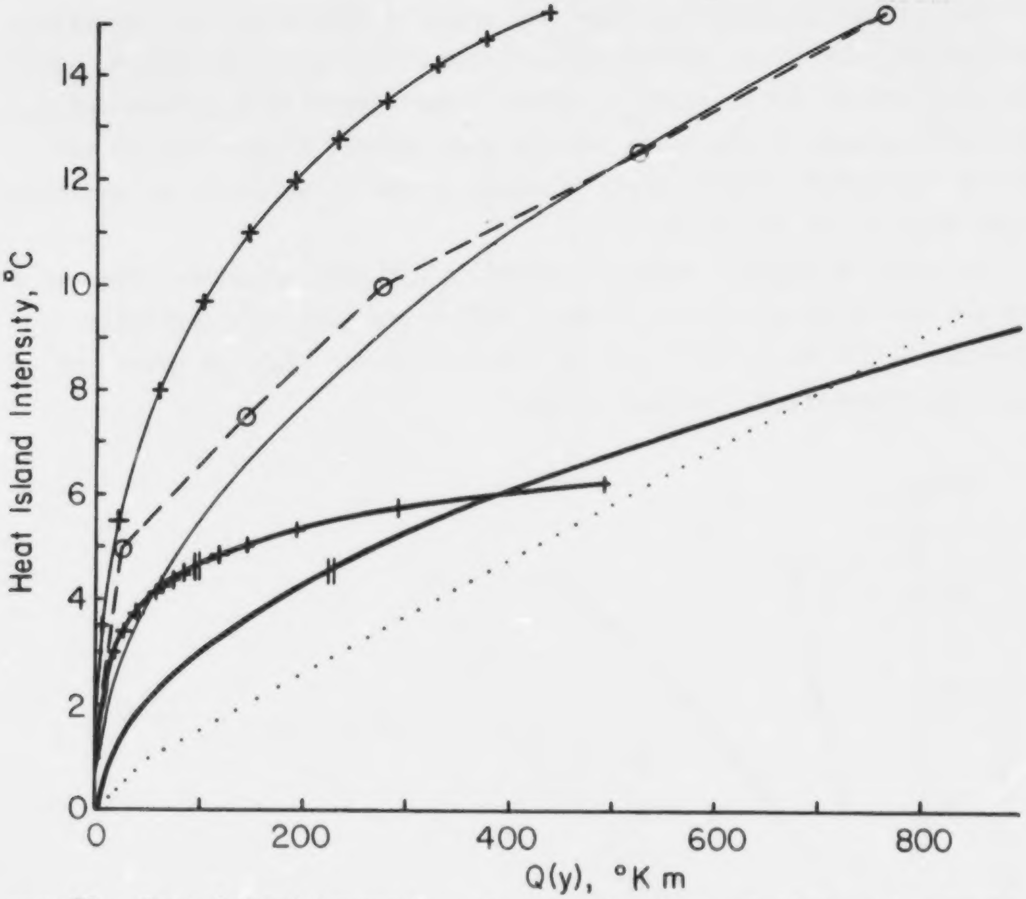

Figure 59. Heat island intensity, $\Delta\theta$, as a function of Q(y). Line types as in Figure 57. Short double lines indicate where the heat island extends above 100 m.

TABLE 20

TEMPERATURES FROM TWO HELICOPTER TRAVERSES

	Upwind Ground Temp. at y = 0	City Core Temp. y = y z = 2 m	Heat Island ΔT	Upwind 100 m Temp. at y = 0 z = 100 m	100 m Potential Temperature Inversion	Geo. Inst. Temp.	Form of Lapse Rate
#24	-17°C	-9°C	8°C	-3°C	15°C	-9°C	linear (helicopter ascent)
#38	-31 °C	-18.5 °C	12.5°C	-16 °C	16°C	-18°C	∿ logarithmic (tethered balloon 1st 10 m)

If the observed heat island intensities of 8°C and 12.5°C are located on the linear and logarithmic plots, respectively, both are found to correspond to Q values of slightly more than 200. This value of Q gives mixing heights of about 60 m in each case. Measured temperatures at the Geophysical Institute, 60 m above the city, are in good agreement with the observed city temperatures, which aids in confirming the original lapse rate assumptions.

CONDUCTIVE/CONVECTIVE AND RADIATIVE ENERGY LOSSES

There are some problems in direct calculation of $Q(y)$. The value of $q(y)$ along a particular path is not generally known, and in addition, $q(y)$ is actually dependent on the temperature at y (see eq. 8) - a fact which we ignored in the solution of our initial equation. In the case of Fairbanks, the mean wind speed is also poorly known, as most of the measured winds probably represent eddies and waves (Section 7). It is, however, possible to set some limits to q and to v with the available data. To do so, we will consider the role of radiative loss.

Let $h(x,y)$ be the total energy per unit area supplied at the surface by the city. This will be the sum of $q(x,y)$, and the net radiative energy loss. If the outlying areas are in radiative equilibrium at temperature T_o, and the incoming longwave radiation is the same in and out of the city, then the net radiative energy loss is $\sigma T^4(x,y) - \sigma T_o^{\ 4} \cong 4\sigma T_o^{\ 3}\ \Delta T(x,y)$ (where ΔT is the heat island intensity at (x,y)) assuming that the average substrate temperature is close to that of the overlying air. Then

$$h(x,y) = q(x,y) + 4\sigma T_o^{\ 3}\ \Delta T(x,y). \tag{8'}$$

Since it is necessary to know q to calculate ΔT, while h is the actual input, this equation is of use only in special circumstances.

One such special circumstance is the case in which q increases linearly along the path of the wind to the city center and the lapse rate is a linear inversion, $\frac{\partial\theta}{\partial z} = \Gamma$. Let $q(0,y) = Ky$. Then from eq (23),

$$Q(y) = \int \frac{q(y)}{\rho c_p v}\, dy = \frac{1}{2}\,\frac{Ky^2}{\rho c_p v}\ , \tag{35}$$

and from eq (19), $\Delta T = \Delta\theta_o = \sqrt{2\Gamma Q(y)} = y \; \frac{\Gamma K}{\rho c_p v}$. (36)

Eq (8') then becomes

$$h(0,y) = \left(K + 4\sigma T_o{}^3 \sqrt{\frac{\Gamma K}{\rho c_p v}}\right) y. \tag{37}$$

If we set $\left(K + 4\sigma T_o{}^3 \sqrt{\frac{\Gamma K}{\rho c_p v}}\right) = J,$ (38)

$$h(0,y) = Jy \quad \text{or } J = \left.\frac{\partial h}{\partial y}\right|_{x=0} \tag{39a}$$

in parallel with

$$q(0,y) = Ky \quad \text{or } K = \left.\frac{\partial \gamma}{\partial y}\right|_{x=0} \tag{39b}$$

Thus for a linear increase in h along the wind and an initial uniform inversion, we also have a linear increase in q(0,y). If J is known, K can be calculated from the defining equation for J, squared:

$$K^2 - 2KJ + J^2 = 16\ \sigma^2 T_o{}^6\ \frac{\Gamma K}{\rho c_p v}\ . \tag{40}$$

From this,

$$K^2 - 2K\left(J + \frac{8\ \sigma^2 T_o{}^6\ \Gamma}{\rho c_p v}\right) + J^2 = 0. \tag{41}$$

Let $\frac{8\ \sigma^2 T_o{}^6}{\rho c_p} = A$ (42)

and $\frac{\Gamma}{v} = B.$ (43)

Eq. 38 demands that K < J, which allows only the solution (Dwight, 1961, eq. 55.1)

$$K = \frac{J^2}{J + AB + \sqrt{2ABJ+(AB)^2}} \tag{44}$$

$$= \frac{J}{1 + \frac{AB}{J} + \sqrt{2\,\frac{AB}{J} + (\frac{AB}{J})^2}} \tag{45}$$

The fraction of the heat energy released by the city which is actually heating the air is $\frac{q}{h}$, which now can be written as:

$$\frac{K}{J} = \left(1 + \frac{AB}{J} + \quad 2\,\frac{AB}{J} + (\frac{AB}{J})^2\right)^{-1} \tag{46}$$

Values of K/J for different values of $\frac{AB}{J}$ are given in Table 21.

TABLE 21

K/J AS A FUNCTION OF AB/J

$\frac{AB}{J}$	K/J
.001	.96
.01	.87
.02	.82
.05	.73
.1	.64
.25	.50
1	.27
3	.13
5	.08
10	.05

The three variables A, B and J represent the regional meteorology, the local micrometeorology and the city heat addition, respectively. Using the gas law to express air density in terms of temperature, T, and pressure, P,

$$A = 6.327 \times 10^{-16} T^7 P^{-1}, \qquad (47)$$

where T is in °K, P, in mb and A in cal cm^{-1} $°\text{K}^{-1}$ min^{-2}.

If Γ is expressed in °K m^{-1} and v in m sec^{-1}, then

$$B = \frac{10^{-4}}{60} \frac{\Gamma}{v} = 1.667 \times 10^{-6} \frac{\Gamma}{v} \quad \text{in °K min cm}^{-2}. \qquad (48)$$

Some values of A, B and AB for meteorological variables typical of temperate-zone cities and of Fairbanks are given in Table 22.

TABLE 22

TYPICAL VALUES, UNITS AS GIVEN IN TEXT

T_0	P	A	Γ	v	B	AB
20°C	700	$1.68\text{x}10^{-1}$	.01	5	$3.33\text{x}10^{-9}$	$5.59\text{x}10^{-10}$
10°C	1000	$9.20\text{x}10^{-2}$	.01	5	$3.33\text{x}10^{-9}$	$3.07\text{x}10^{-10}$
-20°C	1000	$4.20\text{x}10^{-2}$	.15	.25	$1.01\text{x}10^{-6}$	$4.26\text{x}10^{-8}$
-40°C	1000	$2.4\text{x}10^{-2}$	.15	.25	$1.01\text{x}10^{-6}$	$2.44\text{x}10^{-8}$

Note that $\Gamma = \frac{d\theta}{dz} = .01$ is the isothermal case ($\frac{dT}{dz} = 0$) and that the calculations for $\Gamma = .15$ actually refer to $\Gamma = .1522$ as used in the discussion of the influence of the form of the lapse rate.

If the total energy, E, released by the city is known, J may be estimated by assuming a circularly symmetric city of radius R. Let the heat release, h, be zero outside the radius R and increase linearly toward the city center. Then

$$h(x,y) = J\left(R - \sqrt{x^2+(R-y)^2}\right) \quad \text{for } x^2 + (R-y)^2 < R^2 \qquad (49)$$

$$h(x,y) = 0 \qquad \text{for } x^2 + (R-y)^2 \geq R^2.$$

This defines the conical heating distribution used from here on. The total heat release, E, is the area integral of h(x,y) over the city. By defining $r = \sqrt{x^2+(R-y)^2}$, this integral is easily evaluated, giving

$$E = \frac{\pi J R^3}{3} \tag{50}$$

or

$$J = \frac{3E}{\pi R^3} . \tag{51}$$

For Fairbanks and its surroundings in winter, we have from section 8 $E = 10^{10}$ cal min^{-1}.

If R = 5 km, appropriate for the area as a whole, and we assume values for the meteorological variables as given in line 3 of Table 22,

$$J = \frac{3 \times 10^{10}}{\pi(5 \times 10^5)^3} \times 7.64 \times 10^{-8} \text{ cal cm}^{-3} \text{ min}^{-1}$$

giving AB/J = .56, or K/J = .36 - only about 35% of the energy released goes into heating the air. (If a dense fog is present, the 35% is what is left over to heat the air after subtracting the radiation from the fog top.) If R = 1 km, which might be more appropriate for air coming into the city from the north,

$$J = 9.55 \times 10^{-6}, \ AB/J = 4.46 \times 10^{-3} \text{ and } K/J = .91.$$

90% of the energy goes into heating the air in this case.

Note that the above analysis and the definitions for K and J hold only upwind of the city center. Downwind of the maximum value of h at the city center, ΔT will continue to increase as h(0,y) decreases until q of eq (8') becomes zero, i.e., $4\sigma T^3 \Delta T = h(0,y)$. At the point where q = 0, let y = Y. Since from eq (36) ΔT is proportional to y and thus to h = Jy up to y = R, $q = h - 4\sigma T^3 \Delta T$, and ΔT continues to increase while h decreases from y = R to y = Y, q must decrease much more rapidly than it increased, becoming 0 at Y and negative thereafter (Fig. 53). Negative q implies heat transfer from the air to the ground, so the temperature and thus ΔT decreases with y for $y > Y$. Since ΔT increases when $y < Y$, and decreases when $y > Y$, it follows that Y is the coordinate of the maximum heat island intensity. The maximum heat island intensity, $\Delta T(Y)$ must be within the city, i.e., Y must be less than $2R$. This follows from

$$\left.\frac{\partial q}{\partial y}\right|_{x=0} = \frac{dq_o}{dy} = K \qquad \text{for } y < R,$$

$$\left.\begin{aligned} &\text{but } \frac{dq_o}{dy} = \frac{d}{dy}\left(h - 4\sigma T^3 \Delta T\right). \\ &h(0,y) = JR-(y-R)J, \text{ from eq (49)} \\ &\frac{dq_o}{dy} = \frac{d}{dy}\left(JR-(y-R)J - 4\sigma T^3 \Delta T\right) \\ &\qquad = -J - \frac{d}{dy}\left(4\sigma T^3 \Delta T\right). \end{aligned}\right\} \qquad \text{for } R \leq y \leq Y$$

For $R \leq y \leq Y$, $\frac{d}{dy}(4\sigma T^3 \Delta T) > 0$ by the definition of Y,

$$\text{so } -\left.\frac{dq_o}{dy}\right|_{R<y<Y} > J \geq K = \left.\frac{dq_o}{dy}\right|_{y<R} .$$

Since q increases from $q = 0$ at $y = 0$ for $0 \leq y \leq R$ and decreases at a faster rate than it increased for $R \leq y \leq Y$, Y being defined as the point where q is again equal to 0, it is clear that Y must be less than $2R$ (see Fig. 53).

The maximum heat island intensity may be bracketed by noting that $Y \geq R$ and that $\Delta T_{re}(R) \geq \Delta T_{max}$. The upper limit to the heat island intensity is given by $\Delta T_{max} = \Delta T_{re}(R)$. This can be determined from

$$\left. h(y) \right|_{y=R} = 4\sigma T^3 \Delta T_{re} = RJ \tag{52}$$

$$\text{or} \quad \Delta T_{re} = \frac{RJ}{4\sigma T_o^{\,3}} = \frac{3E}{\pi R^2 4\sigma T_o^{\,3}} \tag{53}$$

For the two Fairbanks cases discussed above, this gives

for R = 5 km $\Delta T_{re} = 7.2°K$

for R = 1 km $\Delta T_{re} = 181°K$.

Obviously the upper limit is a very poor approximation to the 1 km case, and in fact the assumptions in this case are so extreme that the $\Delta T/T_o \ll 1$ assumption breaks down. A real energy concentration of this magnitude (720 W m^{-2} at the city core; compare with an estimated 630 W m^{-2} for Manhattan Island, SMIC, 1971) would also almost certainly invalidate our assumption that the circulation induced by the heat island was small.

The actual heat islands predicted at the city core, which are also the lower limits for the maximum heat islands, using the figures listed and eq (36) are:

TABLE 23

PREDICTED HEAT ISLANDS

T °C	P mb	Γ °C m^{-1}	v m sec^{-1}	R km	J cal cm^{-3}	K min^{-1}	Q(R) °K m	ΔT °C
-20	1000	.1522	.25	5	7.64×10^{-8}	2.75×10^{-8}	69.4	4.6
-20	1000	.1522	.25	1	9.55×10^{-6}	8.69×10^{-6}	877	16.3
-20	1000	.15	1	5	7.64×10^{-8}	4.53×10^{-8}	28.5	3.0
-20	1000	.15	1	1	9.55×10^{-6}	9.11×10^{-6}	229	8.4

Note that when the wind speed is increased by a factor of four, the calculated heat islands decrease by somewhat less than a factor of two, as $\frac{K}{J}$ increases with wind speed. Given the crudity of the model for h(x,y), the model for Fairbanks is in reasonable agreement with observation. This in turn suggests that the mean wind through the Fairbanks area is probably within or below the suggested range of .25 to 1 m sec^{-1}, with the upper end of this range, which would correspond to the 1 km radius, being very unlikely.

The case with fog causes problems because of the radiative cooling at the top. Figure 55 showed a hypothetical fog sounding. The algebraic area between the original and final soundings at y must equal Q(y) as before.

But now (for the constant lapse rate Γ)

$$Q(y) = \frac{(\Delta\theta)\,\frac{\Delta\theta}{\Gamma}}{2} - \frac{(Z-\frac{\Delta\theta}{\Gamma})(\Gamma Z-\Delta\theta)}{2}\text{, or}$$

$$Q(y) = \frac{2Z\Delta\theta-\Gamma Z^2}{2} \tag{54}$$

The exact relationship between Z and $\Delta\theta$ is needed to complete this equation, but that relationship depends on the details of radiation and convection, as it will depend on the vertical growth of a fog layer capped by a very steep inversion. We can, however, set some limits.

Let $\Delta\theta'$ be the temperature difference and Z' the mixing depth at y for the fog-free case. It is obvious from Figure 55 that $\Delta\theta \geq \Delta\theta'$, as the area $\frac{(\Delta\theta')^2}{2\Gamma} = Q(y)$. Suppose that $\Delta\theta = m\Delta\theta'$ (m not necessarily an integer). Then

$$\frac{(\Delta\theta')^2}{2\Gamma} = Q(y) = \frac{2Zm\Delta\theta'-\Gamma Z^2}{2}$$

$$\Delta\theta' = \Gamma Z'$$

and

$$\Gamma Z'^2 = 2Zm\Gamma Z' - \Gamma Z^2$$

$$Z^2 - 2mZZ' + Z'^2 = 0$$

$$Z = \frac{2mZ' \pm \sqrt{4m^2Z'^2-4Z'^2}}{2} = Z'(m \pm \sqrt{m^2-1})$$

The minus sign corresponds to the case with a superadiabatic lapse rate above Z, as may be seen from Figure 55 by noting that if $\Delta\theta = m\Delta\theta'$, mZ' is the point at which the foggy sounding and the original sounding cross. So, if

$$\begin{aligned} \Delta\theta &= m\Delta\theta', \\ Z &= (m + \sqrt{m^2-1})\,Z'. \end{aligned} \tag{55}$$

An upper limit to m may be obtained by noting that Z can hardly exceed the value it would have if all of the heat that went into the air were allowed to mix while suppressing radiative loss, and the radiative loss were then taken all at once. This would give the sounding shown as a dotted line in Figure 60 as an intermediate step. In this case we can define

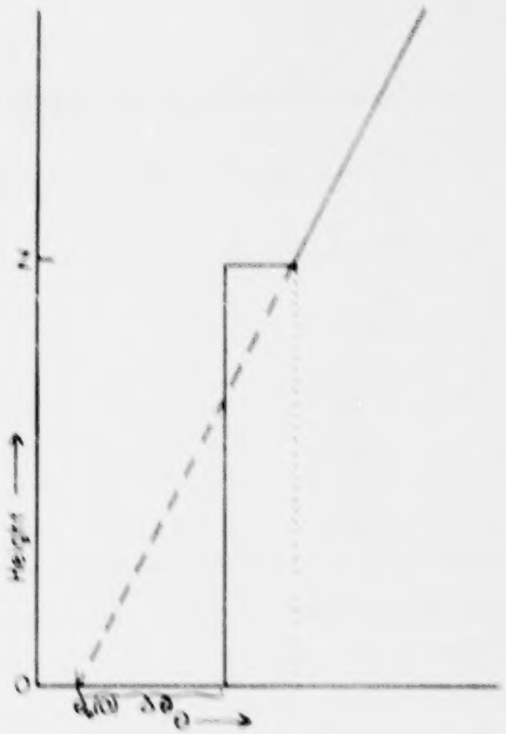

Figure 60. Development of city fog sounding.

$$H(y) = \int \frac{h(y)}{\rho c_p v}\, dy \tag{56}$$

and proceed in exact analogy to eqs. (12) through (18) to obtain

$$Z = \sqrt{\frac{2H(y)}{\Gamma}} \tag{57}$$

or

$$\left(m + \sqrt{m^2 - 1}\right) = \frac{Z}{Z_1} = \sqrt{\frac{H(y)}{Q(y)}} = \sqrt{\frac{J}{K}} \tag{58}$$

$$\frac{\Delta\theta}{\Delta\theta'} = m = \frac{1}{2}\sqrt{\frac{K}{J}}\left(\frac{J}{K} + 1\right) \tag{59}$$

Values of $\sqrt{J/K}$ and m are given in Table 24.

The effect of the lapse rate within the fog is to change our defining equation for q, eq. (8') to $$q = h - 4\sigma T_o^3 (\Delta T - .01Z) \tag{60}$$

TABLE 24. MAXIMUM RATIOS OF FOGGY/CLEAR VALUES OF MIXING DEPTH ($\sqrt{\frac{J}{K}}$) AND $\Delta T(m)$

$\frac{K}{J}$	$\frac{J}{K}$	m
.01	10	5.05
.05	4.5	2.35
.1	3.16	1.74
.3	1.83	1.19
.5	1.41	1.06
.7	1.20	1.02
.9	1.05	1.001
.95	1.03	1.0003
.99	1.005	1.00001

If a linear relationship exists between ΔT and Z, this has the effect of changing the σ. In the lower limit case of $Z = Z'$, for instance, $Z = \Delta T/\Gamma$ and σ must be replaced by $(1 - \frac{.01}{\Gamma})\sigma$. This primarily affects A and thus K/J. In the extreme case that K/J = 0, this would increase ΔT by a factor of $(1 - \frac{.01}{\Gamma})^{-1}$.

The sensitivity of the model to the way a given amount of heating is distributed through a city is definitely worth noting. For the case with a linear lapse rate and the "conical" distribution of heat addition discussed above, it is of some interest to work out the dependence of the model on population ϕ, wind speed v, potential lapse rate Γ, energy consumption per person, s, and the area per person, $G = \pi R^2/\phi$. From eq (19) we have at the city center $\Delta T(r) = \sqrt{2\Gamma Q(R)}$. Consider first the case that $\frac{K}{J} \sim 1$.

$$Q(R) = KR^2/(2\rho c_p v) = KG\phi/(2\rho c_p v\pi), \tag{61}$$

$$K \cong J = \frac{3E}{\pi R^3} = \frac{3s\phi}{\pi R^3} = \frac{3s\sqrt{\pi}}{G^{3/2}\phi^{1/2}} \tag{62}$$.

giving
$$\Delta T = \sqrt{3/(\rho c_p \sqrt{\pi})} \cdot \Gamma^{1/2} v^{-1/2} \phi^{1/4} G^{-1/4} s^{1/2} \tag{63}$$

provided the units are compatible.

For Γ in °K m^{-1}, v in m sec^{-1}, ϕ in persons, G in m^2 $person^{-1}$, s in cal $person^{-1}$ min^{-1}, ρ in kg m^{-3} and c_p in cal gm^{-1} $°K^{-1}$, this becomes

$$\Delta T = \frac{9.2 \times 10^{-3}}{\sqrt{\rho c_p}} \Gamma^{1/2} s^{1/2} \phi^{1/4} G^{-1/4} v^{-1/2}. \qquad (63')$$

Likewise, in the radiation-dominated case $\frac{K}{J} = 0$, $\Delta T = \frac{RJ}{4\sigma T^3}$ from **(7)** and (39a), giving

$$\Delta T = \frac{3sG^{-1}}{4\sigma T_o^3} . \qquad (64)$$

If s is in cal $person^{-1}$ min^{-1} and G is in m^2 $person^{-1}$, this may be written as

$$4.53 \times 10^{-2} \left(\frac{T_o}{273}\right)^{-3} sG^{-1} \qquad (64')$$

For cases with $0 < \frac{K}{J} < 1$, the most common state, the situation is more complex. We have

$$\Delta T = \sqrt{2\Gamma Q(R)} = \sqrt{\Gamma K R^2/\rho c_p v} = \sqrt{\Gamma K G\phi/\pi\rho c_p v} , \qquad (65)$$

but $$K = \frac{K}{J} J = \frac{K}{J} (3s\sqrt{\pi} G^{-3/2} \phi^{-1/2}) \qquad (66)$$

where $$\frac{K}{J} = [1 + \frac{AB}{J} + \sqrt{2\frac{AB}{J} + (\frac{AB}{J})^2}]^{-1};$$

and $$\frac{AB}{J} = 1.98 \times 10^{-16} T^7 P^{-1} \Gamma v^{-1} s^{-1} G^{3/2} \phi^{1/2} ,$$

where the units in (67) are the same as for (63'), with the addition that T is in °K and P is in mb.

For $.05 \leq AB/J \leq .25$ (the half of the transistion zone nearer convective dominance)

$$\frac{K}{J} \approx \frac{1}{2.8} \left(\frac{AB}{J}\right)^{-1/4}$$

giving $$\Delta T \overset{\sim}{\alpha} \Gamma^{3/8} G^{-7/16} \phi^{3/16} v^{-3/8} s^{5/8}. \qquad (68)$$

For $.25 \leq \frac{AB}{J} \leq 1$, $\frac{K}{J} \approx \frac{1}{4\sqrt{AB/J}}$, and $\Delta T \overset{\sim}{\alpha} \Gamma^{1/4} G^{-5/8} \phi^{1/8} v^{-1/4} s^{3/4}$. (69)

The factor which determines which of the various equations above will be valid in a particular case is $\frac{K}{J}$, which, from (46) and Table 21 , is a monotonic decreasing function of $\frac{AB}{J}$. $\frac{AB}{J} = 10$ gives a case which is 95% dominated by radiation; $\frac{AB}{J} = .001$ gives a case 95% dominated by conduction. As an illustration of the values of $\frac{AB}{J}$ to be expected in real cases, Table 25 was made up from Table 4.3, p 58 in the SMIC report (1971). Note that the values given for s are based solely on anthropogenic heating and may be serious underestimates in temperate-zone cities where such factors as albedo, evapotranspiration, and thermal lag of the substrate must also be taken into account. Given reasonable values of Γ and v ($.1 \leq \Gamma v^{-1} \leq .002$) most values of $\frac{K}{J}$ will fall between about .2 and .8. Thus the transitional case, with exponents changing, is likely to be the most important one, giving for the general case

$$\Delta T = \frac{9.2 \times 10^{-3}}{\sqrt{\rho c_p}} \Gamma^{1/2} s^{1/2} \phi^{1/4} G^{-1/4} v^{-1/2} \frac{K}{J} \qquad (70)$$

Table 26 and Figures 61-63 were set up to show the effect of changing one variable at a time in a hypothetical city with a population of 200,000 persons, area per person of 400 m^2 $person^{-1}$, heat release of 10^5 cal $person^{-1}$ min^{-1} ($\simeq$ 7 KW $person^{-1}$), potential lapse rate of $.03°K^{-1}$ ($\frac{dT}{dz} = 2°/100m$) and wind speed of 1 m sec^{-1}. In each case the light line gives the relationship if radiative transfer is ignored; the heavy line includes the effect of varying $\frac{K}{J}$.

In summary, if $\Gamma s^{-1} G^{3/2} \phi^{1/2} v^{-1}$ is sufficiently small, ΔT is proportional to $\Gamma^{1/2} v^{1/2} \phi^{1/4} G^{-1/4} s^{1/2}$, in qualitative agreement with previous work. As $\Gamma s^{-1} G^{3/2} \phi^{1/2} v^{-1}$ increases, the influence of Γ, v and φ on the heat island intensity dimishes and that of G and s increases until in the extreme case of radiative equilibrium the heat island is due entirely to the energy release per unit area. At this point, however, the circulation induced by the heat island would no longer be negligible, and the analysis is inapplicable.

TABLE 25. COMBINATIONS OF ϕ, G AND k OBSERVED FOR URBAN AREAS BASED ON SMIC (1971) TABLE 4.3

	R km	ϕ 10^6 people	G m^2 $person^{-1}$	S 10^3 cal min^{-1} $person^{-1}$	AB/J	
					for ϕ in 10^6 persons	Γ in °K m^{-1} v in m sec^{-1}
Washington-Boston Complex	166	33	2636	161	$19\phi^{1/2}\Gamma v^{-1}$	$108\Gamma v^{-1}$
Nordrhein-Westfalen	104	16.8	2021	115	$18\phi^{1/2}\Gamma v^{-1}$	$73\Gamma v^{-1}$
Same, Industrial Area	57	11.3	913	128	$4.8\phi^{1/2}\Gamma v^{-1}$	$16\Gamma v^{-1}$
Los Angeles County	56	7.0	1428	148	$8.3\phi^{1/2}\Gamma v^{-1}$	$22\Gamma v^{-1}$
Los Angeles	33	7.0	500	148	$1.7\phi^{1/2}\Gamma v^{-1}$	$4.5\Gamma v^{-1}$
Moscow	17	6.4	137	241	$.15\phi^{1/2}\Gamma v^{-1}$	$.38\Gamma v^{-1}$
Hamburg	15.4	1.8	408	72	$2.5\phi^{1/2}\Gamma v^{-1}$	$3.4\Gamma v^{-1}$
West Berlin	8.6	2.3	102	29	$.80\phi^{1/2}\Gamma v^{-1}$	$1.2\Gamma v^{-1}$
Manhattan	4.3	1.7	35	301	$.015\phi^{1/2}\Gamma v^{-1}$	$.02\Gamma v^{-1}$
Fairbanks,* SMIC	3.4	.03	1233	312	$3.1\phi^{1/2}\Gamma v^{-1}$	$.54\Gamma v^{-1}$
Fairbanks, this report	5.1**	.045	1819	143	$12.2\phi^{1/2}\Gamma v^{-1}$	$2.6\Gamma v^{-1}$
Fairbanks North Star Borough, this report	78.1**	.065	294860	143	$25080\phi^{1/2}\Gamma v^{-1}$	$6394\Gamma v^{-1}$

$\frac{AB}{J} = 2.24 \times 10^{-2}\ s^{-1}\ G^{3/2}\ \phi^{1/2}\Gamma v^{-1}$, evaluated for T = 0°C, P = 1000 mb

R is derived from $\sqrt{\frac{area}{\pi}}$

**Based on actual areas of 31.35 mi^2 and 7400 mi^2

*Fairbanks figures are not in agreement with our values

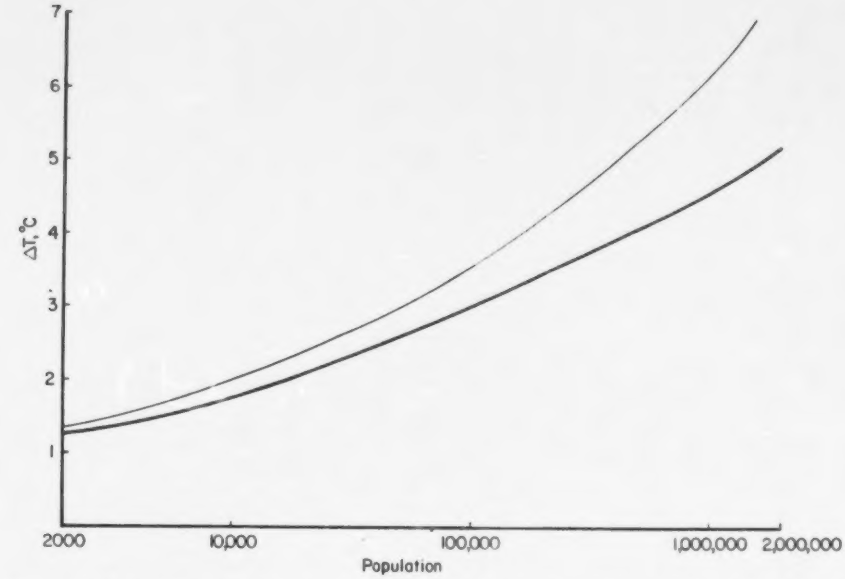

Figure 61. Dependence of city center heat island intensity on population. Heavy lines include the effect of thermal radiative loss, light lines give heat island intensity neglecting radiative effects.

Figure 62. (Below) Dependence of city center heat island intensity on energy release per person (solid lines) and potential lapse rate (dashed lines). Light and heavy lines as in Figure 61.

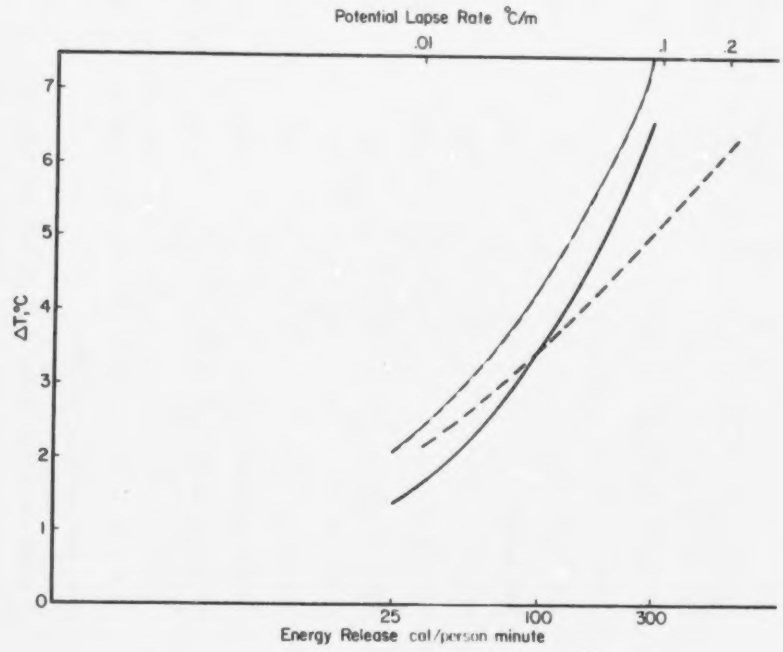

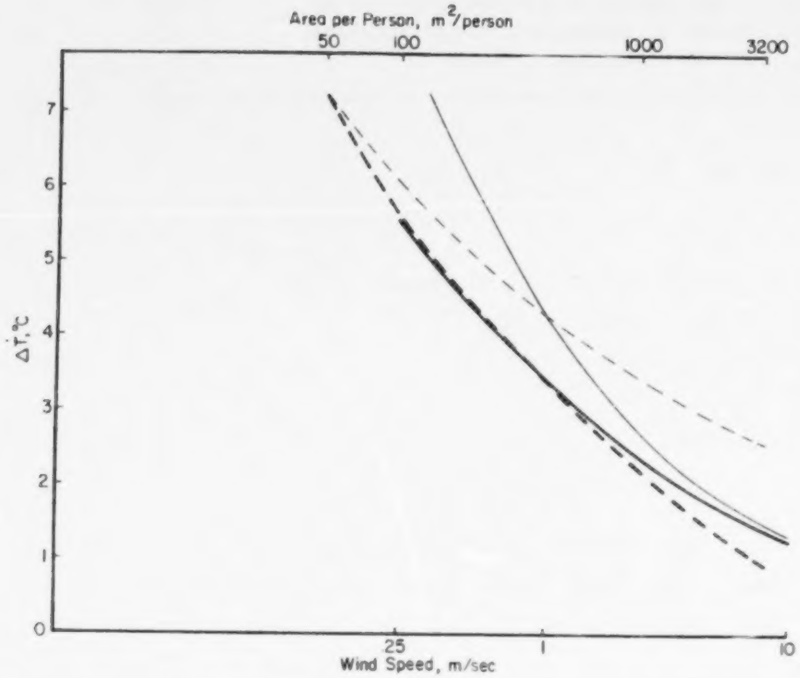

Figure 63. Dependence of city center heat island intensity on wind speed (solid lines) and area per person (dashed lines). Light and heavy lines as in Figure 61.

TABLE 26. VARIATION OF ΔT (FROM EQUATION 70) WITH POPULATION, AREA PER PERSON, ENERGY RELEASE PER PERSON, LAPSE RATE AND WIND SPEED. TEMPERATURE IS 0°C AND AIR PRESSURE IS 1000 mb

a: $G = 400 m^2 \text{ person}^{-1}$

$S = 100 \times 10^3 \text{ cal min}^{-1} \text{ person}^{-1}$

$\Gamma = .03°K\ m^{-1}$

$v = 1\ m\ sec^{-1}$

ϕ =	2×10^3	2×10^4	2×10^5	2×10^6	2×10^7	persons
$\frac{K}{J}$ =	.933	.884	.804	.679	.507	
ΔT =	1.3	2.1	3.5	5.2	6.9	°C

b: $\phi = 2 \times 10^5$ persons

$S = 100 \times 10^3 \text{ cal min}^{-1} \text{ person}^{-1}$

$\Gamma = .03°K\ m^{-1}$

$v = 1\ m\ sec^{-1}$

G =	50	100	200	400	800	1600	3200	$m^2 \text{ person}^{-1}$
$\frac{K}{J}$ =	.999	.925	.879	.804	.693	.543	.368	
ΔT =	7.2	5.6	4.5	3.5	2.5	1.7	.9	°C

c: $\phi = 2 \times 10^5$ persons

$G = 400\ m^2 \text{ person}^{-1}$

$\Gamma = .03°K\ m^{-1}$

$v = 1\ m\ sec^{-1}$

S =	25	50	75	100	150	200	300	$\times 10^3 \text{ cal min}^{-1} \text{person}^{-1}$
$\frac{K}{J}$ =	.647	.734	.777	.804	.836	.857	.881	
ΔT =	1.4	2.2	2.9	3.5	4.4	5.2	6.6	°C

d: $\phi = 2 \times 10^5$ persons

$G = 400 m^2 \text{ person}^{-1}$

$S = 100 \times 10^3 \text{ cal min}^{-1} \text{ person}^{-1}$

$v = 1\ m\ sec^{-1}$

Γ =	.01	.03	.06	.1	.15	.2	$°K\ m^{-1}$
$\frac{K}{J}$ =	.881	.804	.734	.672	.615	.572	
ΔT =	2.2	3.5	4.5	5.3	5.9	6.4	°C

e: $\phi = 2 \times 10^5$ persons

$G = 400\ m^2 \text{ person}^{-1}$

$S = 100 \times 10^3 \text{ cal min}^{-1} \text{ person}^{-1}$

$\Gamma = .03\ °K\ m^{-1}$

v =	.25	.5	1	2	5	10	$m\ sec^{-1}$
$\frac{K}{J}$ =	.647	.734	.804	.857	.906	.933	
ΔT =	5.6	4.5	3.5	2.6	1.7	1.3	°C

REFERENCES

1. Atwater, Marshall A. The radiation budget for polluted layers of the urban environment. J. Appl. Met, 10, 1971, pp. 205-214.

2. Atwater, M. A. and J. P. Pandolfo. Tundra Environmental Changes Induced by Urbanization. Climate of the Arctic, ed. G. Weller and S. A. Bowling, Geophysical Institute, Fairbanks, 1975, pp. 312-315.

3. Benson, C. S. Ice Fog--Low Temperature Air Pollution Defined with Fairbanks, Alaska as Type Locality. Cold Regions Research and Engineering Laboratory Research Report 121, 1970.

4. Benson, C. S. and S. A. Bowling. The Sub-arctic Heat Island as Studied at Fairbanks, Alaska. Climate of the Arctic, ed. G. Weller and S. A. Bowling, Geophysical Institute, Fairbanks, 1975, pp. 309-311.

5. Bowling, S. A. Radiative Cooling Rates in the Presence of Ice Crystal Aerosols. Ph.D. Dissertation, University of Alaska, May 1970.

6. Bowling, Sue Ann, Takeshi Ohtake and Carl S. Benson. Winter Pressure Systems and Ice Fog in Fairbanks, Alaska. J. of Appl. Met., 7, 1968, pp. 961-968.

7. Childers, Joseph M. and James P. Meckel. Flood of August 1967 at Fairbanks, Alaska. Hydrologic Investigations Atlas HA-294. U. S. Geological Survey, 1967.

8. Duckworth, Fowler S. and James S. Sandberg. The Effect of Cities upon Horizontal and Vertical Temperature Gradients. Bull. Am. Met. Soc., 35., 1954, pp. 198-207.

9. Dwight, H. B. Tables of Integrals and Other Mathematical Data, fourth edition. MacMillan, New York, 1961.

10. Fahl, Charles B. Internal Atmospheric Gravity Waves at Fairbanks, Alaska. M. S. Thesis, University of Alaska, Fairbanks, 1969.

11. Haurwitz, Bernhard. Oscillations in a Basin of Cold Air. Atmosphere, 11, 1973, pp. 141-144.

12. Holmgren, B., L. Spears, C. Wilson and C. S. Benson. Acoustic Soundings of the Fairbanks Temperature Inversions. Climate of the Arctic, ed. G. Weller and S. A. Bowling, Geophysical Institute, Fairbanks, 1975, pp. 293-306.

13. Holty, Joseph, G. Air Quality in a Subarctic Community, Fairbanks, Alaska. Arctic, 26, 1973, pp. 292-302.

14. Landsberg, Helmut. Inadvertent Atmospheric Modifications through Urbanization. Weather and Climate Modification, ed. W. N. Hess, Jr. Willey and Sons, New York, 1974, pp. 726-763.

15. Leahey, Douglas M. and James P. Friend. A Model for Predicting the Depth of the Mixing Layer Over an Urban Heat Island with Applications to New York City. J. Appl. Met., 10, 1971, pp. 1162-1173.

16. Ludwig, F. Urban Air Temperatures and Their Relation to Extra-Urban Meteorological Measurements. Papers presented at the Symposium on Survival Shelter Problems, American Society of Heating, Refrigerating and Air-Conditioning Engineers. January 19-22, 1970, San Francisco, California, 1970, pp. 40-45.

17. Myrup, Leonard O. A Numerical Model of the Urban Heat Island. J. Appl. Met. 8, 1969, pp. 908-918.

18. Nappo, Carmen J., Jr. A Numberical Model of the Urban Heat Island. Conference on the Urban Environment and Second Conference on Biometeorology, Am. Met. Soc. Philadelphia. Oct. 31-Nov 2, 1972, pp. 1-4.

19. Ohtake, Takeshi, Studies on Ice Fog. Geophysical Institute Report UAG R-211 University of Alaska. Final Report APO-00449, June 1970.

20. Oke, T. R. City Size and the Urban Heat Island. Conference on the Urban Environment and Second Conference on Biometeorology. Am. Met. Soc., Philadelphia, 1972, pp. 144-146.

21. Robinson, Elmer and Bell, Gordon B. Jr. Low-level Temperature Structure Under Alaskan Ice Fog Conditions. Bull. Am. Met. Soc., 37, 1956, pp. 506-513.

22. SMIC Report. Inadvertent Climate Modification. Report on the Study of Man's Impact on Climate. MIT Press, Cambridge, 1971. 307 p.

23. Summers, Peter W. An Urban Heat Island Model: Its Role in Air Pollution Problems, with Applications to Montreal. Paper presented at the "First Canadian Conference on Micrometeorology" in Toronto, 12-14 April, 1965.

24. Wilson, C. R. and C. B. Fahl. Infrasonic Pressure Waves in the Auroral Zone. Final Report, contract E22-2768 (N) ESSA. Geophysical Institute, University of Alaska, 1969.